NORTHWESTERN UNIVERSITY

The Multifunctional Role of Substrate-Binding Proteins in Heme Uptake and Antimicrobial

Resistance

A DISSERTATION

SUBMITTED TO THE GRADUATE SCHOOL

IN PARTIAL FULLFILLMENT OF THE REQUIREMENTS

for the degree

DOCTOR OF PHILOSOPHY

Field of Biological Sciences

By

Kari J. Tanaka

EVANSTON, ILLINOIS

March 2019

ABSTRACT

The Multifunctional Role of Substrate-Binding Proteins in Heme Uptake and Antimicrobial

Resistance

Kari J. Tanaka

Pathogenic bacteria scavenge essential nutrients including metals, amino acids and peptides to survive within the hostile host environment. Bacteria utilize ATP-binding cassette (ABC) transporters, powered by the energy of ATP hydrolysis, to move substrates across cellular membranes. The substrate-binding protein (SBP) shuttles substrate in the periplasm and directs the substrate specificity of the transport system. The focus of this dissertation is the multifunctional substrate specificity of SBPs at the interface of the host–pathogen interactions that are necessary for nutrient uptake and antimicrobial resistance. Nontypeable *Haemophilus influenzae* (NTHi) is an opportunistic pathogen and has four Cluster C SBPs, nthiHbpA (heme-binding protein), nthiOppA (oligopeptide-binding protein), nthiSapA (sensitivity to antimicrobial peptides) and NTHI0310 (putative peptide-binding protein). Unlike other SBP families, some members of the Cluster C family recognize two distinctly different substrates, their canonical substrates and heme. As a heme auxotroph, NTHi relies on host hemoproteins as a source of the essential nutrient. The work in this thesis identifies the heme specificity of the NTHi Cluster C SBPs, defines their binding affinities for canonical and heme substrates, and uncovers ligand-specific sites in the binding pocket for canonical substrates and heme. These studies provide insight into the overlapping function of these Cluster C SBPs in heme uptake and the multisubstrate binding of their canonical substrates and heme to maintain virulence in the host environment.

ACKNOWLEDGEMENTS

I would like to express my deepest gratitude to my thesis advisor Heather Pinkett for her constant support and insightful advice. This research was made possible by her unlimited enthusiasm, heartfelt encouragement and dedication to her students. Heather's energizing optimism made the everyday failures of science less daunting. She inspired me to come up with new ideas and experiments that helped me push these projects forward.

I would also like to thank my committee, Kelly Mayo, Alfonso Mondragon, and Thomas O'Halloran, for all of their guidance throughout the years. A special thanks to our collaborator Kevin Mason at Nationwide Children's Hospital.

It has been a great pleasure working with my colleagues in the Pinkett Lab. I would particularly like to thank Austin Rice for his invaluable advice during my early days in the lab, and Saemee Song for her honest and engaging discussions.

To my fellow teatime buddies, Clarence Chan and Kasia Soczek, thank you for making the 4th floor of Cook a great place to work. I am grateful for the many friends I have found over the years, Anne d'Aquino, Agustina D'Urso, Patrick Hankins, Adam Hockenberry, and Roli Mandhana Kasat…it was great sharing our time at Northwestern together!

LIST OF ABBREVIATIONS

ABC, ATP-binding cassette

AMP, antimicrobial peptides

ATP, adenosine triphosphate

cBD1, chinchilla β-defensin 1

CD, circular dichroism

CV, column volume

DBD, DNA-binding domain

DdpA, dipeptide-binding protein

Dpp, dipeptide

DppA, dipeptide-binding protein

EDC, 1-ethyl-3-(3-dimethylaminopropyl) carbodiimide hydrochloride

GdnHCl, guanidine hydrochloride

hBD2, human β-defensin 2

hBD3, human β-defensin 3

HbpA, heme-binding protein

HEPES, 4-(2-hydroxyethyl)-1-piperazineethanesulfonic acid

hNP1, human α-defensin 1

IPTG, isopropyl β-D-1-thiogalactopyranoside

kDa, kilodalton

LIC, ligation independent cloning

MCSG, Midwest Center for Structural Genomics

MES, 2-(N-morpholino)ethanesulfonic acid

MppA, murein tripeptide-binding protein

NBD, nucleotide-binding domain

NHS, N-hydroxysuccinimide

Ni-NTA, nickel-nitrilotriacetic acid

NikA, nickel-binding protein

NTHi, nontypeable *Haemophilus influenzae*

OD, optical density

OM, otitis media

Opp, oligopeptide

OppA, oligopeptide-binding protein

PAGE, polyacrylamide gel electrophoresis

PDB, protein data bank

PDR, pleotropic drug resistance

PDRE, pleiotropic drug response elements

PepT, peptide, opine and nickel uptake

RMSD, root-mean-square deviation

RU, response units

Sap, sensitivity to antimicrobial peptide

SapA, sensitivity to antimicrobial peptide-binding protein

SBP, substrate-binding protein

SDS, sodium dodecyl sulfate

SPR, surface plasmon resonance

TAD, transactivation domain

TEV, tobacco etch viral

TMD, transmembrane domain

XBD, xenobiotic-binding domain

ZnPP, zinc protoporphyrin IX

3D, three dimensional

DEDICATION

To my parents, Linda and Ron, and my sister, Dani,

Thank you for all of your love and support along the way.

To Mihai,

Thank you for encouraging me to enjoy this great adventure.

TABLE OF CONTENTS

LIST OF TABLES AND FIGURES

CHAPTER 1:

Selective Substrate Uptake: The Role of ATP-Binding Cassette (ABC) Importers in Pathogenesis*

1.1. Introduction

Bacterial colonization is dependent on the ability to obtain essential nutrients from surrounding environments. Bacteria have evolved to utilize a variety of strategies to acquire the necessary nutrients for homeostasis and pathogenesis. To resist bacterial colonization, a host can increase the antibacterial agents at the site of infection and/or limit the availability of nutrients to bacteria (1). Bacteria respond to host-mediated nutrient deprivation, antibacterial defenses and other stressors, often taking advantage of changes in the host microenvironment associated with disease manifestation, by adapting strategies to overcome the host's immune system. Understanding how bacteria 'sense' and 'respond' to changes in host microenvironments will increase our understanding of the virulence factors that contribute to the pathogen's overall fitness or the ability to cause disease. Bacterial transport proteins are necessary for nutrient uptake and are a major factor in host-pathogen interactions. Mutagenesis studies that target the components of ATP-binding cassette (ABC) transporters have revealed a subset of these transporters play a significant role in the survival and proliferation of pathogens within the host. This chapter summarizes research on a range of ABC importers with a role in virulence and highlights some of the ways researchers are targeting transport proteins to decrease pathogenicity.

1.2. ABC Transporters: Structure and Function

A diverse group of transport proteins maintain a delicate balance of transport activities across cellular membranes. One family of transport proteins, ABC transporters, which consists of both exporters and importers, are conserved from bacteria to humans. Expression and transport activity of ABC transporters are tightly regulated to balance the need for essential nutrients and

the effects of substrate toxicity. ABC exporters are responsible for the transport of diverse substrates such as antibiotics, lipids and proteins. ABC importers transport specific substrates across the membrane into the cytoplasm of bacteria and archaea (2). ABC importers transport a broad range of substrates including sugars, metals, peptides, amino acids, and other metabolites (3). Exporters and importers share the same mechanism of ATP binding and hydrolysis to power the translocation of substrates across the membrane (4).

1.2.1. *Type I, II, and III ATP-Binding Cassette (ABC) Importers*

ABC importers are further divided into three categories; Type I, Type II and Type III transporters (also known as energy-coupling factor (ECF) transporters) (5). This distinction evolved out of the differences in overall architecture and variations in the transport mechanism of each subtype. Type I and II ABC importers utilize a substrate-binding protein (SBP) to deliver substrate to the transporter. The SBP is located in the periplasm of Gram-negative bacteria and is tethered to the cytoplasmic membrane or transporter in Gram-positive bacteria (Figure 1.1) (6). These SBPs recognize and deliver substrates to the cognate ABC transporter. The SBPs are categorized into several clusters based on overall structure of the proteins (7). Despite architectural differences, all SBPs contain at least two domains or lobes with a pocket at the interface for substrate binding.

Type I and II transporters consist of transmembrane domains (TMD) embedded in the lipid bilayer that form the translocation channel and nucleotide-binding domains (NBD) for hydrolyzing ATP. While there are several conserved motifs in the NBDs that play a role in ATP binding, sequence conservation amongst TMDs is low. However, the overall topology between types of ABC transporters seems to be conserved; Type I ABC transporters typically have 6

helices per TMD while Type II have 10-12 helices. TMDs and NBDs dimerize and assemble the minimal unit of an importer, with the SBP as the fifth component of the complex (Figure 1.1) (2). Some importers also contain an accessory domain as part of the NBD, often conferring the ability to regulate transport activity (8). Different from Type I and II importers, ECF transporters consist of four components, which include the substrate-specific binding component (EcfS), transmembrane component (EcfT) and two nucleotide-binding domain components (EcfA and EcfA'). EcfT, EcfA and EcfA' are the conserved components which make up the energizing module, while EcfS is substrate specific (9). The EcfS is embedded in the lipid membrane and binds to substrates, replacing the need for the SBPs present in Type I and II importers (10). The general architecture and assembly of ABC transporters are depicted in Figure 1.1.

1.2.2. *Mechanism of Substrate Transport*

In addition to the unique architecture, the mechanism of transport differs between the classes of importers. While there are variations in the details of the mechanisms of Type I and II transporters, the TMDs rearrange providing alternating access from the one side of the bilayer to the other, allowing for unidirectional transport. Structural studies of ABC transporters in complex with SBPs have revealed how each SBP forms a complex with the TMDs of its cognate transporter to deliver substrate to the translocation pathway. Binding of substrate by the SBP and formation of the transporter complex determines selectivity for substrate transport (for comprehensive reviews on the mechanism and selectivity of ABC transporters see (5,11-13)). Alternatively, the S component of the ECF transporter binds substrate and rearranges position to deliver it across the lipid bilayer (14). In a mechanism unique to Type III transporters, a subclass of ECF transporters bind a number of EcfS components interchangeably (10). These transporters
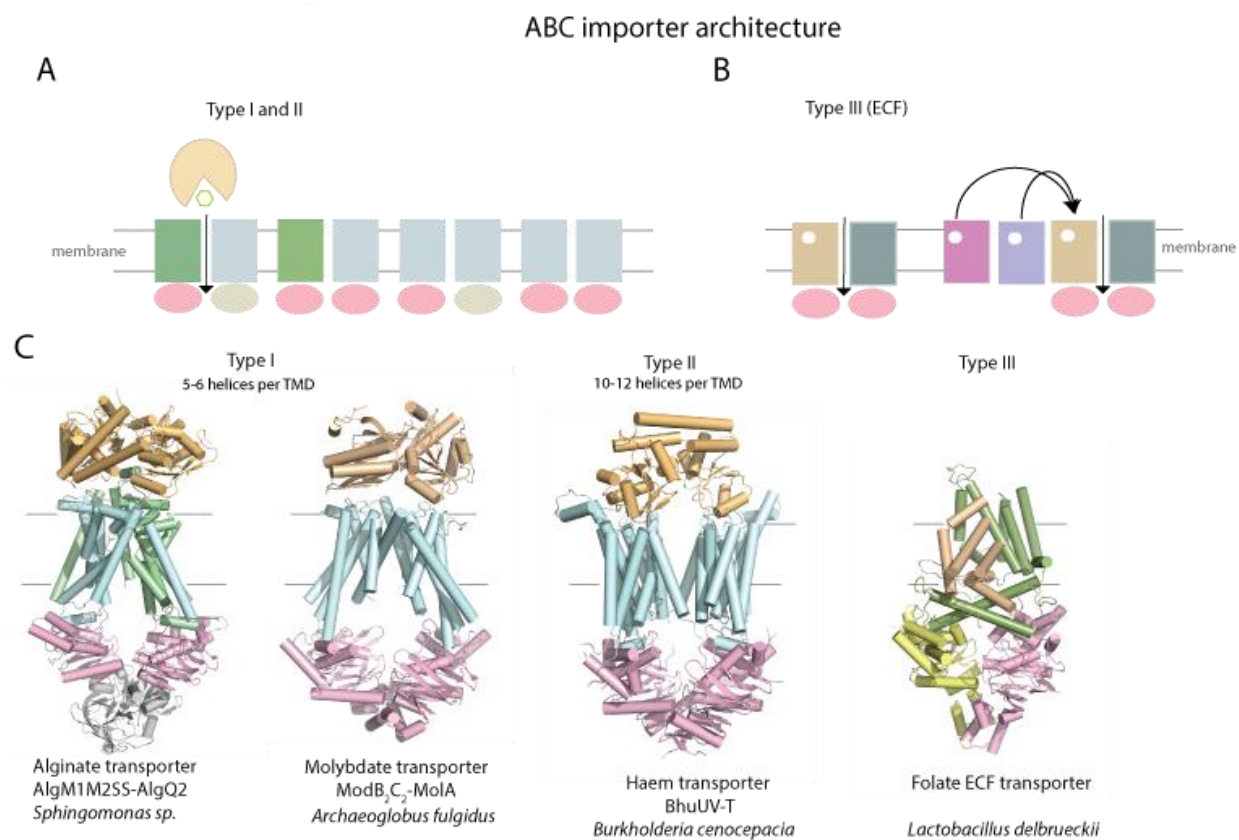
Figure 1.1 Protein architecture and assembly demonstrates diversity of ABC transporters.

(A) ABC transporter assembly for Type I and II importers. The transmembrane domain (TMD), nucleotide binding domain (NBD) and substrate binding protein (SBP) are represented by ovals, rectangles and spheres with an opening for substrate binding, respectively. Importers consist of homo- and heterodimers of TMD and NBD components. (B) For Type III ABC transporters, each transporter is comprised of the energizing module and (EcfT, EcfA, EcfA') and EcfS or multiple EcfS components share an energizing module. (C) Four representative examples of ABC transporters based on the Type I, Type II and Type III classification. Type I Alginate transporter AlgM1M2S$_2$-AlgQ2 from *Sphingomonas sp.* (PDB ID: 4TQU) and Molybdate transporter MolB$_2$C$_2$-ModA from *Archaeoglobus fulgidus* (PDB ID:2ONK). Type II heme transporter BhuU$_2$V$_2$ in complex with SBP, BhuT, from *B. cenocepacia* (PDB ID: 5B58). The

TMDs are colored in light cyan or light green, NBDs in light yellow or light pink and the SBPs are colored light orange. Accessory domains in Type I transporters are colored grey. For the Type III transporter, Folate ECF transporter from *Lactobacillus delbrueckii,* the NBD components are colored in light pink, the S-component in wheat and the T-component in light purple.

are composed of the same EcfT and EcfA and EcfA' modules but utilize different EcfS components depending on which substrate is transported (Figure 1.1) (15).

1.3. ABC Transporters: Nutrient Acquisition and Pathogen Virulence

Nutrient acquisition is essential for all bacteria, commensals and pathogens, to establish colonization in the host. Many importers play an essential role in nutrient delivery; for example, ECF transporters for riboflavin are commonly found in the *Listeria monocytogenes*, *Bacillus subtilis* and *Clostridium difficile* while the Type I zinc importer, ZnuABC is present in *Brucella abortus*, *Yersinia pestis*, *and Proteus mirabilis* (16,17). Pathogenic bacteria can rapidly adapt to changing host microenvironments, particularly those associated with infectious diseases, through nutrient acquisition by select ABC transporters. In this manner, nutrient acquisition is critical for pathogen virulence, or ability to cause disease. The mechanisms of nutrient acquisition then, are key virulence determinants used by pathogens to mediate disease. (16,17). While these essential nutrient acquisition systems are expected to impact virulence of a bacterial pathogen, in many cases there remains a lack of information linking these systems to pathogen virulence, primarily assessed by phenotypic characterization of transporter mutants in animal models of infectious diseases. While many of these key transport systems in pathogens remain to be identified, a few select ABC importers have been shown to be critical to the virulence of bacteria, establishing these proteins as virulence factors (Table 1.1). These virulence factors transport an array of substrates including transition metals, peptides and amino acids. In this chapter, we take a closer look at ABC importers as virulence determinants of pathogenic bacteria, often supported by loss of virulence through genetic deletion of components of essential ABC transporter genes.

Table 1.1. Select ABC transporters that play a role in full virulence.

Substrate	Name	Organism	Transporter composition*
Metal transporters			
Zinc	ZnuABC	B. abortus, S. Typhimurium, C. jejuni, M. catarrhalis, uropathogenic E. coli, A. baumannii, Y. pestis, P. mirabilis	znuA znuC znuB / znuA znuC znuB
Manganese and iron	SitABCD	Avian pathogenic E. coli, APEC O78 strain χ7122, B. henselae	sitA sitB sitC sitB [1, 2]
Manganese and zinc	MntABC	S. Typhimurium, N. gonorrhoea	mntA mntB mntC / mntC mntB mntA
Manganese and zinc	PsaABC	S. pneumoniae	psaB psaC psaA
Nickel and cobalt	CntABCDF (formerly Opp1ABCDEF)	S. aureus	cntF cntD cntC cntB cntA
Amino acid transporter			
Glutamate	GltTM, SBP (NMB1964)	N. meningitides	gltM gltT NMB1966
Glutamine	GlnHPQ	S. Typhimurium, N. gonorrhoeae, Group B Streptococci, S. pneumoniae (spd1098–1099, spd0411–0412)	glnP-H glnQ / glnQ glnP glnH
Alanine	DalS, SBP of putative D-alanine transporter	S. Typhimurium	stm1633 stm1634 stm1635 stm1636
Cysteine	CtaP, SBP of putative oligopeptide transporter	L. monocytogenes	lmo0135 lmo0136 lmo0137
Lysine, Ornithine	SBP1, SBP3, SBPs putative amino acid transporter	M. catarrhalis	mrc1689 lysine mrc1690 ornithine mrc1694 mrc1695 [3]
Methionine	MetNIQ	M. catarrhalis	metQ metI metN
Methionine	MetQNP	S. pneumoniae	sp_0148 metQ metN metP
Peptide transporter			
Peptides	OppABCDF	M. catarrhalis and B. thruingiensis	oppA oppF oppD oppC oppB / oppA oppB oppC oppD oppF
AMPs	SapABCDF	Nontypable H. influenzae and H. ducreyi	sapZ sapF sapD sapC sapB sapA / sapA sapB sapC sapD
AMPs	YejABEF	B. melitensis (BMNI_I0006-BMNI_I00010) and S. Typhimurium	yejA1 yejA2 yejB yejE yejF / yejA yejB yejE yejF

1. Liu MF, Bouhsira E, Boulouis HJ, Biville F: The *Bartonella henselae* SitABCD transporter is required for confronting oxidative stress during cell and flea invasion. Research in Microbiology 2013, 164(8):827-837.

2. Sabri M, Caza M, Proulx J, Lymberopoulos MH, Bree A, Moulin-Schouleur M, Curtiss R, Dozois CM: Contribution of the SitABCD, MntH, and FeoB metal transporters to the virulence of avian pathogenic *Escherichia coli* O78 strain chi 7122. Infection and Immunity 2008, 76(2):601-611.

3. Otsuka T, Kirkham C, Johnson A, Jones MM, Murphy TF: Substrate Binding Protein SBP2 of a Putative ABC Transporter as a Novel Vaccine Antigen of *Moraxella catarrhalis*. Infection and Immunity 2014, 82(8):3503-3512.

4. Caspi R, Billington R, Ferrer L, Foerster H, Fulcher CA, Keseler IM, Kothari A, Krummenacker M, Latendresse M, Mueller LA et al: The MetaCyc database of metabolic pathways and enzymes and the BioCyc collection of pathway/genome databases. Nucleic Acids Research 2016, 44(D1):D471-D480.

∗ Representation from BioCyc Database unless noted (4). Not all gene directions in operon are represented.

1.3.1.   Metal Transporters

All bacteria require essential metals to carry out biological processes. Iron, cobalt, nickel, copper, zinc, and manganese are all trace elements that play a role in a myriad of biological processes, including enzyme cofactors, necessary structural components of proteins, or resistance to oxidative stress (18). To fulfill this need for trace metals, bacteria utilize several metal transport systems that tightly regulate the uptake of metals, allow for expulsion of excess metals to avoid toxicity, and maintain homeostasis. To defend against the invasion of bacteria, mammals have developed ways to restrict the availability of essential metals in the host environment, a process called *nutritional immunity* (19,20). For example, to limit a pathogen's access to iron, the host sequesters nutrients via lactoferrin or transferrin bound iron and hemopexin in complex with heme (21). Bacteria have adapted to iron sequestration by utilizing siderophores and receptors that can bind these host-derived proteins for iron acquisition (22,23). Once acquired, iron and heme substrates are transported into the cytoplasm by a series of transport proteins, such as the TonB-dependent system, symporters, and ABC importers. While the type of transport proteins that are involved in pathogenicity is broad and covered in many comprehensive reviews (19,24,25), we have selected a few metal ABC importers to highlight the role they play in maintaining bacterial virulence.

Zinc is required for the proper folding and stability of proteins in the cell and serves as a catalyst for many enzymes. Even though zinc is an essential nutrient, it also plays a role in the host defense mechanism as high levels of zinc can be toxic to a bacterium (25). In addition to other transport proteins, ZnuABC, a high affinity zinc MZT (Manganese/Zinc/Iron Chelate Uptake) family transporter, contributes to pathogen survival in the infected host. ZnuA, ZnuB and ZnuC encode for the substrate binding protein, the transmembrane domain and the

nucleotide-binding domain, respectively. In *Brucella abortus*, an intracellular pathogen capable of infecting domestic animals and occasionally humans, *znuA* is required for growth in zinc-limited conditions. Loss of ZnuA decreased the ability of *B. abortus* to replicate in RAW 264.7 macrophages and increased clearance in BALB/c mice (26). In *S. enterica* serovar Typhimurium, a *znuA* mutant strain was also less virulent in BALB/c and DBA-2 mice compared to the wildtype strain (27). These data correlate with a previous study of a *S.* Typhimurium *zur (znu* regulatory gene)* and *znuC* knockout (28). A *znuA* mutant knockout in *Campylobacter jejuni* shows that the SBP is essential for colonization of the chick gastrointestinal tract (29). For *Moraxella catarrhalis*, an otitis media (OM) pathogen associated with clinical exacerbation of chronic obstructive pulmonary disease (COPD), *znuABC* is necessary for invasion of human adenocarcinoma epithelial A549 cells and persistence in respiratory tract of BALB/c mice (30).

While *znu* mutations resulted in a marked decrease in virulence in some pathogens, others showed no phenotype with loss of the *znu* system. However, bacterial attenuation was observed when *znu* deletions were combined with other mutations or when mutant strains were coinfected with wildtype strains. In uropathogenic *Escherichia coli* (UPEC), loss of ZnuA and ZupT (ZRT-, IRT-like Protein family) proteins decreased the bacterial load in the murine urinary tract and kidneys in both a single-strain infection and when the mutant was coinfected with the wild type strain (31). In *Y. pestis*, deletion of *irp2*, the Ybt siderophore synthetase, in the *znuABC* mutant background resulted in a significant loss of virulence due to a defect in zinc acquisition (32,33). While the *znuABC* mutant has a severe *in vitro* growth defect, the *irp2 znuABC* mutant is attenuated in the septicemic plague mouse model (32). Further, zinc uptake in *Y. pestis* is a concerted effort between components of the Ybt system, ZnuABC, and possibly a second high-affinity zinc transporter, yet to be identified, which all contribute to virulence (33,34). During

coinfections of *Acinetobacter baumannii*, an opportunistic and nosocomial pathogen, the loss of the TMD strain results in wildtype outcompeting the *znuB* mutant for colonization in lungs and livers of C57BL/6 mice (35). In *Proteus mirabilis,* a common cause of complications in urinary tract infections, the NBD *znuC* mutant strain failed to survive in the bladder and kidneys of CBA/J mice when coinfected with wildtype, indicating that ZnuABC contributes to the fitness of *P. mirabili*s in murine urinary tract infections (36). Co-challenge studies show that ZnuABC is not required to colonize the host but offers a competitive advantage during infections.

The ability to transport manganese into the cell is critical for the detoxification of free radicals and protection against oxidative damage caused by hydrogen peroxide. SitABCD, YfeABCD, PsaABC, and MntABC have all been implicated in manganese transport, and their role in divalent cation transport also places them in the MZT family (37,38). These importers play a role in virulence in *S.* Typhimurium and *Neisseria gonorrhoea* (39). In *N. gonorrhoeae*, a mucosal pathogen often associated with the genitourinary tract, MntABC is the Mn^{2+} and Zn^{2+} transporter. MntC, the SBP, recognizes both substrates with the same binding pocket and has a similar affinity to each substrate, approximately 1 μM (40). Individual mutations of *mntAB* and *mntC* show a significant reduction in invasion of primary cervical epithelial cells, and both mutants are deficient in forming biofilms (40). In *Bartonella henselae*, a bacterium commonly transmitted to humans through a cat flea or cat bite, deletion of the SBP and NBD, *sitA* and *sitB*, decreases the ability for the pathogen to survive in cat fleas. Interestingly, the *B. henselae sitAB* knockout does not impact the invasion of human endothelial cells but has a decreased rate of survival when compared to the control (41).

Iron, in its many forms, is required for essential processes in the bacteria, and iron deficiency can impact nucleotide synthesis, ATP production, and the activity of numerous

critical enzymes (18,42). SitABCD along with other transport proteins, MntH (NRAMP family) and Feo (GTPase), import ferrous iron. In avian pathogenic *E. coli*, APEC O78 strain χ7122, *sitABCD* mutant strain was partially attenuated in its ability to colonize the lungs, livers and spleens of infected chickens and was further attenuated in a coinfection model with wildtype. Loss of both divalent cation transporters, *sitABCD mntH* demonstrated the greatest reduction in bacterial load in the lungs, liver and spleen. Interestingly, the bacterial load of the *sitABCD feo* mutant was lower in the lungs and spleen, but not the liver, suggesting tissue tropism (43). In contrast, MntH and Feo single and double mutants did not reduce bacterial load, suggesting an important role for SitABCD in avian pathogenic *E. coli* colonization. Additionally, *S.* Typhimurium requires both divalent cation transporters, MntH and SitABCD, for full virulence in wildtype *Nramp*^{G169} mice following intraperitoneal infection, with only partial attenuation for each individual mutation (44). Single mutations of *Y. pestis yfeAB* or *mntH* did not show a significant loss in virulence. However, the *yfeAB mntH* double mutant shows a substantial decrease of virulence in the bubonic plague mouse model compared to the parent strain. Furthermore, double mutants were fully avirulent in a mouse model of pneumonic plague (33). It is interesting to note that a *feoB yfeAB* double mutant in *Y. pestis* also results in a decrease of virulence in the bubonic plague mouse model when compared to the parent strain, whereas single mutations did not (45).

For nickel and copper, studies indicate the ability to properly regulate the transport of these metals is important for the survival of bacterial pathogens (1). Copper is a common cofactor for oxidases and plays a role in the formation of reactive oxygen species (ROS) (25). However, due to copper toxicity and antibacterial properties (46,47), bacteria utilize a number of mechanisms, including copper exporters, to transport copper out of the cytoplasm where it is detoxified or

released into the extracellular space (1,48,49). Nickel is a common cofactor of many enzymes, including urease, an enzyme that hydrolyzes urea into ammonia and carbamate, and is important for maintaining a neutral cytosolic pH (50). Nickel uptake has been shown to be essential for colonization of pathogens, including *S. aureus* and the human gastric pathogen *Helicobacter pylori* (51). Nickel import is controlled by several uptake systems, including a member of the Peptide, Opine and Nickel Uptake (PepT) transporter family, CntABCDF, and a recently discovered nickel transporter, NiuBDE. Recent work has identified gastric *Helicobacter* species that have acquired nickel transporter genes through horizontal gene transfer (52). Whereas NiuBDE and NixA function independently to transport nickel, both transporters participate in nickel-dependent urease activation at pH 5 and promote survival of *H. pylori* in the acidic environment of the stomach. However, only NiuBDE transports transport nickel for urease activation at neutral pH and is essential for colonization of the mouse stomach suggesting preferential transport of nickel with changing microenvironments (52). *S. aureus* CntABCDF, originally annotated as *opp1*, is a cobalt and nickel transporter that impacts urease activity and bacterial colonization in the systemic and urinary tract infection models. BALB/c mice infected with the *cnt* operon deletion strain were twice as likely to survive compared to infection with wildtype, and in the urinary tract infection mouse model, bacterial load of kidneys and bladders was lower for the *cnt* mutant strain (53).

1.3.2. *Amino Acid Transporters*

With limited resources, pathogenic bacteria, such as *S. aureus* and *Salmonella,* rely on numerous host amino acids and require multiple amino acid transporters to fulfill their metabolic requirements for growth, persistence, and virulence (54,55). Since amino acids are essential

nutrient sources for carbon and nitrogen, as well as, recycling amino acids for protein synthesis in bacteria, they are central to the host–pathogen metabolic interaction. Amino acids also play a role in cellular responses of pathogens. Increased levels of asparagine in the host induces expression of bacterial virulence genes during *Streptococcus pyogenes* infection (56). *Francisella tularensis* and *Mycobacterium tuberculosis* require *de novo* tryptophan synthesis to circumvent the depletion of host tryptophan as a result of the active T cell response (56). *Chlamydia trachomatis* evades host nitric oxide production by limiting arginine, which deprives nitric oxide radicals (iNOS) of substrate (57). For euedaphic human pathogenic bacteria, such as *Bacillus anthracis* and *L. monocytogenes*, ammonia is the primary nitrogen source in the non-host environment (58); in contrast, L-glutamine and L-glutamate are widely available nitrogen source in the host environment (59). Additionally, the host increases L-glutamine levels to activate immune defenses, which is necessary to maintain function of lymphocytes and macrophages (60). Nutrient uptake by amino acids transporters is important for bacterial survival, and many of these transporters have been identified as virulence factors utilized by pathogens during successful infection.

L-glutamate, an essential amino acid for bacterial growth and intermediate product for ammonium assimilation, is a precursor for the synthesis of the antioxidant glutathione (61,62). *Neisseria meningitides*, an exclusively human pathogen, requires glutamate for growth *in vitro* and the intracellular milieu (63). Specifically, the SBP GltM (*NMB1964*) and the TMD GltT (*NMB1965*) of the meningococcal L-glutamate ABC transporter, a homolog of phospholipid-uptake MlaBDEF transporter in *E. coli*, imports glutamate under low Na^+ conditions (64,65). This transporter is essential for survival during infection of epithelial cells and resistance to neutrophil oxidative burst (65-67). The null *N. meningitidis ΔgltT ΔgltM* mutant was defective in

the internalization into human umbilical vein endothelial cells and the human adenocarcinoma epithelial A549 cells (68). A recent study showed GltT-GltM is necessary for glutamate uptake, which is used to produce glutathione, for increased meningococcal survival during infection of human brain microvascular endothelial cells (69).

Like glutamate, L-glutamine also serves as the primary nitrogen source of pathogenic bacteria (70). The glutamine GlnHPQ transporter is a member of the Polar Amino Acid Uptake Transporter (PAAT) family. GlnH, the SBP, is found in the periplasm in Gram-negative bacteria, and *E. coli* GlnH has an affinity of 0.3 μM for glutamine (71). GlnHPQ in combination with glutamine synthetase, glnA, is required for virulence of *S.* Typhimurium. Double mutants of the glutamine synthetase and the SBP or the NBD, *ΔglnA ΔglnH* or *ΔglnA ΔglnQ*, resulted in a 10^4-fold decrease in competitive growth of the mutant strains and attenuated growth in mice compared to the wildtype strain (72). The glutamine ABC transporter is required for virulence of Group B streptococci. Group B streptococci can cause sepsis in newborns and adults with chronic conditions, such as, diabetes or liver disease and *Streptococcus pneumoniae*, an opportunistic pathogen in the human respiratory tract, causes ear and sinus infections, pneumonia, and meningitis (73). In Gram-positive *S. pneumoniae*, deletion mutants of the fused TMD and SBP, GlnP_H and the NBD, GlnQ, showed significant attenuation in the ability to cause pneumonia and septicemia in a mouse infection model (74). When the macrophage-like cell line J774A.1 was infected with *gln* mutants, the number of internalized and viable pneumococci was significantly lower than wildtype. These phagocytosis studies suggest the Gln uptake system might play a role in resistance to oxidative stress during host infection (74). In Group B streptococci, a *ΔglnQ* mutant shows decreased fibronectin adherence, lower invasion of human adenocarcinoma epithelial A549 cells *in vitro*, and decreased virulence in neonatal rats

(75). Inactivation of *L. monocytogenes glnPQ* abolished glutamine uptake, lowered the response of type I interferon in infected bone marrow-derived macrophages, and down-regulated transcription of virulence factors, such as, *hly*, *plcA*, *plcB*, and *actA* (76). Liver and spleen colonization of C57BL/6 mice intravenously injected with the *ΔglnPQ* mutant was reduced compared to the wildtype strain, leading to a 30-fold and a 10-fold decrease in bacterial load of the liver and spleen, respectively (76).

As precursors for membrane fatty acids, BCAAs are key co-regulators of growth and virulence of pathogenic bacteria. Interestingly, the *livHMGF* BCAA transporter, a member of the Hydrophobic Amino Acid Uptake Transporter (HAAT) family, has two SBPs. The leucine/isoleucine/valine (LIV) SBP, also known as LivJ, has been co-crystallized bound to isoleucine, leucine and valine with dissociation constants of 0.4, 0.4, and 0.7 μM, respectively (77,78). Additionally, LivJ weakly interacts with alanine, serine, threonine and phenylalanine (79,80). LivK, known as the leucine-specific (LS) SBP, recognizes leucine with a binding affinity of 0.4 μM and surprisingly, phenylalanine with an affinity of 0.18 μM (81). The structure of LivK bound to leucine and phenalanine identified residues in the binding pocket responsible for determining substrate specificity for the bulkier hydrophobic amino acids in comparison to LivJ (82). Interestingly, the *ΔlivHMGF* mutant has decreased virulence in disease models dependent upon serotype-specific phenotypes. Loss of *livHMGF* in *S. pneumoniae* serotype 4 strain TIGR4 leads to lower virulence in the pneumoniae mouse model, a modest decrease in virulence in the systemic model, which is not statistically significant, and no difference in the nasopharyngeal infection model. However, in the *S. pneumoniae* serotype 3 clinical isolate 0100993, the *ΔlivHMGF* mutant is attenuated in the pneumoniae and systemic model (83).

The ability to bind and import amino acids is important for bacteria to establish infection.

In many cases, loss of substrate binding proteins (SBPs) of amino acid uptake ABC transporters attenuates infection. Recently, Murphy *et al*. demonstrated that deletion of several amino acid SBPs in *M. catarrhalis*, including the lysine and ornithine transporters, showed a reduced ability to invade human adenocarcinoma epithelial A549 cells (84). In the Gram-positive human pathogen, *L. monocytogenes*, the SBP of cysteine transporter, CtaP, was shown to contribute to virulence in a murine model of intravenous infection. The *ΔctaP* deletion mutant had increased membrane permeability and acid sensitivity, reduced bacterial adherence to host cells, and lower colonization of the gastrointestinal tract of mice (85).

Expression of DalS, the SBP of D-alanine ABC transporter (*STM1633-STM1636*) in *S.* Typhimurium, limits exposure to oxidative damage elicited by D-amino acid oxidase (DAO) in neutrophils. The *ΔdalS* mutant was more susceptible to DAO-dependent killing during host infection (86). In addition, the *ΔdalS* strain showed decreased replication in the RAW 264.7 macrophage cells compared to the wildtype strain. The mean survival time of C57BL/6 mice orally infected with wildtype *S.* Typhimurium was a day shorter than mice infected with *ΔdalS* deletion mutant (87).

MetQ is the SBP of the methionine-uptake MetQNP ABC transporter in *S. pneumoniae*, and is another serotype-specific virulence factor (88). Coinfection of wildtype and *ΔmetQ* strains of *S. pneumoniae* serotype 3 clinical isolate 0100993 showed attenuated colonization of the *metQ* mutant in the nasopharynx and spleens of CD1 mice (83). However, for single-strain infections, virulence of the *ΔmetQ* mutant in CD1 mice was unchanged compared to wildtype in the *S. pneumoniae* serotype 3 strain (89). In contrast, bioluminescent imaging in real-time showed a *ΔmetQ* mutation in *S. pneumoniae* serotype 2 strain D39 showed significantly attenuated virulence in an acute pneumonia mouse model (90). Similarly, *metQ* of the methionine MetNIQ

transporter plays no role in epithelial cell invasion of *M. catarrhalis*, but facilitates persistence in the murine lungs (84).

1.3.3. *Peptide Transporters*

Small peptides are transported by the PepT sub-family of ABC importers. This subset is classified by structure and sequence identity and includes well-characterized peptide transporters, *dppABCDF*, *oppABCDF*, and *sapABCDF*. Interestingly, as mentioned above the PepT family also includes *nikABCDF* and *CntABCDF*, which are not known to import peptides, but share the overall structural similarity to the peptide transporters in this family (91). Peptide transporters are necessary for the import of peptides derived from host proteins, like hemoglobin and proteasomal degraded proteins (92,93) as a source of nutrients, and for importing environmental cues for cellular functions, such as, chemotaxis, conjugation, and sporulation (94-96). The dipeptide transporter, *dppABCDF* (97), has been implicated in virulence, but only the *oppABCDF, sapABCDF and yejABEF* systems are directly identified as virulence factors (98-100).

In addition to their role in metabolic activity, the *sap* and *yej* systems recognize antimicrobial peptides (AMPs) produced by the host innate immune system. A wide range of organisms, including eukaryotes, plants, and bacteria, produce AMPs (101). During infection by pathogenic bacteria, host epithelial cells up-regulate the expression of AMPs and recruit AMP-secreting cells to the infection site, such as macrophages or neutrophils. Peptide ABC transporters recognize small cationic AMPs, including α-defensins, β-defensins, cathelicidins, and polymyxins. The role of ABC transporters in peptide uptake and AMP resistance is vital for pathogen survival and replication in the hostile host environment.

Bacteria scavenge peptides from the environment, which provide a source of carbon, nitrogen, and/or amino acids, during homeostasis and pathogenesis. *Lactococcus lactis* OppA, the SBP of the *opp* system, binds peptides from 4aa up to 35aa long (102). Structural and functional studies indicate that OppA from *L. lactis* can bind peptides of varying length 5, 8, 9, 12 and 20aa, with an affinity range from 0.1-100μM, with the highest affinity for 9aa peptides (103). *M. catarrhalis oppA* is necessary for invasion of human adenocarcinoma epithelial A549 cells (84). Pulmonary clearance of the Δ*oppA* mutant strain of *M. catarrhalis* was increased compared to the parent strain in the mouse model (104). Deletion of *oppB*, the TMD, in *Bacillus thuringiensis*, which is closely related to the pathogen causing food-borne gastroenteritis *Bacillus cereus*, significantly reduced the mortality rate of *Galleria mellonella* insect larvae by *B. thruingiensis* spores (105). The *opp* system is linked to the up-regulation of other virulence-associated genes, such as, *speB*, for cell adhesion and *plcR*, a virulence regulator (105,106). However, the *opp*-transported peptide and the signal transduction pathway to induce virulence genes are still unknown.

The *sapABCDF* system is a key virulence factor of AMP resistance, *in vivo* colonization, and persistent survival in the host environment. The AMP resistance of the *sap* operon was first described in *S.* Typhimurium and *Dickeya dadantii* (previously known as, *Erwinia chrysanthemi*) (107,108). Nontypeable *Haemophilus influenzae* (NTHi), the causative agent of middle ear infection, has increased *sap* promoter activity during colonization of the chinchilla model of OM (109). SapA, the SBP, is thought to be specific for AMPs with positive charges, including cathelicidin, melittin, and defensins (110). Although the structure of SapA bound to AMPs has not been solved, deletion of *sapA* increases sensitivity of NTHi to chinchilla β-defensin 1 (cBD1) (109). Loss of *sapA* also leads to a decrease in human bronchial epithelial cell

and chinchilla middle ear epithelial cell adhesion of NTHi (111). Virulence of NTHi was attenuated in the chinchilla middle ear and nasopharynx by the Δ*sapA* mutant (109). Importantly, humans infected with a Δ*sapA* mutant of *Haemophilus ducreyi*, a causative agent of the sexually transmitted infection that causes skin ulcers, formed pustules at half the rate of the parent strain (112). The TMDs of the sap operon have also been proven to play a role in virulence in these pathogens. AMPs are translocated across the cellular membrane via the TMDs. The permease-deficient Δ*sapBC* strain exposed to sub-lethal concentrations of human cathelicidin (hLL-37) and human β-defensin 3 (hBD3) showed localization and accumulation of the AMPs in the periplasm and on the NTHi lipid membranes (113). While the *sap* operon in *H. ducreyi* has not been linked to defensin resistance, *sapB* and *sapC* are necessary for hLL-37 resistance and virulence in the host. The *sapBC* mutant had decreased pustule formation in human volunteers even at dose 10-fold higher that the parent strain, and resulted in the full attenuation of *H. ducreyi* virulence (114). Additionally, *sapD* is associated with potassium homeostasis, and deletion of the NBD attenuated survival of NTHi in the chinchilla model (115).

YejABEF confers resistance to cationic and cyclic AMPs, such as melittin, protamine, polymyxin B, and β-defensins (116). In murine macrophage cells, a microarray showed that *S.* Typhimurium *yejB*, *yejE* and *yejF* are induced at least 2-fold during infection (100). Additionally, expression of *yej* genes increased when *Brucella melitensis*, which can be transmitted to humans by the stable fly from farm animals, was treated with polymyxin B (117). Deletion of the TMD, Δ*yejE*, or the entire operon, Δ*yejABEF*, in *B. melitensis* display decreased ability to invade and replicate in activated macrophages. These mutants had a bacterial load four orders of magnitude lower than the parent strain by the end of the incubation period (117). *S.* Typhimurium Δ*yejF*, the NBD, also had attenuated replication in hBD3 and human β-defensin 4

(hBD4) expressing intestine 407 cells, human β-defensin 2 (hBD2) expressing HeLa cells, and human β-defensin 1 (hBD1) and hBD2 expressing Caco-2 cells (116). The attenuated growth of *B. melitensis* and *S.* Typhimurium mutants in mouse Peyer's patches, liver and spleen demonstrate the role of the *yej* transporter in bacterial survival during infection (116,117). While the structure and substrate selectivity of *yejA* is not as well characterized as other peptide SBPs, the *yej* system is essential for AMP resistance and bacterial virulence.

1.4. Targeting Pathogenesis: Advances and Therapeutic Approaches

Bacterial pathogens are a significant threat to human health, and the continued emergence of antimicrobial resistance has only amplified this danger. The mechanisms utilized by bacteria to acquire essential nutrients within the host and the nutrient sequestration of the immune response during infection can be capitalized upon to thwart the colonization of bacteria. Understanding the structure of ABC importers, defining the specificity of substrate translocation, and deciphering how these transporters fit into the overall survival mechanism of an organism has led to interesting approaches to combating these diseases.

1.4.1. Substrate Mimics

ABC importers act as a natural gateway into the cell. Antibiotics that mimic transporter substrates can exploit these uptake pathways in a 'Trojan horse' mechanism. Bacteriocins are natural antibiotics produced by bacteria to give them a competitive advantage over their neighbors. These antibiotics mimic essential nutrients, such as iron-siderophore complexes or peptides, and are imported to the cell by ABC transporters (118). A peptidyl nucleoside antibiotic, pacidamycin, is imported by the *nppA1A2BCD* system and inhibits translocase I,

MraY, in *Pseudomonas aeruginosa* (119,120). The *E. coli yejABEF* system imports microcin C, a peptide-nucleotide antibiotic, which blocks the synthesis of tRNA^{asp} (121). The SBP of *E. coli* an iron-siderophore transporter, FhuD, binds a siderophore-antibiotic conjugate that inhibits seryl-tRNA synthetase known as albomycin (Figure 1.2B) (122). ABC importers also play a role in the uptake of synthetic antibiotics. The dipeptide transporter, *dppABCDF*, imports orthine carbamoyltransferase inhibitor phaseolotoxin and translation initiation inhibitor kasugamycin (123,124). Additionally, kasugamycin and translation termination inhibitor blasticidin are imported via the *oppABCDF* system in *E. coli* (124).

1.4.2. Inhibition of Substrate Binding

Inhibitors that specifically target the SBPs of ABC transporters have also proven to be successful drug candidates. *S.* Typhimurium ZnuABC is one on such example. Two zinc-binding compounds, RDS50 and RDS51, were shown to inhibit *S.* Typhimurium ATCC14028 growth and decreased pathogen invasion of intestinal epithelial Caco-2 cells. The crystal structure of the RDS51-Zn(II)-ZnuA complex reveals that RDS51 (1-[(2-chlorophenyl)methyl]-4-phenyl-1H-pyrrol-3-hydroxamic acid) binds near the zinc-binding site of the SBP (Figure 1.2D). RDS51 bridges the globular domains by forming hydrophobic contacts with residues on both sides of the binding pocket and coordinates with the zinc ion, either disrupting ZnuABC complex formation or preventing the release of zinc (125).

1.4.3. Vaccine Targets

Vaccines are an alternative approach to antibiotics, and production of antibodies against the SBPs has proven to be a promising therapeutic. SBP *OppA*-immunized mice challenged with
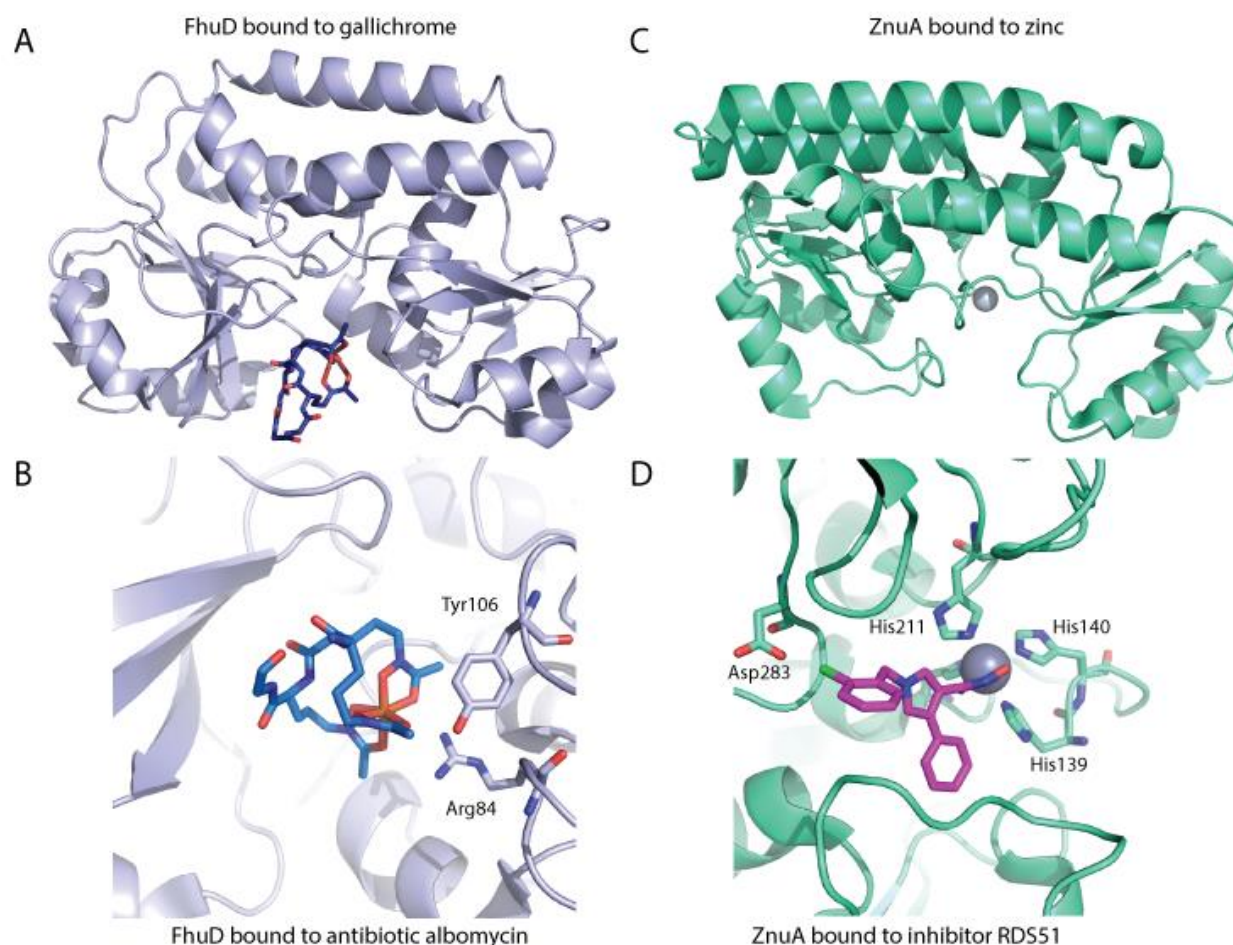
Figure 1.2. Substrate mimics that target ABC importer substrate binding proteins are promising targets for current therapies. (A) Crystal structure of FhuD bound to gallichrome, a ferrichrome analog (PDB ID:1EFD), and (B) antibiotic albomycin (PDB:1K7S). Substrates, gallichrome and albomycin, are dark blue and blue, respectively. (C) Crystal structure of ZnuA bound to zinc (PDB ID:4BBP, shown as grey sphere) and (D) zinc and inhibitor RDS51 complex (PDB ID:4BBP, shown as grey sphere and magenta sticks, respectively). For panels B and D, residues involved in inhibitor binding are labeled and shown as sticks.

Y. pestis had an increased survival time in comparison to the control group (126). Additionally, mice immunized with OppA had a significant reduction of *M. catarrhalis* colonies in the pulmonary clearance model (127). Further work is needed to elucidate the mechanism of *oppA* virulence and how *OppA*-raised antibodies protect against bacterial infection. A co-immunization study of *S. pneumoniae*, PiuA and PiaA, showed using the two iron SBPs antigens produced additive protection in mice (128). Mechanistic studies explained how anti-PiaA and anti-PiuA polyclonal rabbit antibodies did not inhibit growth of *S. pneumoniae* in iron-restricted conditions, indicating these antibodies protect mice against *S. pneumoniae* infection by promoting opsonophagocytosis, not restricting iron transport by the SBPs (129). Immunization with recombinant manganese SBP, MntC, elicits an anti-MntC IgG response capable of protecting mice against *S. aureus* (130). Structural and functional studies revealed the mechanism for MntC-induced immune protection. The MntC monoclonal antibodies interact with each of the globular lobes of MntC, including the binding pocket, potentially blocking the SBP-TMD interface and manganese binding (Figure 1.3) (131). In addition, a *S. aureus* vaccine that incorporates multiple antigens that target different virulence mechanisms, including MntC, has been successful in clinical trials (132).

1.5. Thesis Summary and Objective

There are many factors that influence bacterial survival and virulence within the host. As highlighted in Chapter 1, many bacteria colonize different tissues with a range of efficiencies, reflecting tissue tropism. Pathogens encounter a hostile host environment *in vivo* (e.g. fluctuations in pH, oxidative stress, toxins, nutrient sequestration, and microbiota); therefore, changing microenvironments may impact the ability of the bacteria to acquire necessary nutrients

3A MntC bound to manganese

3B

MntC bound to zinc and monoclonal antibody
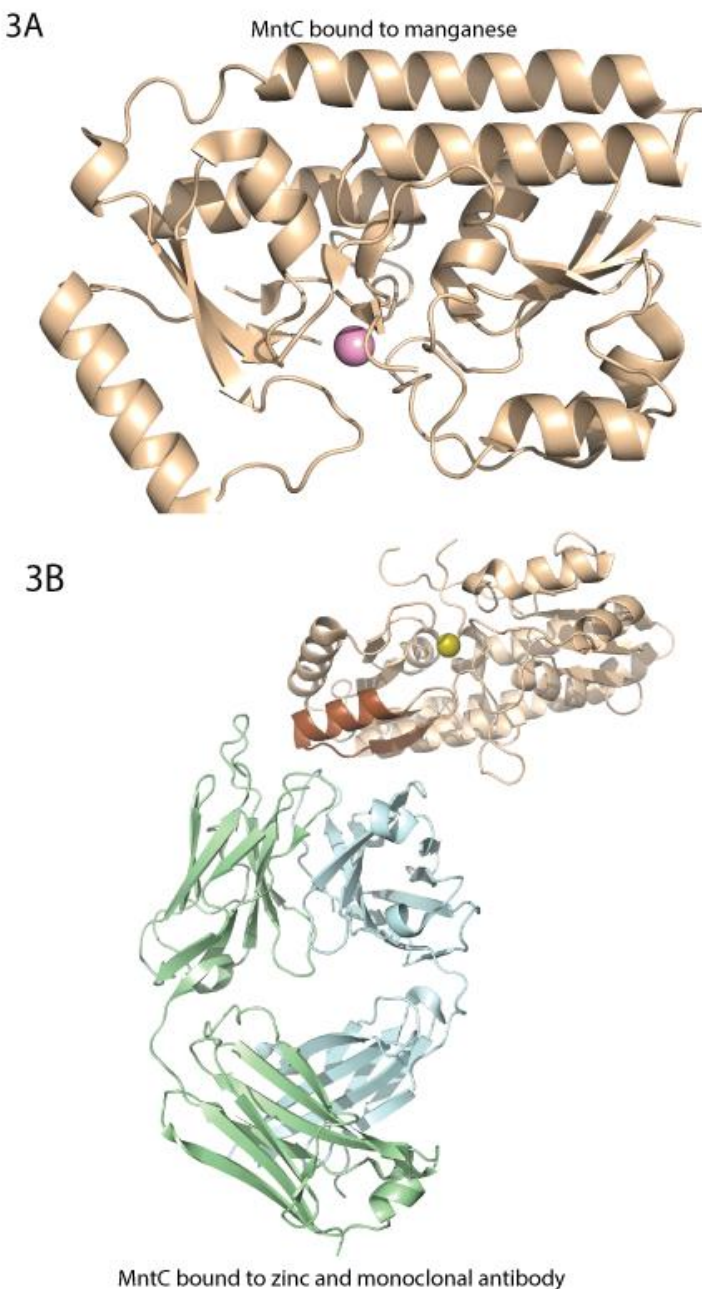
Figure 1.3. Anti-SBP antibodies have proven successful vaccine candidates. (A) Cartoon of crystal structure of MntC bound to manganese (PDB ID: 4K3V, shown as pink sphere) and (B) MntC with Fab fragment for antibody mAB 305-78-7 and iron (PDB ID:5HDQ). The Fab fragments heavy chain is colored in cyan while the light chain in light green. The residues implicated in antibody binding are colored brown.

for virulence. ABC transporters are pivotal for the transport of numerous diverse and essential substrates. For many of the transport systems covered in Chapter 1, loss of substrate delivery by the SBP affects microbial virulence. Recognition of the substrate by the SBP is the first step in substrate selectivity and is critical to microbial fitness in host microenvironments.

The work in this thesis focuses on substrate specificity and affinity of multifunctional SBPs that are necessary for nutrient uptake and antimicrobial resistance. This project focused on the four Cluster C SBPs from NTHi, nthiHbpA, nthiOppA, nthiSapA and NTHI0310. NTHi is a widespread Gram-negative commensal that colonizes the human nasopharynx. As an opportunistic pathogen, NTHi is one of the principal bacteria isolated from the middle ear during OM infections (133). NTHi infections can also exacerbate other upper and lower respiratory tract diseases and induce complications for patients with chronic obstructive pulmonary disease and cystic fibrosis (134-136). OM has a high spontaneous rate of recovery, but can also lead to complications like chronic OM, recurrent acute OM, OM with effusion and other respiratory diseases, such as acute sinusitis and pneumonia (137).

OM is the leading cause of antibiotic prescriptions for children in the US, even though antibiotic therapy has only modest benefits while increasing the risk of adverse drug side effects and antibiotic resistance (138). There is a vaccine to protect against *H. influenzae* infections. However, the Hib vaccine is only effective against preventing infections caused by *H. influenzae* serotype b and does not provide protection against unencapsulated NTHi. NTHi adapts to its changing microenvironments and defends against the host's immune response by overcoming nutrient restriction, mitigation of oxidative stress, sequestration of antibodies, inhibition of chemotaxis, and resistance to AMPs (139-141).

To circumvent host-mediated defenses, NTHi manages a complex network of transport

proteins to scavenge heme from the host environment. In Chapter 2, we probe the heme specificity and binding affinity of all four NTHi Cluster C SBPs using surface plasmon resonance (SPR). Surprisingly, I discovered shared heme specificity among all NTHi SBPs as well as for six *E. coli* Cluster C SBPs and observed the heme binding affinity of these proteins, nthiOppA < nthiHbpA < NTHI0310 < nthiSapA, ranged from about 200 nM to 1 μM. The functional overlap of these four Cluster C SBPs is advantageous for NTHi to maintain access to heme in the host environment.

In Chapter 3, we explore the multisubstrate specificity of nthiOppA for heme and peptides. The crystal structure of nthiOppA bound to a novel hexapeptide features a flexible substrate-binding pocket to accommodate the larger peptide. Heme binding of nthiOppA was modeled with ligand-docking studies and predicted a heme-specific cleft in the binding pocket. Using SPR competition assays, I uncovered peptide binding of nthiOppA can disrupt heme binding but does not completely abolish it. This led to the discovery that individual nthiOppA domains play differential roles in substrate binding, one domain drives heme binding and the other directs peptide binding. NthiOppA accommodates heme and peptide in ligand-specific sites of the binding cavity for its mutltifunctional role in nutrient uptake.

The Sap transport system is at the interface of two pathways essential for NTHi survival, nutrient acquisition and resistance to AMPs. In Chapter 4, we examine the AMP binding affinity of nthiSapA. NthiSapA mediates defensin AMPs hNP1, hBD2, and hBD3 antimicrobial activity against NTHi. Using SPR, I observed nthiSapA has a high binding affinity for these defensin AMPs. NthiSapA maintained the same high binding affinity for simplified AMP fragments that contained only the loop regions of hNP1, hBD2 and hBD3. I also discovered peptide binding was independent of the loop structure of these AMP fragments. The high AMP binding affinity

suggests nthiSapA prioritizes substrate binding to prevent NTHi sensitivity to defensins.

Chapter 5 summarizes the work presented in this thesis and highlights future directions for this project. Here, I consider the interplay between transport systems with overlapping function for bacteria to maintain access to essential nutrients in the host. We also examine the possible role of multifunctional substrate binding in complex formation and the regulation of these transport systems. The conclusion addresses the ultimate goal of this work, how SBPs and their cognate transporters can be used to improve the design of targeted therapeutics.

CHAPTER 2:

Heme Affinity of Nontypeable *Haemophilus influenzae* (NTHi) Cluster C Substrate-

Binding Proteins*

2.1. Introduction

2.1.1. *Heme Acquisition: Hemophores, Outer Membrane Receptors, ABC Importers and Degradation in NTHi*

Iron is an essential nutrient for bacteria that acts as a redox cofactor in cellular machinery of key processes, including respiration and metabolism. Heme is the most abundant source of iron in the human host, most of which is found in hemoprotein complexes such as hemoglobin, haptoglobin, myoglobin, serum albumin and hemopexin. The limited bioavailability of heme leads bacteria to compete with the host for resources using a complex network of heme acquisition and utilization proteins. Many bacteria supplement the heme uptake pathway with their own biosynthetic pathway for heme production. However, NTHi lacks the necessary enzymes to synthesize heme and must rely on host hemoproteins as a source of the essential nutrient for aerobic respiration (142,143).

To circumvent host-mediated nutrient restriction, NTHi has developed a network of proteins with overlapping function for heme acquisition and utilization. The NTHi pathway (Figure 2.1A) employs outer membrane receptors (*hup*, *hgpA*, *hgpB, hgpC, hxuC*, and *hemR*) to bind rarely available free heme, strip hemoproteins of their substrates, and capture heme-binding siderophores (144-148). Each outer membrane receptor recognizes a unique combination of host hemoproteins or free heme for utilization in the uptake pathway. In the case of HxuC, the key nutrient is also delivered by a hemophore, HxuA (149). Most heme receptors are powered by the TonB/ExbB/ExbD complex, anchored in the inner membrane, spanning the periplasm to harness the energy of the bacteria's proton motive force to transport heme across the outer membrane.

Once in the periplasm, heme is shuttled to ATP-binding cassette (ABC) transporters in the inner membrane. Members of the PepT subfamily of ABC transporters play a role in the heme
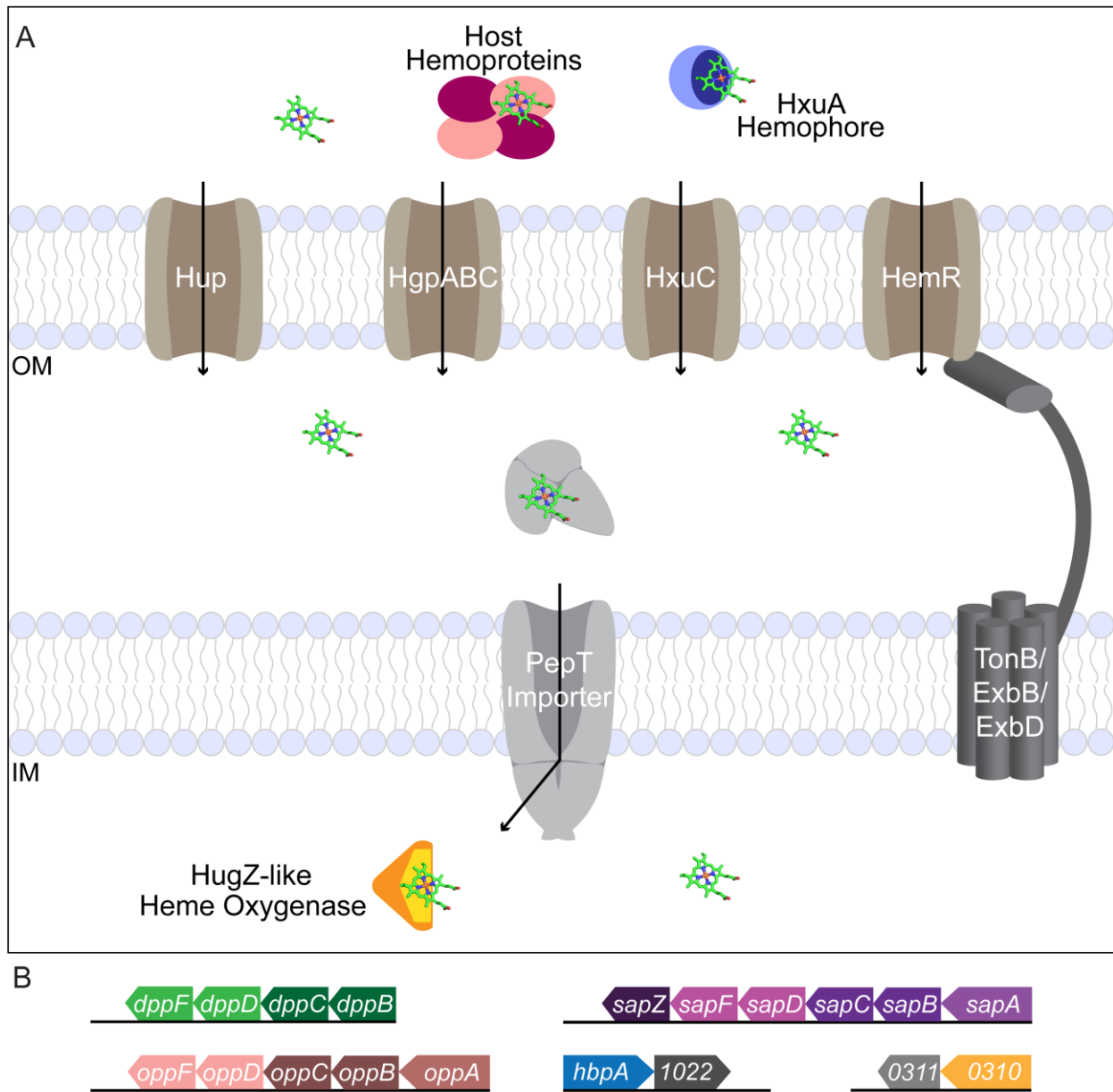
Figure 2.1. Multiple outer membrane receptors and ABC transporters mediate heme uptake in NTHi. (A) The human host has many heme reservoirs targeted by NTHi for nutrient scavenging. NTHi has many heme outer membrane receptors to scavenge the essential nutrient from the host environment. The TonB/ExbB/ExbD complex provides energy to the outer membrane receptors to transport the heme across the membrane. ABC transporters in the inner

membrane import heme into the cytoplasm. Heme is then targeted to cytoplasmic hemoproteins or heme oxygenase for degradation (adapted from Faraldo-Gomez, 2003) (150). (B) The gene clusters of NTHi Cluster C SBPs and PepT importers. The *opp* and *sap* operons contain the SBP, two TMDs and two NBDs. The *dpp* operon includes the TMDs and NBDs without the corresponding *dppA* SBP. The remaining gene clusters include the orphan SBPs, *hbpA* and *NTHI0310*.

uptake pathway (151). NTHi has three ABC transporters in the PepT family, gene clusters *dpp* (dipeptide), *opp* (oligopeptide), and *sap* (sensitivity to antimicrobial peptides) (Figure 2.1B). *In vivo* studies have demonstrated the Dpp and Sap importers are important for heme uptake. Deletion of components in the *dpp* or *sap* operons reduced the ability of the bacteria to utilize heme and recover after heme-iron starvation, respectively (110,152-154). Dpp and Sap transporters are essential parts of the NTHi heme uptake network. To date, the role of the Opp importer in heme uptake has not yet been explored.

In the cytoplasm, free heme promotes lipid peroxidation and produces reactive oxygen species, which results in apoptosis (155). Heme-trafficking and heme-sequestering proteins promote the storage of heme and regulate heme utilization to protect against free heme toxicity. Hemoproteins are necessary for electron transport, preventing oxidative stress, gas sensing, and oxygen transport. In addition to acting as a cofactor, heme can be degraded by heme oxygenase to produce iron for essential cellular processes including iron-sulfur formation and enzyme catalysis (156). Putative heme iron utilization protein from the *hbpA* gene cluster, *NTHI1022*, shares 46% sequence identity to *H. pylori* HugZ, a heme oxygenase (157).

2.1.2. *Cluster C Substrate-Binding Proteins (SBPs) in the Periplasmic Space*

Bacterial ABC importers require SBPs to acquire substrate in the periplasm and deliver it to the transporter. SBPs are defined by their substrate specificity and grouped into classes based on structural conservation, Clusters A-F (3). Substrates of the Cluster A SBPs are generally metal ions or chelated-metal molecules, and SBPs in the Cluster C family shuttle a wide range of substrates from nickel ions to AMPs. SBPs from both of these families are known to play a role in heme uptake. *H. influenzae* heme-binding protein (HbpA), a member of the Cluster C family,

was the first SBP identified to bind heme (158). Additional heme SBPs are found in the Cluster A (Iron Chelate Uptake Transport, FeCT) family, including *Yersinia enterocolitica* HemT, *Y. pestis* HmuT, *Shigella dysenteriae* ShuT, *Bordetella pertussis* BhuT and *P. aeruginosa* PhuT, but homologs of these Cluster A SBPs have not been identified in the NTHi genome.

There are four SBPs from the Cluster C family in the NTHi genome, *hbpA*, *oppA*, *sapA*, and *NTHI0310* (Figure 2.2). Each of the SBPs have specificity for a distinctive canonical substrate. NthiHbpA (also known as GbpA) mediates import of glutathione, nthiOppA transports a broad range of peptides and nthiSapA shuttles AMPs (154,159,160). The predicted topology and high sequence similarities to Cluster C SBPs led us to identify NTHI0310 as a member of this family. This putative peptide-binding protein shares the highest sequence identity with nthiOppA (Table 2.2), but its canonical substrate specificity has yet to be discovered.

With more Cluster C SBPs than PepT transporter gene clusters in NTHi, orphan SBPs have versatility in complex assembly within this family and share importers for substrate uptake. NTHi lacks the gene encoding *dppA*, and nthiHbpA (55% sequence identity to ecDppA) is an orphan SBP without an encoded transporter in its operon. In *H. influenzae*, HbpA recognizes the Dpp transporter and delivers substrate for import into the cell (154). Similar to hiHbpA, orphan SBP NTHI0310 likely utilizes one of the PepT importers for substrate delivery.

One striking feature of the Cluster C family is that members play dual roles in nutrient uptake, importing their canonical substrates and heme. Previous studies have characterized the heme-binding capability of some Cluster C SBPs, and their roles in importing heme into the cell. In *H. influenzae*, HbpA is necessary to use heme as an iron source during growth, and SapA is essential for NTHi survival in heme-starved growth conditions (110,161). In *E. coli*, the Cluster C nickel SBP, NikA, binds heme *in vivo* and has been suggested to play a role as a heme
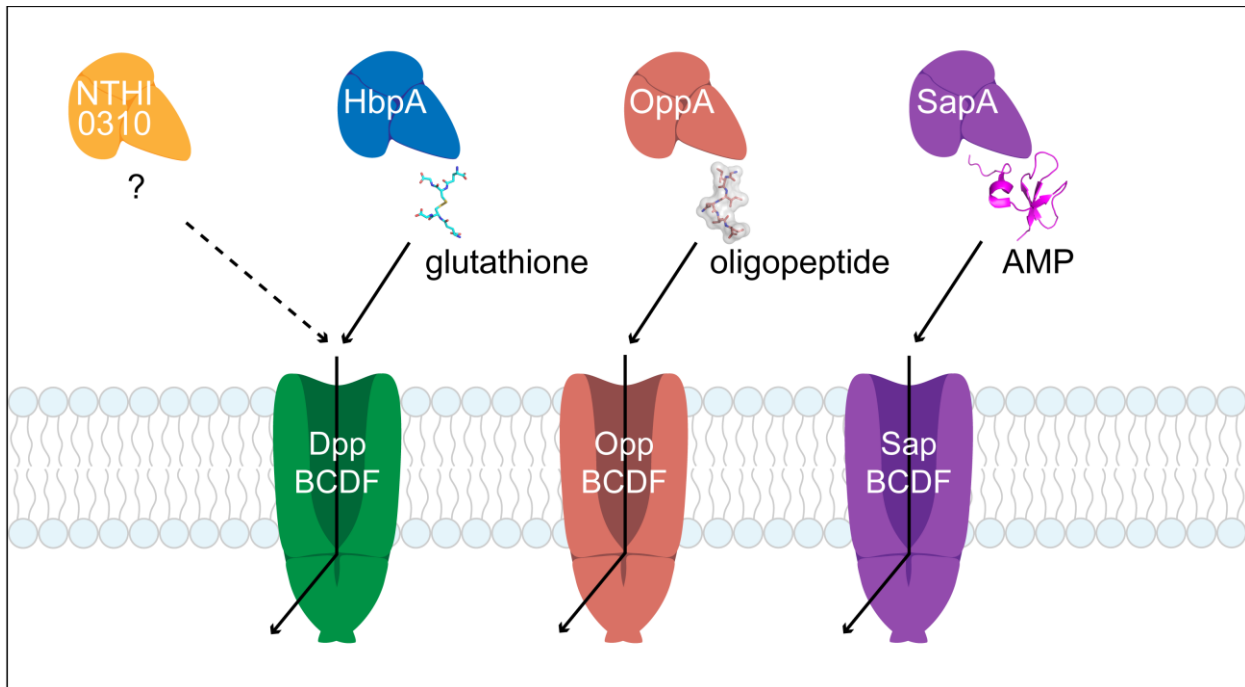
Figure 2.2. Canonical substrate binding of the NTHi Cluster C SBPs. NthiHbpA is necessary for the uptake of glutathione, nthiOppA is responsible for the import of oligopeptides and nthiSapA recognizes a specific group of peptides, AMPs. For NTHI0310, its canonical substrate has not yet been identified.

chaperone in the periplasm (162). An orphan SBP in *E. coli*, MppA delivers its murein tripeptide substrate to the Opp transporter, and both ecMppA and ecDppA are dependent on the Dpp transporter for heme uptake (163,164). In *E. coli*, a double *mppA dppA* deletion mutant was not able to use heme as an iron source during growth (164). These *in vivo* studies highlight the overlapping functionality of some Cluster C proteins and their roles in the heme uptake network for this heme auxotroph.

Overlapping function of multiple heme receptors and ABC importers in the uptake pathway ensure bacteria have access to the essential nutrient in the host. Utilizing a combination of outer membrane receptors, each specific for different hemoproteins, allows NTHi to exploit the many forms of heme in the host environment. *In vivo* studies have identified some Cluster C proteins are involved in the heme uptake pathway and led to the hypothesis that the NTHi Cluster C SBPs also bind heme. SPR was used to compare the heme specificity and binding affinity of nthiHbpA, nthiOppA, nthiSapA, and NTHI0310. This work highlights the multifunctional roles of Cluster C systems and how each SBP has the potential to contribute to this vital pathway for NTHi survival.

2.2. Experimental Procedures

2.2.1. *Materials*

A 10 mM heme stock solution was prepared by dissolving hemin chloride (Strem Chemicals, ferriprotoporphyrin IX chloride, Cat. No. 16009-13-5) in 100% DMSO, and the heme concentration was confirmed using the pyridine-hemochromagen method (165). A 1.54 mM stock solution of heme was also dissolved in 100 mM NaOH (1 mg/mL is the maximum solubility of heme in NaOH). Zinc protoporphyrin IX (ZnPP) was used as a fluorescent analog of

heme (Frontier Scientific, Cat. No. Zn625-9). A 1.60 mM stock solution was prepared by dissolving ZnPP in 100 mM NaOH. All heme and ZnPP solutions were aliquoted to limit freeze-thaw cycles of the solutions and stored at -80°C.

2.2.2. *Bioinformatics Analysis*

The genome of NTHi 86-028NP was searched for Cluster C SBPs using BLAST queries. Four of these SBPs were identified in NTHi, HbpA, OppA, SapA, and a putative peptide-binding protein (NTHI0310). Percent identity and percent similarity comparisons between NTHi SBPs were calculated from pairwise sequence alignments (Table 2.2) generated by LALIGN using a BLOSUM50 matrix (EMBL-EBI). Alignment of NTHi SBPs was performed using ClustalW and superimposed with the secondary structure of nthiOppA in Jalview v2 (166).

2.2.3. *Expression Vectors of SBPs*

Expression constructs were amplified from the genomic DNA of the clinical strain of NTHi 86-028NP and *E. coli* str. K-12 substr. MG1655. Each construct was amplified without their predicted periplasmic signal sequence, nthiHbpA (residues 20-549), nthiOppA (residues 21-541), nthiSapA (residues 24-564), NTHI0310 (residues 24-514), ecDdpA (residues 26-516), ecDppA (residues 29-535), ecMppA (residues 23-537), ecNikA (residues 23-524), ecOppA (residues 27-543), and ecSapA (residues 22-547) with the primers described in Table 2.1. The SBP constructs were cloned into the pET-21b vector using the NdeI and XhoI restriction sites to create constructs fused to a C-terminal His$_6$-tag. All plasmids were verified by sequencing (ACGT Inc.).

Table 2.1. Cluster C SBP constructs.

	Res. Start	Res. End	MW (Da)	Est. pI	Primers
nthiHbpA	20	549	60099.7	6.25	F: CACATATGATGGCTTGTGATCAATCTAGCTCGGCAAATAAA
					R: CACTCGAGTTTACCATCAACACTCACACCATAAAAAGCG
nthiOppA	21	541	59837.2	6.24	F: CACATATGATGGTTATAGTGCCTGAAGGAACACAATTAGATG
					R:CACTCGAGATGTTTAATAATATAAAGATTGCGTAAGTAAATATG ATCTTGTG
nthiSapA	24	564	62867.4	6.90	F: CACATATGATGGCGCCAAGTGTTCCAACATTTTTAACTGAAAAT
					R: CACTCGAGGTGTTTCTCCTGAATAAAATATAAGGTGGAAAAATC
NTHI0310	24	514	57239.7	5.89	F: CACATATGATGTGTGATAAATTGGATAGTCCTAAGCCTATTTCG
					R: CACTCGAGTTGACTTTGAACCTTTCTCCACAAATCTTTACT
ecDdpA	26	516	56029.2	6.10	F: CACATATGATGGCCGTACCAAAAGATATGCTGGTGATT
					R: CACTCGAGTTTACTCATGGTATTGATATTGAAGACCTGTTC
ecDppA	29	535	58531.3	6.04	F: CACATATGATGAAAACTCTGGTTTATTGCTCAGAAGGATCT
					R: CACTCGAGAAACATCACTTCGAAAACGTCTCTATCGAA
ecMppA	23	537	58742.7	8.29	F: CACATATGATGGCAGAAGTTCCGAGCGCAC
					R: CACTCGAGATGCTTCACAATATACATAGTCCGACTGTA
ecNikA	23	524	57426.3	5.83	F: CACATATGATGGCTGCACCAGATGAAATCACCAC
					R: CACTCGAGAGGTTTCACCGGTTTAATCTGTTCGAAC
ecOppA	27	543	59484.1	6.11	F: CACATATGATGGCTGATGTACCCGCAGGCGT
					R: CACTCGAGGTGCTTCACAATGTACATATTCCGGGTAT
ecSapA	22	547	60580.6	6.79	F: CACATATGATGGCGCCTGAATCTC CCCCG
					R: CACTCGAGTGGTTTTTTCACCTCATCCTGTTTCTCG

2.2.4. SBP Expression and Purification

SBP proteins were expressed in *E. coli* BL21(DE3) grown in 1 L cultures of Luria Broth media supplemented with 100 μg/mL ampicillin. Cells were grown at 37°C to early log phase (OD_{600} of 0.4) and then cooled to 16°C. After the incubator cooled, protein expression was induced (OD_{600} of 0.8) with 400 μM isopropyl 1-thio-β-D-galactopyranoside (IPTG). Cells were cultured overnight and harvested by centrifugation at 5000 rpm and stored at -80°C. Each step of the protein purification was carried out at 4°C. Bacterial cells were resuspended in buffer A (25 mM HEPES pH 8, 500 mM NaCl, 15 mM imidazole pH 8) and lysed with a S-4000 sonicator (Misonix Sonicators). The cell debris was removed by centrifugation at 17,000 rpm for 1 h, and the soluble fraction was loaded on to an equilibrated nickel-nitrilotriacetic acid (Ni-NTA) affinity chromatography column (Thermo Fisher Scientific, Cat. No. 88223). The 5 mL column was rinsed with 10 column volumes of buffer A, followed by 5 column volumes buffer B (buffer A, supplemented to 25 mM imidazole pH 8). The SBPs were eluted with 8 column volumes of buffer C (buffer A, supplemented to 250 mM imidazole pH 8). Eluted protein (determined by SDS-PAGE to be >95% pure) was dialyzed overnight in buffer D (25 mM HEPES pH 7.5, 500 mM NaCl). The protein was applied to a HiLoad 16/600 Superdex 200 size-exclusion chromatography column (GE Healthcare). Buffers for nthiHbpA and NTHI0310 were supplemented with 5 mM 2-mercaptoethanol. Protein fractions were pooled and concentrated to 20 mg/mL. Proteins were stored in buffer D at -80°C until needed.

2.2.5. Ligand-free SBP Purification

To remove any ligand bound to the SBP during protein expression, the SBP was chemically denatured and refolded on the nickel affinity column. The bacteria cells were

resuspended, sonicated, and centrifuged as noted above. After the soluble fraction was applied to the affinity column and washed with 10 column volumes of buffer A (25 mM HEPES pH 8, 500 mM NaCl, 15 mM imidazole pH 8), the protein was then denatured with 20 column volumes of denaturing buffer (6 M GdnHCl, 25 mM HEPES, 15 mM imidazole, pH 8). The column was rinsed with 10 column volumes of refolding buffers with decreasing concentrations of GdnHCl (buffer A supplemented with 3, 1.5, 1 and 0.5 M GdnHCl). To remove remaining GdnHCl, the column was washed with 1 column volume buffer A, and the protein was eluted with 8 column volumes of buffer C. The protein was dialyzed, applied to the Superdex column, and stored as mentioned above.

2.2.6. *Native PAGE Heme Shift Assay*

Heme-binding of SBPs was tested using native PAGE analysis. Chemically denatured and refolded protein samples of 5 μg were mixed with 5, 10, 15, 20, 25, and 50 molar ratios of heme (dissolved in NaOH). Samples were incubated on ice for 30 min and then combined with 4x sample loading buffer (40% glycerol). Non-denaturing Laemmli running buffer was prepared without detergent (25 mM Tris base, 192 mM glycine) and chilled at 4°C. Before loading the samples, 8% continuous polyacrylamide gels were pre-run at 150 V for 1 h on ice. Electrophoresis was performed at 150 V for 1.5 h on ice and gels were stains with Coomassie Brilliant Blue.

2.2.7. *Zinc Protoporphyrin Fluorescence Titration Assay*

A solution of 1 uM of nthiSapA was prepared in reaction buffer (25 mM Tris pH 7.5, 150 mM NaCl, and 10mM NaOH) for fluorescence titration experiments. A working solution of 200

uM ZnPP diluted in reaction buffer and was titrated in steps of 0.1 to 2 uM. After each titration step, samples were stirred for 1 min, and then left to rest for 3 min in the dark at RT. Samples were excited at 425 nm and the emission spectra were collected from 550 nm to 750 nm, in 2 nm steps. A 1 mm excitation slit and a 1 mm emission slit were placed in the instrument before data collection. UV-grade 4 mL polyacrylic cuvettes were used (VWR International, Cat. No. 58017-875). All fluorescence intensity experiments were performed using an ISS PC1 photon-counting steady-state fluorometer (ISS Inc.). The change in ZnPP fluorescence at 596 nm versus the ZnPP concentration was fit to a single-site binding model using GraphPad Prism 6.0.

2.2.8. *Heme Binding Affinity by Surface Plasmon Resonance (SPR)*

The heme affinities of the SBPs were measured by SPR. SBPs were immobilized on a Series S CM5 sensor chip (GE Healthcare, Cat. No. 29104988) using a standard amine-coupling method. Proteins were immobilized in PSP-P (20mM phosphate buffer, 2.7 mM KCl, 137 mM NaCl, 0.05% Surfactant P20, pH 7.4) running buffer (GE Healthcare, Cat. No. 28-9950-84). All SPR buffers were filtered immediately before use. Protein samples of 20 mg/mL in 25 mM HEPES pH 7.5, 500 mM NaCl were diluted to 2 mg/mL with a final buffer concentration of 10 mM HEPES pH 7.5, 50 mM NaCl. For the best immobilization of the SBPs, lowering the salt concentration increases the amount of protein immobilized. The recommended amine-coupling protocol dilutes the sample in 10 mM sodium acetate with a pH about 1.5 lower than the theoretical pI of the protein. I tested 10 mM sodium acetate pH 4.5 for immobilization of SBPs, but the proteins did not completely recover after immobilization and heme binding was reduced.

For flow channel 1, the reference channel, the dextran surface was activated by equal parts 1-ethyl-3-(3-dimethylaminopropyl)   carbodiimide   hydrochloride   (EDC)   and   N-

hydroxysuccinimide (NHS) and blocked by ethanolamine pH 8.5 (GE Healthcare, amine-coupling kit Cat. No. BR100050). SBPs were immobilized in flow channels 2, 3, and 4; low levels of protein were immobilized to minimize non-specific binding and mass transfer. SBPs were injected after sensor-surface activation by EDC/NHS mixture for a contact time of 15-20 min at a flow rate of 7 μL/min to immobilize 1000-2000 RU of protein; the surface was then blocked with ethanolamine. The surface of the chip was equilibrated in running buffer (25 mM HEPES pH 7.5, 150 mM NaCl, 0.1% Tween 20, 2% DMSO) at a flow rate of 100 μL/min for at least 3 h. Ensuring the chip (i.e. the proteins) has adequate time to equilibrate after immobilization is essential for successful data collection.

The data were obtained using single-cycle kinetic experiments in triplicate. For each replicate, five analyte (heme) injections were prepared by 2-fold serial dilution. The analyte samples were consecutively injected by increasing heme concentrations over all four channels to determine the binding constants of the SBPs. The association time of each analyte injection was 1 min, followed by a final 5 min dissociation step. SBP kinetic experiments were run at a flow rate of 40 μL/min at 25°C. The sensor surface was regenerated after each experiment with two 30 s injections of running buffer, supplemented with 0.1% SDS, at a flow rate of 50 μL/min. All experiments were performed with the Biacore T200 instrument (GE Healthcare) according to the manufacturer's instructions.

Models used for fitting of the experimental data are part of the Biacore evaluation software. The reference channel was subtracted from all experimental data. The data were initially fit by applying a single-state 1:1 binding model. As expected, the statistics and fit quality of these preliminary fits were poor. Kinetic rate constants and equilibrium dissociation constants were determined by fitting the data globally to the 1:1 two-state reaction model using

the Biacore T200 evaluation software v3.0 (GE Healthcare). In this model, k_{a1} and k_{d1} are the forward and reverse rate constants for complex formation, and k_{a2} and k_{d2} are the forward and reverse rate constants for the two-state binding. A more detailed description of the parameters and equations is provided in the Biacore T200 Software Handbook (28-9768-78, Ed. AA, pg. 160-202).

2.3. Results

2.3.1. Conserved 3D Structure of Cluster C SBPs

The overall structure of SBPs is comprised of two globular α/β domains, each with a few α–helices surrounding a core β–sheet. Most SBPs bind their selected substrate at the interface of domains I and II. Structural homology was used to identify SBPs in the Cluster C family (3). A unique structural feature of Cluster C SBPs is a third globular domain, domain I_B, inserted into domain I_A (Figure 2.3A). This increases the size of the substrate-binding pocket and helps this class of proteins bind a diverse range of substrates. SBPs are grouped by topology subclasses that describe the threading of the secondary structure between the α/β domains. The β–sheet topology of Class I is $\beta_2\beta_1\beta_3\beta_4\beta_5$, in comparison the topology of Class II is $\beta_2\beta_1\beta_3\beta_n\beta_5$, where the β_n strand is substituted by a strand from the opposite domain (167). This crossover between domain I and II, known as domain dislocation, characterizes Cluster C proteins as Class II SBPs. Figure 2.3 compares the ligand-bound structures of ecDppA (PDB code 1DPP), *Glaesserella parasuis* (formerly known as *Haemophilus parasuis*) HbpA (PDB code 3M8U), ecMppA (PDB code 3O9P), ecNikA (PDB code 3DP8), and *S.* typhimurium OppA (PDB code 2OLB). Comparing Cluster C complexes highlights the high degree of overall structural similarity of these SBPs.

ABC transporters play a vital role in heme uptake in bacteria. To uncover how heme is
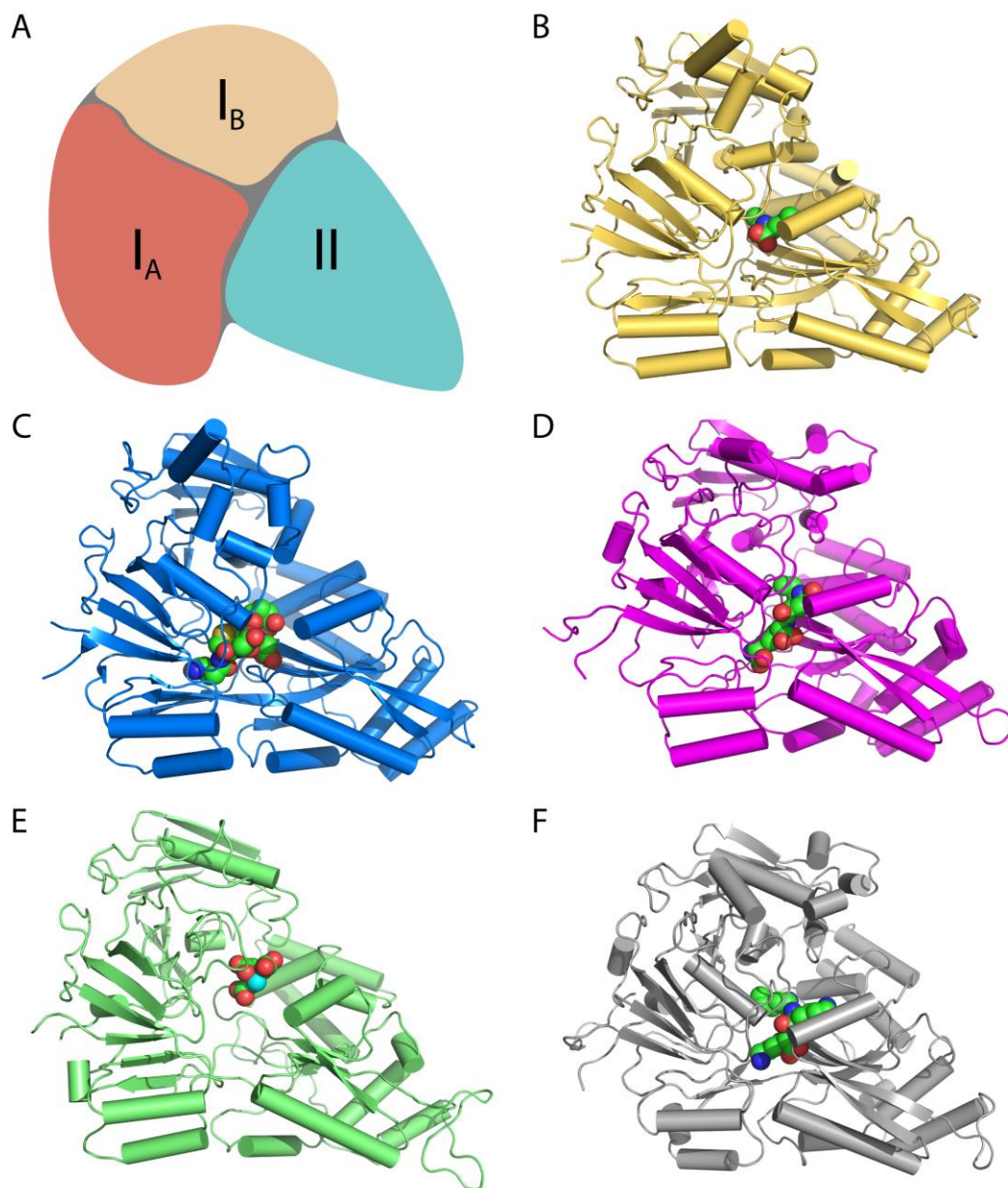
Figure 2.3. Overall 3D structure of Cluster C SBPs. (A) Cartoon of Cluster C SBP labeled by individual domains I_A, I_B and II. Substrate-bound Cluster C proteins have a well-conserved closed conformation, (B) ecDppA bound to glycyl-lysine (PDB code 1DPP), (C) gpHbpA bound to oxidized glutathione (PDB code 3M8U), (D) ecMppA bound to murein tripeptide (PDB code 3O9P), (E) ecNikA bound to butane-1,2,4-tricarboxylate-chelated nickel (PDB code 3DP8), and (F) seOppA bound to tri-lysine (PDB code 2OLB).

shuttled to the inner membrane of this "heme-loving" pathogen, I looked at the conservation of heme ABC transport systems in NTHi. Since Cluster A heme SBPs are not found in the NTHi genome, NTHi Cluster C proteins provide the vital link in the uptake pathway between the outer membrane receptors scavenging heme from the host and the ABC importers delivering the nutrient to the cytoplasm. A BLAST search of the NTHi genome was used to identify all Cluster C proteins and a protein sequence alignment was performed to illustrate the similarities of these SBPs (Figure 2.4). Despite the low sequence identity between the NTHi Cluster C SBPs (Table 2.2), these proteins have high sequence similarity and are predicted to have a similar overall structural topology. The structural conservation of Cluster C SBPs and the functional similarity between some of these proteins in the heme network led us to investigate the heme specificity of each of the NTHi SBPs proteins, as well as six *E. coli* Cluster C SBPs.

2.3.2. *Native PAGE Analysis of Heme-bound State Identifies Heme Specificity of Cluster C Family*

A survey of the heme specificity of well-characterized *E. coli* and NTHi Cluster C SBPs showed that heme-binding is a shared characteristic of all ten proteins tested. SBPs ecDdpA (dipeptide), ecDppA, ecMppA, ecNikA ecOppA, ecSapA, nthiHbpA, nthiOppA, nthiSapA, and NTHI0310 were expressed without their predicted signal sequence (Table 2.1) and purified under chemically denaturing and refolding conditions to remove any bound ligand. These proteins are similar in size ranging from 56-63 kDa, and in general, the ligand-free SBPs migrate in the native gel based on their estimated pI values (Figure 2.5, A and B). Ligand-free ecDdpA and ecMppA migrate the least of all the SBPs, whereas ligand-free ecNikA migrates the furthest into the gel. Surprisingly, using Native PAGE assays all 10 SBPs demonstrated heme binding
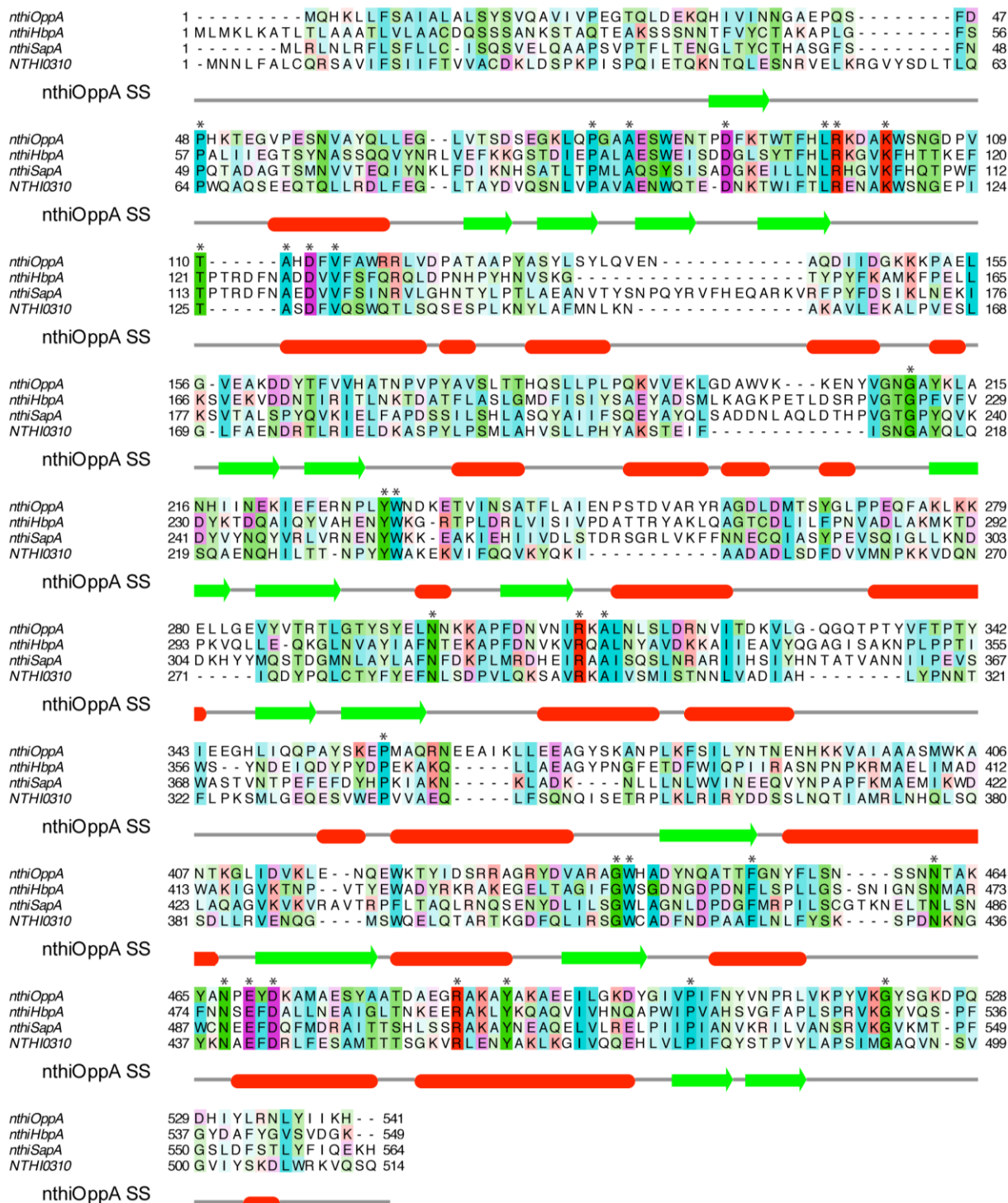
Figure 2.4. Protein sequence alignment shows high similarity of NTHi SBPs. Alignment of nthiHbpA, nthiOppA, nthiSapA, and NTHI0310 by Jalview. Asterisks mark conserved residues.

Secondary structure of nthiOppA is shown below the alignment with α–helices and β–strands represented by red cylinders and green arrows, respectively.

Table 2.2. Protein sequence identity and similarity of NTHi SBPs.

	Identity (%)			Similarity (%)		
	nthiHbpA	nthiSapA	NTHI0310	nthiHbpA	nthiSapA	NTHI0310
nthiOppA	24.9	22.2	26.8	52.4	50.9	60.4
nthiHbpA	-	32.1	21.6	-	62.9	52.0
nthiSapA	-	-	20.8	-	-	52.2
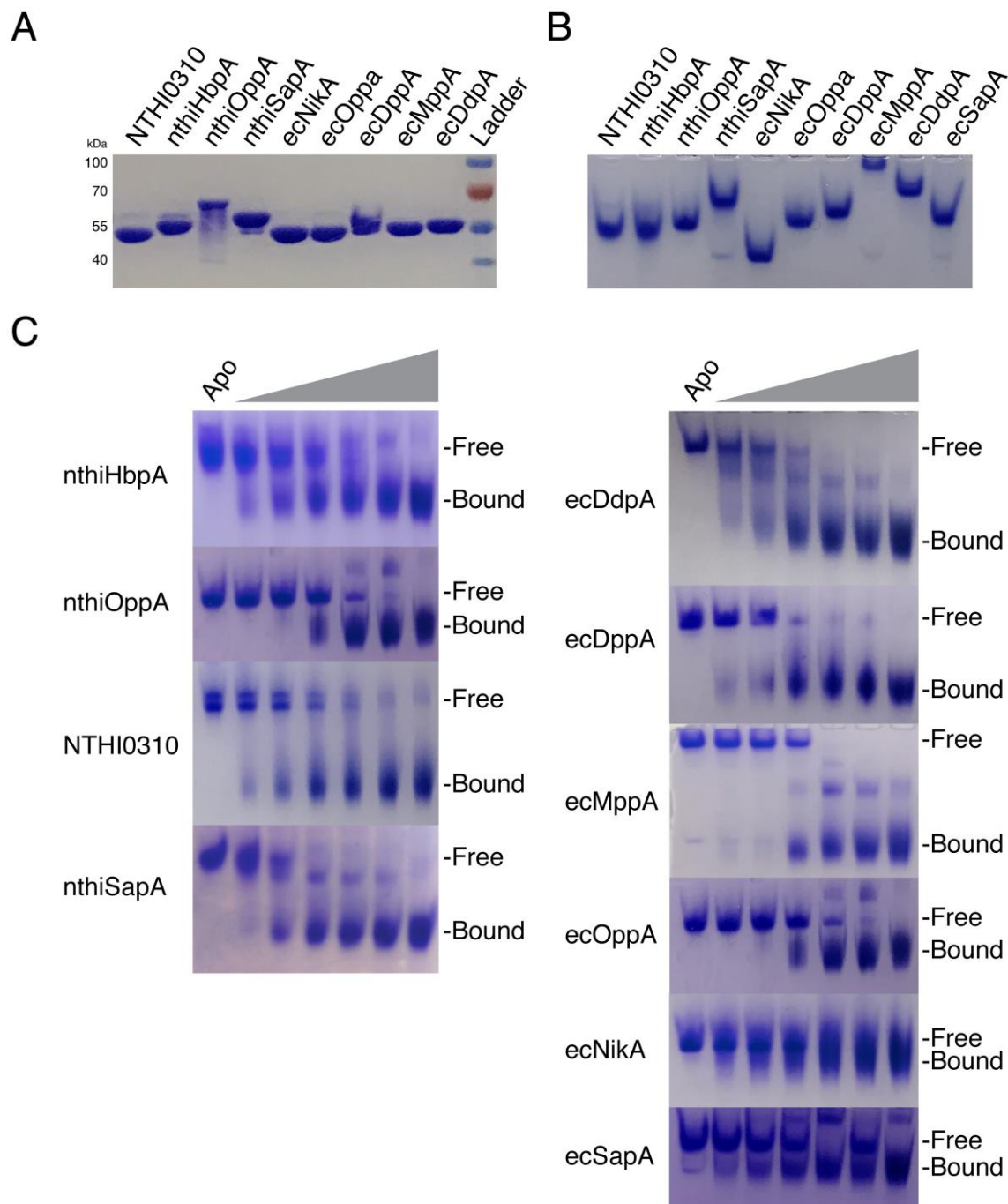
Figure 2.5. Heme specificity of all NTHi and *E. coli* Cluster C SBPs. (A) SDS-PAGE of Cluster C SBPs. (B) Native PAGE assay show ligand-free Cluster C SBPs migrate at different rates. (C) Cluster C proteins bind heme in native PAGE assay and SBPs shift from unbound state to heme-bound state based on heme concentration.

(Figure 2.5C). All SBPs are fully bound by heme at a 1:50 protein to heme ratio. Heme binding enhances the ability of the ligand-bound SBPs to migrate further into the gel. The degree of migration varies for each SBP and is not dependent on the initial migration of the ligand-free protein. For example, ecNikA has a small shift after binding heme, in comparison to more dramatic shifts of ecDdpA and ecMppA bound to heme. In contrast, NTHI0310 has a dramatic shift upon heme binding as well as being one of the ligand-free SBPs that migrates the furthest in the gel. The variable migration distance between heme-bound SBPs may be dependent on any number of factors, including the changes in surface charge and compactness of tertiary structure between the ligand-free and ligand-bound conformations.

It is difficult to obtain heme-binding constants using native PAGE assays. Additionally, heme is insoluble in aqueous solutions and is only dissolved in strong base or solvent. This makes measuring the heme-binding affinities of the SBPs difficult using common biophysical techniques that are sensitive to buffer composition. One advantage of SPR is a high sensitivity for small-molecules in dilute solvent and allowed us to overcome these challenges of heme-binding experiments.

2.3.3. Heme Affinity of Cluster C SBPs in NTHi

Previous studies have reported a wide range of heme equilibrium dissociation constants of the Cluster C SBPs. The heme affinity of ecNikA has previously been measured by tryptophan fluorescence quenching, K_D value of 530 nM (162). Two other *E. coli* SBPs, DppA and MppA, bind heme with estimated binding constants of 10 and 50 µM, respectively; a mutant strain lacking both of these SBPs was not able to use heme as an iron source during growth (164). Despite its namesake, hiHbpA was reported to have weak heme affinity with a K_D value of 655

µM (154). The equilibrium dissociation constants of ecDppA, ecMppA and hiHbpA were calculated using native PAGE gel shift assays. One major disadvantage of these assays is that the samples were not at equilibrium during electrophoresis (168). Heme-binding affinities of homologs for the other NTHi Cluster C SBPs have not previously been published. The limitations of the calculated heme affinity for some of the Cluster C SBPs led us to investigate the heme specificity and affinity of each of the NTHi SBPs.

To determine the shared heme-binding functionality of the NTHi Cluster C SBPs, I examined the heme specificity and binding affinity of the proteins. The heme-protein binding kinetics of nthiHbpA, nthiOppA, nthiSapA, NTHI0310 and ecNikA were measured by SPR. The single-cycle kinetics method was used to measure heme binding of the immobilized SBPs, which includes five serial injections with increasing concentrations of heme followed by an extended dissociation step. All four of the NTHi SBPs bind heme with variable affinity (Figure 2.6). The heme affinity calculated by spectroscopic analysis of ecNikA provided a reference for the heme affinity measured by SPR. The SPR calculated heme affinity of ecNikA, K_D value of 526 nM, closely matches the previously reported K_D value of 530 nM (162). Heme binds to nthiOppA with the highest affinity, K_D value of 244 nM. The heme affinities of nthiHbpA and NTHI0310 are similar, with K_D values of 382 nM and 420 nM, respectively. NthiSapA showed a slightly lower heme binding with a K_D value of 1.1 µM. A fluorescence titration assay was used to measure the ZnPP (heme analog) equilibrium constant of nthiSapA, K_D value of 0.93 µM (Figure 2.7). The SPR sensograms for each SBP were fit to a two-state reaction model and indicate a 1:1 binding ratio of heme to SBP. The kinetic rate constants and equilibrium dissociation constant for each of the SBPs are summarized in Table 2.3. The differences in the heme affinities between the SBPs are largely explained by variability in the initial association rates. The larger initial
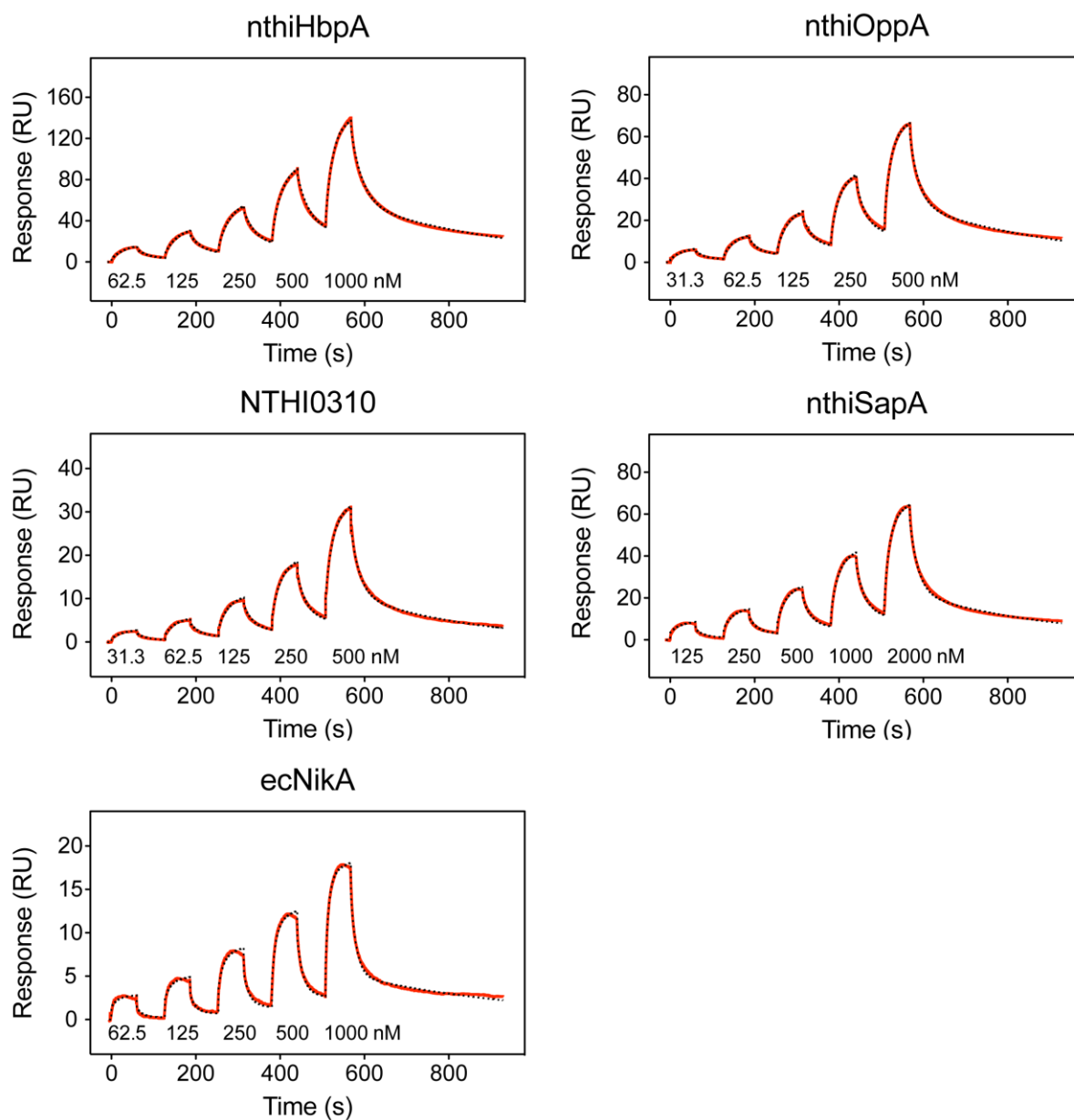
Figure 2.6. NTHi Cluster C SBPs bind heme with a range of affinity. Single-cycle kinetic analysis of heme binding was performed using five analyte injections over immobilized NTHi SBPs. For the association phase, increasing concentrations of heme were injected in series followed by a final dissociation phase. Representative data in each sensogram is depicted by a red line and fit by a 1:1 two-state reaction model to determine kinetic constants and equilibrium dissociation constants, which is displayed by a dashed black line.
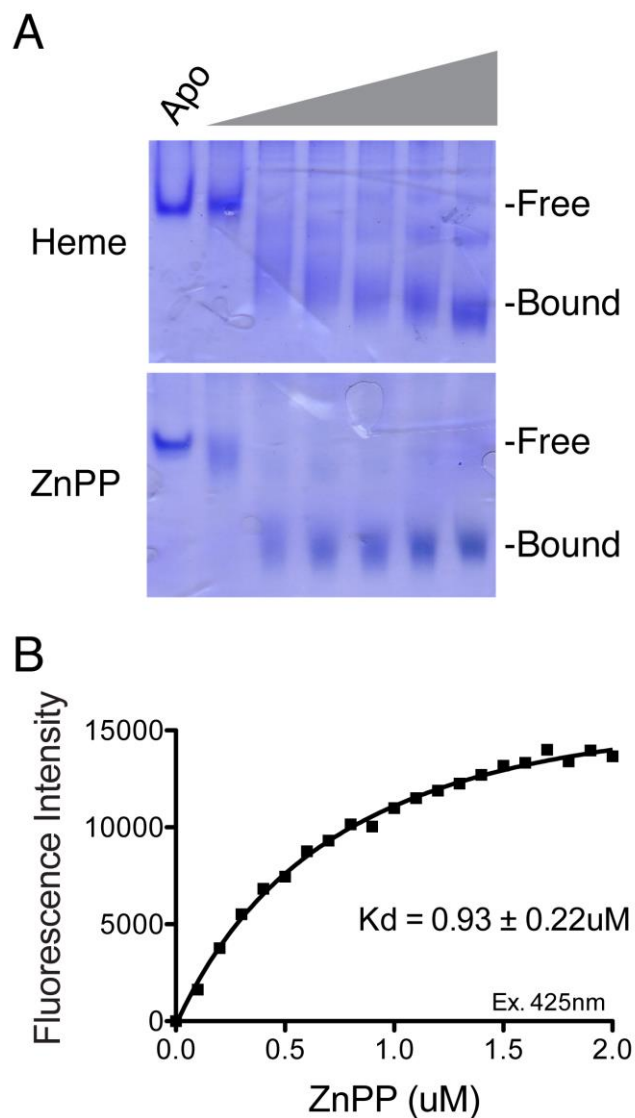
Figure 2.7. Heme analog, ZnPP, binds nthiSapA with a similar affinity as heme. (A) Native PAGE gel shows ZnPP-bound nthiSapA migrates at the same molar ratio as heme. (B) A fluorescence titration assay was used to determining the ZnPP binding affinity of nthiSapA. Data from a representative replicated is shown in black squares and fit using a single-site binding model represented by a black line.

Table 2.3. Kinetic and equilibrium constants of NTHi Cluster C SBPs.

	k_{a1} $M^{-1}s^{-1}$	k_{d1} s^{-1}	k_{a2} s^{-1}	k_{d2} s^{-1}	K_D nM
nthiOppA	5.88 (0.21) x 10^4	3.98 (0.06) x 10^{-2}	5.57 (0.08) x 10^{-3}	3.14 (0.05) x 10^{-3}	244 (11)
nthiHbpA	3.46 (0.15) x 10^4	3.44 (0.31) x 10^{-2}	4.65 (0.11) x 10^{-3}	2.19 (0.07) x 10^{-3}	382 (20)
nthiSapA	1.77 (0.03) x 10^4	4.82 (0.14) x 10^{-2}	5.07 (0.19) x 10^{-3}	3.41 (0.07) x 10^{-3}	1100 (24)
NTHI0310	4.21 (0.08) x 10^4	4.23 (0.16) x 10^{-2}	5.42 (0.10) x 10^{-3}	3.90 (0.06) x 10^{-3}	420 (18)
ecNikA	5.38 (0.46) x 10^4	7.66 (0.36) x 10^{-2}	4.34 (0.28) x 10^{-2}	2.52 (0.20) x 10^{-3}	526 (76)

* Standard deviation of triplicates shown in parentheses

association rate indicates an increase in the heme-bound nthiOppA complex formation frequency. Despite their variation in their individual canonical substrates, the NTHi SBPs share specificity for heme.

2.4. Discussion

Despite Cluster C SBPs canonical substrates ranging in diversity and size from a nickel ion to AMPs, their unifying characteristic has previously been their overall structure conserved from a common ancestor (169). This work has identified multisubstrate heme specificity is a shared characteristic of all ten Cluster C SBPs tested. A survey of Cluster C gene clusters in *Haemophilus* strains show a range in the number of these proteins, from just two SBPs to as many as seven SBPs (Figure 2.8). The Dpp (including HbpA) and Sap transport systems were found in all species except *H. haemoglobinophilus* and *H. pittmaniae*, respectively. Some of the *Haemophilus* strains also have a *dppA* in their *dpp* gene clusters. Interestingly, there is also a second oligopeptide transport system, Opp2, in half of the *Haemophilus* strains. Orphan putative peptide SBPs are found in almost all of the *Haemophilus* strains. These functionally overlapping Cluster C SBPs and their cognate PepT importers are conserved in *Haemophilus*.

To better characterize heme trafficking in the periplasm, I calculated the binding affinities of the NTHi SBPs and found a range from 244 nM for nthiOppA to 1.1 µM for nthiSapA. Considered a low-affinity heme-binding protein, nthiSapA plays a crucial role in the heme uptake pathway for NTHi survival after heme starvation (110). Data from the heme binding studies coupled with previously published data demonstrates that the heme affinity of the individual SBP is not a determinant of the role these proteins play in the heme uptake pathway. Even in bacteria that employ high-affinity heme SBPs, such as HmuT, PhuT and ShuT, there are

Species	DppA	OppA	SapA	HbpA	OppA2	Orphan	
NTHi		OppA	SapA	HbpA		0310	
H. influenzae		OppA	SapA	HbpA		0213	
H. aegyptius		OppA	SapA	HbpA		1553	
H. parainfluenzae		OppA	SapA	HbpA	OppA2	0985	
H. paracuniculus	DppA	OppA	SapA	HbpA	OppA2	2190	7660
H. pittmaniae		OppA		HbpA		1326	
H. ducreyi			SapA	HbpA	OppA2	7075	
H. sputorum	DppA		SapA	HbpA	OppA2	5765	
H. parahaemolyticus	DppA		SapA	HbpA	OppA2		
H. paraphrohaemolyticus	DppA		SapA	HbpA	OppA2		
H. haemolyticus			SapA	HbpA		0813	
H. haemoglobinophilus			SapA			1990	

Figure 2.8. Conserved Cluster C SBPs in *Haemophilus*. The Cluster C SBPs in heme uptake pathway of *Haemophilus*. The Dpp transporter has been identified in all species except *H. haemoglobinophilus*. The Opp, Sap and Opp2 transporters are present in all species with the corresponding SBP. Orphan putative peptide Cluster C SBPs are shown in yellow and labeled by gene number.

functional overlapping heme transport systems. Deletion of the *hmu* locus in *Y. pestis* did not eliminate the ability of the mutant strain to utilize heme or colonize mice in the systemic infection model, indicating another heme transport system is sufficient for virulence in the mouse model (170). In addition, functionally similar heme trafficking proteins in the cytoplasm, such as *P. aeruginosa* PhuS, have comparable heme affinity to Cluster C SBPs. In *P. aeruginosa*, cytoplasmic heme trafficking protein PhuS delivers its substrate to heme oxygenase HemO and helps prevent heme-related oxidative stress with a K_D value of 410 nM (171). Taken together, these heme-binding proteins demonstrate heme affinity does not dictate functionality or limit the essential role of these proteins in the heme uptake pathway for bacterial survival and pathogenesis. Even as the lowest affinity SBP, nthiSapA plays a role in NTHi survival.

In the dynamic and perilous host environment it is advantageous for NTHi to manage multiple heme SBPs to ensure the pathogen maintains access to the essential nutrient (Figure 2.9). This functional overlap between the Cluster C SBPs, particularly the unknown heme-binding capability of nthiOppA and NTHI0310 demonstrated here, has previously made it a challenge to fully characterize the heme uptake pathway. The identification of heme specificity for all four Cluster C SBPs is the first step to understanding the unique and essential role each SBP plays in the transport of the essential nutrient heme. The multisubstrate binding of these Cluster C SBPs and the recognition of the canonical and heme substrates for these proteins is explored further in Chapter 3. Better understanding of the interplay between these multifunctional Cluster C SBPs will help us uncover how pathogens adapt and overcome host-mediated defenses.
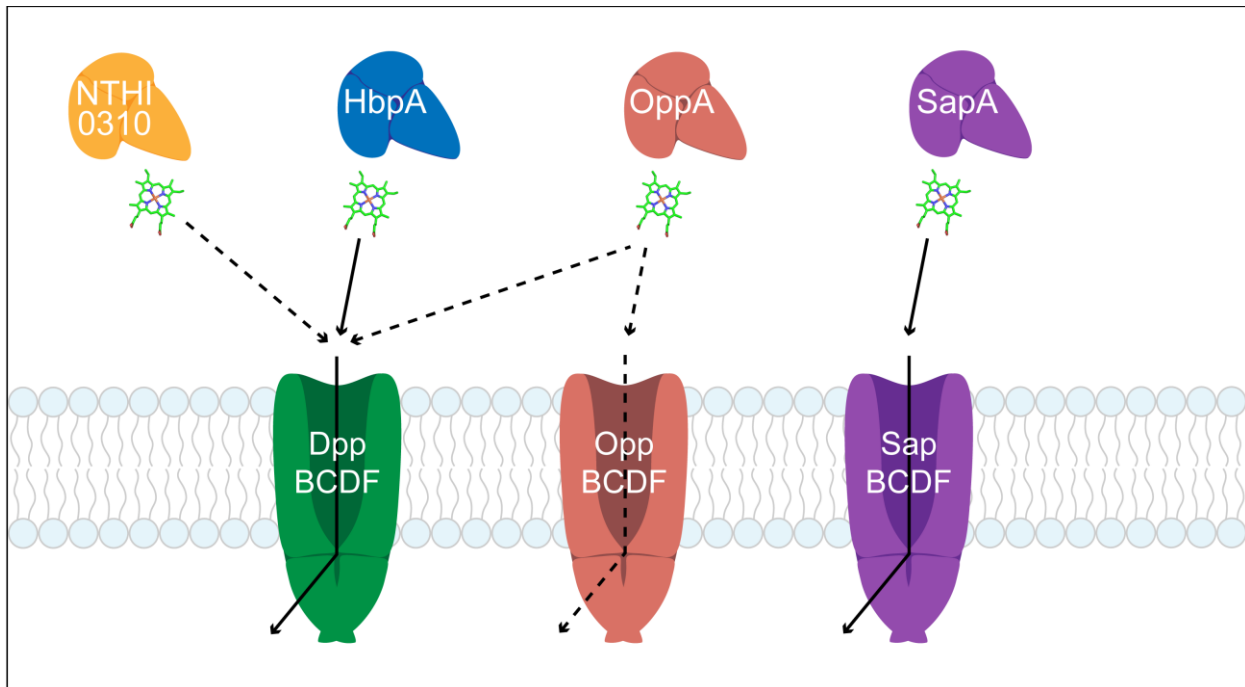
Figure 2.9. Multiple heme Cluster C SBPs in NTHi. All of the NTHi Cluster C SBPs have heme specificity with a range affinity from about 200 nM to 1 μM, nthiOppA < nthiHbpA < NTHI0310 < nthiSapA. The overlapping function of these SBPs helps the bacteria maintain access to heme in the host environment. Heme shown in green.

CHAPTER 3:

Oligopeptide-Binding Protein (OppA) from NTHi has Ligand-Specific Sites to Accommodate Peptides and Heme in the Binding Pocket*

3.1. Introduction

3.1.1. Oligopeptide ABC Importer in Nutrient Uptake

The oligopeptide (Opp) transport system is the ABC transporter responsible for the uptake of a range of peptides, supplying pathogens with essential nutrients as a source of carbon, nitrogen and amino acids. The role of the Opp transport system in heme uptake has not previously been tested. However, as demonstrated in Chapter 2, nthiOppA binds the essential nutrient heme. Nutrient acquisition through the Opp system influences many cellular processes, including internalization of quorum sensing peptides, biofilm production, modifying the cell surface, and antibiotic resistance (105,119,172,173).

3.1.2. OppA Homologs in Gram-Negative and Gram-Positive Bacteria

In Gram-negative bacteria, the SBP OppA has been shown to select for peptides between 3-5 amino acids with high affinity for tri- and tetrapeptides (174). Crystal structures of peptide bound OppA from *S.* typhimurium, *Y. pestis, E. coli*, and *Burkholderia pseudomallei* show peptide specificity is independent of amino acid sequence of the peptides as protein-peptide interactions occur mainly through the peptide backbone (175-178). Gram-positive *Lactococcus lactis* OppA binds peptides 4-35 amino acids long with a preference for nonapeptides (102). Large binding cavities of oligopeptide homologs llOppA, *B. subtilis* AppA, and *Enterococcus faecalis* PrgZ allow these proteins to fully enclose hepta- and nonapeptides in their substrate-binding pockets (103,179,180). OppA mediated peptide transport is a necessary component of nutrient uptake and signaling pathways for survival and virulence of pathogens (104,106).

This work examines the peptide and heme substrate specificity of nthiOppA. I solved the structure of nthiOppA bound to a range of hydrophobic peptides and uncovered the peptide

specificity of Gram-negative OppA extends beyond pentapeptides. *In silico* analysis of heme docking coupled, with substrate competition assays and individual domain analysis, allows us to propose how multisubstrate specificity may occur in nthiOppA. This work highlights the multifunctional roles of nthiOppA with the interplay between the peptide and heme transport networks.

3.2. Experimental Procedures

3.2.1. *Materials*

All peptides were solubilized according to manufacture recommendations. Peptides P1[KKK], P3[LGG], and P6[Brady] (bradykinin, RPPGFSPFR) were purchased from Sigma-Aldrich. Custom peptides P2[MGG], P4[GIINTL], and P5[Long] (YLGANGRGGGS) were synthesized by GenScript.

3.2.2. *NthiOppA Crystallization*

Crystallization of the co-purified peptide nthiOppA complex (25 mM HEPES pH 7.5, 500 mM NaCl) was achieved by the vapor diffusion in sitting drops at 22°C. NthiOppA crystals were obtained with a 1:1 ratio of 10 mg/mL protein and reservoir solution containing 0.1 M sodium acetate at pH 4.6 and 2.4 M ammonium sulfate. Crystals usually appeared within 24 h. Co-crystallization of nthiOppA with peptides was achieved using a 1:10 refolded OppA to peptide mixture yielding final concentrations of 1 mM peptide and 6 mg/mL protein in binding buffer (25 mM HEPES pH 7.5, 150 mM NaCl). The mixture was incubated on ice for 30 min. Co-crystals grew in the same reservoir solution and conditions. All crystals were briefly soaked in cryoprotectant consisting of reservoir solution supplemented with 15% v/v glycerol, harvested with a nylon loop and flash-cooled in liquid nitrogen.

3.2.3. *Structure Determination of NthiOppA*

Diffraction data were collected at the Advanced Photon Source (Argonne, IL) LS-CAT beamline 21-ID-D with an Eiger X 9M detector (DECTRIS AG). The diffraction data were integrated using XDS (181) and scaled with AIMLESS, from the CCP4 suite (182). The initial model for nthiOppA was determined using the molecular replacement pipeline Balbes (183), and model building was further improved with ARP/warp (184) from the online CCP4 platform. The output model was manually rebuilt over several cycles with Coot (185). Each peptide was built in the observed electron density, and the models were refined with REFMAC (186). Validation statistics of the final models were calculated with Molprobity (187). Details of data quality and structure refinement are summarized in Table 3.1 and Table 3.2. Coordinate files have been deposited in the Protein Data Bank under the accession codes 6DQQ, 6DQR, 6DQT, 6DQU, 6DTF, 6DTG, and 6DTH. Structural figures, analysis of nthiOppA substrate-bound states and sequence-independent structural alignments with root-mean-square deviation (RMSD) calculations were performed in PyMOL v2.0 (Schrödinger, LLC). Protein-peptide hydrogen bond lengths calculated in LigPlot+ v1.4 (188).

3.2.4. *Thermal Shift Assay*

Peptide binding candidates were identified using a thermal shift assay of nthiOppA. Reactions of 2 μg refolded nthiOppA, 5x SYPRO Orange (Thermo Fisher Scientific, Cat. No. S6650), and 1 mM peptide in binding buffer (25 mM HEPES pH 7.5, 150 mM NaCl) for a final volume of 10 μL were placed in a clear 384-well PCR plate (Greiner, Cat. No. 785201) with optical sealing tape (Bio-Rad, Cat. No. 223-9444). The plate was spun at 1500 rpm for 30 s to remove bubbles in the wells. Samples were incubated at room temperature for 1 h. The plate was

Table 3.1. Data collection and refinement statistics: Co-purified, P2^{MGG}, P3^{LGG} and P4^{GIINTL}.

Statistics	OppA Structures			
	co-purified +nthiOppA	P2^{MGG} +nthiOppA	P3^{LGG} +nthiOppA	P4^{GIINTL} +nthiOppA
Space group	$P2_1 2_1 2_1$	$P2_1 2_1 2_1$	$P2_1 2_1 2_1$	$P2_1 2_1 2_1$
Data Collection				
Unit cell Dimensions, Å				
a	49.99	47.57	49.52	47.90
b	90.90	92.19	90.95	92.96
c	108.78	108.37	108.86	108.34
Unit Cell Angles, °				
α	90.0	90.0	90.0	90.0
β	90.0	90.0	90.0	90.0
γ	90.0	90.0	90.0	90.0
Resolution, Å	46.67-1.85	35.75-2.08	36.63-1.95	35.88-1.65
	(1.89-1.85)	(2.14-2.08)	(2.00-1.95)	(1.68-1.65)
Wavelength, Å	1.0782	1.0781	1.0781	1.0781
Completeness, %	99.4 (99.5)	99.1 (99.9)	99.6 (99.8)	99.9 (99.9)
R_{merge}	0.077 (0.538)	0.080 (0.670)	0.091 (0.665)	0.059 (0.589)
Average $I/\sigma I$	18.6 (4.2)	15.6 (3.1)	15.3 (3.7)	16.9 (3.0)
Redundancy	13.3	11.1	10.9	9.0
Total reflections	572217	323020	397113	527954
Unique reflections	42868	29098	36506	58988
Refinement				
R_{work}/R_{free}	0.1598/0.2069	0.1770/0.2344	0.1664/0.2048	0.1598/0.2069
Number of atoms				
All atoms	4586	4333	4349	4521
Protein	4169	4115	4157	4115
Water	375	184	153	357
Average B-factor, Å2				
All atoms	33.3	49.3	37.1	32.1
Protein	32.6	49.1	36.9	31.4
Water	40.0	50.7	38.9	39.2
RMSD				
Bond lengths, Å	0.017	0.013	0.010	0.017
Bond angles, °	1.695	1.483	1.410	1.695
Ramachandran statistics				
Favored, %	98.1	97.1	97.7	97.5
Allowed, %	1.7	2.7	2.3	2.3
Outliers, %	0.2	0.2	0.0	0.2

*Data for the highest-resolution shell are given in parentheses. All structures were determined using single crystals.

Table 3.2. Data collection and refinement statistics: P1^{KKK}, P5^{Long} and P6^{Brady}.

Statistics	OppA Structures		
	P1^{KKK} +nthiOppA	P5^{Long} +nthiOppA	P6^{Brady} +nthiOppA
Space group	$P2_1 2_1 2_1$	$P2_1 2_1 2_1$	$P2_1 2_1 2_1$
Data Collection			
Unit cell Dimensions, Å			
a	47.80	50.09	47.87
b	92.33	90.92	92.89
c	108.36	108.73	108.12
Unit Cell Angles, °			
α	90.0	90.0	90.0
β	90.0	90.0	90.0
γ	90.0	90.0	90.0
Resolution, Å	46.73-1.75	46.66-1.90	46.44-1.96
	(1.78-1.75)	(1.94-1.90)	(2.01-1.96)
Wavelength, Å	1.0782	1.0782	1.0782
Completeness, %	97.9 (93.8)	99.8 (100.0)	99.9 (100.0)
R_{merge}	0.055 (0.525)	0.080 (0.880)	0.084 (0.717)
Average $I/\sigma I$	16.5 (2.7)	15.6 (2.6)	11.6 (2.4)
Redundancy	9.1	8.8	8.8
Total reflections	436486	352161	310840
Unique reflections	48105	39899	35422
Refinement			
R_{work}/R_{free}	0.1753/0.2212	0.1696/0.2089	0.1908/0.2540
Number of atoms			
All atoms	4392	4415	4308
Protein	4105	4162	4098
Water	249	212	165
Average B-factor, Å2			
All atoms	33.3	34.6	37.1
Protein	41.2	34.2	36.9
Water	41.6	37.4	47.7
RMSD			
Bond lengths, Å	0.010	0.010	0.008
Bond angles, °	1.317	1.403	1.262
Ramachandran statistics			
Favored, %	97.7	97.9	96.1
Allowed, %	2.1	1.9	2.7
Outliers, %	0.2	0.2	0.2

*Data for the highest-resolution shell are given in parentheses. All structures were determined using single crystals.

heated from 25 to 95°C with a heating rate of 0.5°C min^{-1}. The fluorescence intensity was measured with an excitation wavelength of 470 nm and emission wavelength of 580 nm. The thermal shift assay was performed using a BioRad CFX384 Real-Time Detection System (Bio-Rad). Analyze data using Excel worksheet 'DSF Analysis.xls' and GraphPad template 'DSF GraphPad Boltzmann.pzf' (ftp://ftp.sgc.ox.ac.uk/pub/biophysics) (189).

3.2.5. In Silico Heme Docking Studies

Ligand docking of heme was conducted with ROSIE (Rosetta Online Server that Includes Everyone) Ligand Docking Protocol (190). Along with the structure of nthiOppA, other previous solved structures for *G. parasuis* HbpA (PDB code 3M8U) and *E. coli* NikA (PDB code 3DP8) were used for docking studies. The gpHbpA structure has 74% sequence identity to nthiHbpA. The solvent-free structure of each SBP was used as the template and heme with a 2$^+$ formal charge was used as the ligand. The substrate-binding pocket was probed with a 7 Å search radius starting at x = 38.0, y = 43.5, and z = 10.5, the search radius was centered at the interior of the protein. For each protein, 200 structures were generated and ranked based on calculated lowest interface energy. Of the 20 top-ranked ligand poses for nthiOppA, heme was docked in the same position in the substrate-binding pocket in 18 of the solutions. For hiHbpA and ecNikA there were 11 and 19 solutions with the same location, respectively. For the remaining solutions in the top 20, the heme molecule is overlapped with the most common ligand pose, but the porphyrin ring is slightly rotated. Top-scoring docking models were displayed using PyMOL.

3.2.6. SPR Competition Assay

After nthiOppA immobilization (3300 RU), the chip was equilibrated in running buffer as

described above. For the competition assay, analytes were injected for 1 min at a flow rate of 40 µL/min at 25°C. A 500 nM heme injection was used to calculate the heme response. Individual injections of P1^{KKK}, P2^{MGG}, and P5^{Long} were measured at 250 nM, 1.5 mM and 250 nM, respectively. Maintaining the concentration of each analyte, combined mixtures of heme and peptide were injected. The sensor surface was regenerated after each experiment with two 30 s injections of running buffer, supplemented with 0.1% SDS, at a flow rate of 50 µL/min. The response for each analyte was observed in triplicate. All experiments were performed with the Biacore T200 instrument (GE Healthcare) according to the manufacturer's instructions.

3.2.7. *NthiOppA Domain Truncations NthiOppA$_{1A1B}$ and NthiOppA$_2$*

Domain construct nthiOppA$_{1A1B}$ was created by site-directed mutagenesis of nthiOppA, domain II was deleted and replaced with two glycine residues to fuse the C-terminal end of domain I$_A$ to domain I$_B$ (21-290 GG 510-541). NthiOppA$_2$ (291-509) was cloned into the pET-21b vector using the *NdeI* and *XhoI* restriction sites to add a C-terminal His$_6$-tag to the domain. The following primers were used: nthiOppA$_{1A1B}$ forward primer TTGCTAGGCGAAGTATAC GTTACTCGTACCGGCGGCTATGTGAATCCACGCTTAGT, nthiOppA$_{1A1B}$ reverse primer GTAAGGTTTCACTAAGCGTGGATTCACATAGCCGCCGGTACGAGTAACGTATACTT, nthiOppA$_2$ forward primer CACATATGCTAGGAACTTATTCTTATGA, and nthiOppA$_2$ reverse primer CACTCGAGGTTAAAGATTGGTACGATAC. All plasmids were verified by sequencing (ACGT Inc.). The nthiOppA expression and purification conditions were used for nthiOppA$_{1A1B}$ and nthiOppA$_2$.

3.2.8. Circular Dichroism (CD) Spectroscopy

The nthiOppA domain samples were diluted to 16 µM in 5 mM Tris pH 7.5, 15 mM NaCl. CD far-UV spectra were collected using a 0.1 cm quartz cuvette from 260-190 nm in the step scan mode, with 2 nm bandwidth, 4 s response time, and 1.0 nm step speed. Each spectrum is the accumulation of three scans. CD analysis was performed using a J-815 CD spectrometer (JASCO). The spectra show strong helical and β–sheet secondary structure characteristics indicating nthiOppA$_{1A1B}$ and nthiOppA$_2$ are well-folded domains (Figure 3.9A and 3.9B).

3.2.9. Intrinsic Tryptophan Fluorescence Quenching

Solutions of 100 nM nthiOppA, nthiOppA$_{1A1B}$, and nthiOppA$_2$ were prepared in reaction buffer (25 mM HEPES pH 7.5, 150 mM NaCl) for steady-state fluorescence experiments. P4^{GIINTL} was titrated into the protein solution in steps of 0.2 or 10 uM. After each titration step, samples were stirred for at least 5 min, and then left to rest for at least 5 min at RT. Samples were excited at 295 nm and the fluorescence maximum was observed at 329 nm. UV-grade polyacrylic cuvettes with 1 cm path length and excitation and emission slits of 1 mm were used for data collection. All fluorescence intensity experiments were performed using a PC1 photon-counting steady-state fluorometer (ISS). The percent quenching of tryptophan fluorescence at 329 nm versus the P4^{GIINTL} concentration was fit to a single-site binding model using GraphPad Prism 6.0.

3.3. Results

3.3.1. Crystal Structure of Co-purified Peptide NthiOppA Complex

NthiOppA was expressed without the periplasmic signal sequence in *E. coli* and natively

purified the protein using a C-terminal His$_6$-tag. Crystallized nthiOppA was co-purified with bound endogenous peptide, indicated by the additional electron density in the substrate-binding pocket. SBPs are frequently co-purified with their substrates, and OppA homologs have demonstrated a broad specificity for peptides (191,192). The structure was solved by molecular replacement to a resolution of 1.85 Å with space group $P2_1\ 2_1\ 2_1$ and one monomer in the asymmetric unit. In general, SBPs have two structurally conserved globular domains consisting of a β–sheet that is flanked by α-helices (α/β–domains), and the five-strand sheet at the core of each domain is connected by two strands to the opposite α/β–domain. The substrate-binding pocket is formed at the interface of these domains. Specific to the Cluster C SBP family, domain I of nthiOppA is divided into two sub-domains; domain I$_A$ is stitched together from residues 26-41, 210-290 and 510-541 and domain I$_B$ includes residues 42-209. Domain II spans residues 291-509 (Figure 3.1A). The addition of domain I$_B$ makes Cluster C proteins larger than other SBPs in other clusters, and this allows for an expanded binding cavity to accommodate the larger substrates associated with this family of SBPs (3).

When compared to open unbound ecOppA (RMSD = 4.42 Å), structural alignment of nthiOppA indicates a conformational change to the closed peptide-bound state (Figure 3.1B). In the ligand-bound nthiOppA complex, domains I and II rotate toward the center of the protein to bury the peptide in the substrate-binding pocket. Interestingly, even though domains I$_A$ and I$_B$ are structurally independent, they rotate as a rigid domain in respect to domain II. The angle of rotation between the two domains is approximately 35° from the open to the closed conformations. The co-purified peptide binds near the hinge region at the interface between the domains, and domain II provides a binding cleft with the majority of protein-peptide interactions for the bound peptide in the substrate-binding pocket.
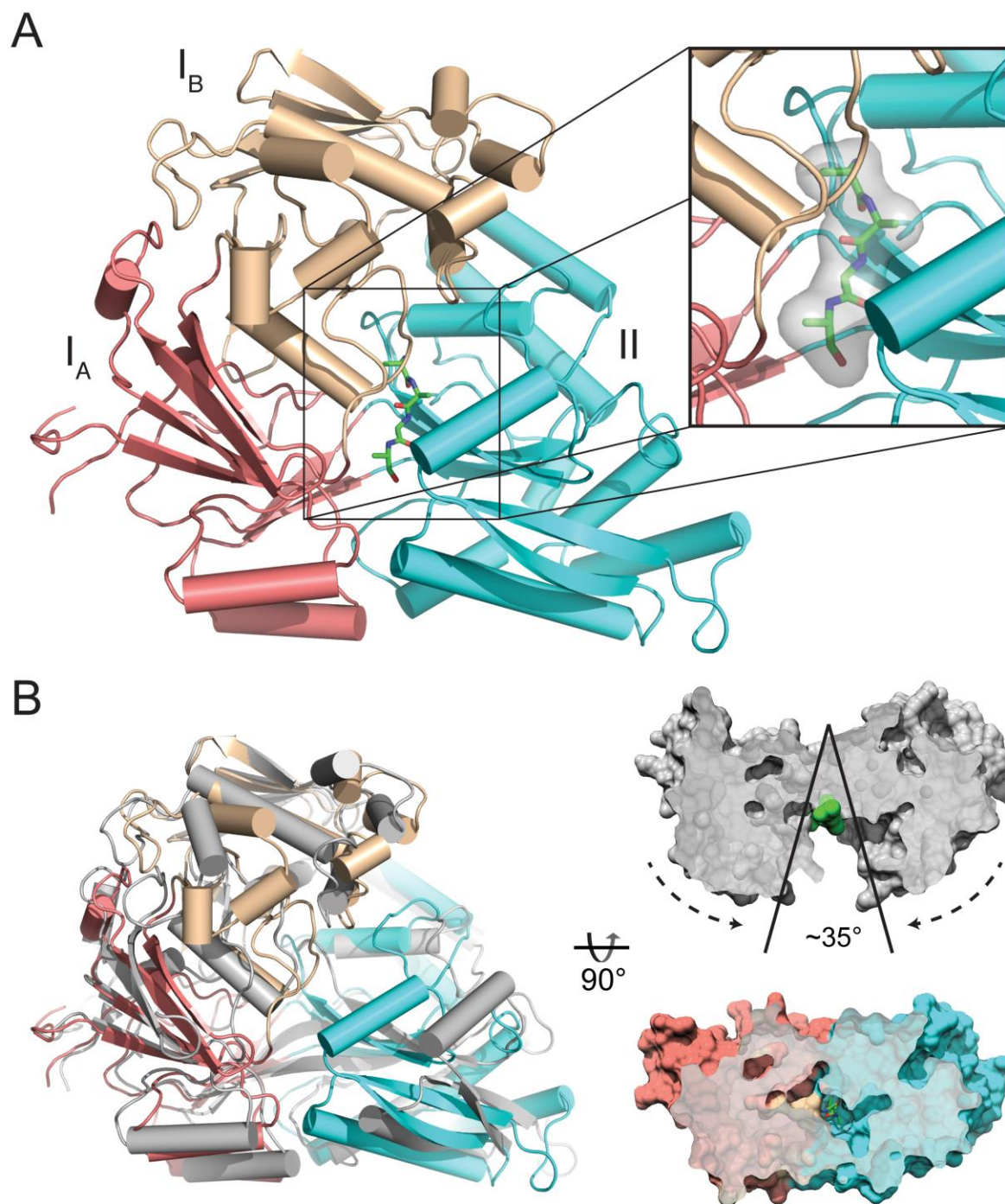
Figure 3.1. Crystal structure of nthiOppA in closed ligand-bound conformation. (A) The crystal structure of nthiOppA, colored by domain (I$_A$, salmon; I$_B$, wheat; II, cyan), bound to co-purified peptide, in green. Inset: surface and stick representation of the co-purified peptide in

substrate-binding pocket. (B) Cartoon representation of the ligand-bound structure of nthiOppA aligned with the open unbound ecOppA structure in gray (PDB code 3TCH), and surface representation cross-sections of ecOppA and nthiOppA. Based on the alignment with nthiOppA, the green spheres in the open unbound ecOppA structure highlight the binding site where peptide interacts with the SBP to form the closed conformation.

3.3.2. *Characterization of NthiOppA Peptide Interactions*

The peptide specificity of nthiOppA was tested using a range of peptides with varying physical properties. Peptides identified as Gram-negative or Gram-positive OppA substrates as well as peptides with an increase in hydrophobicity and length were used in a thermal shift assay. Peptides that increased the stability of nthiOppA (melting temperature, T_m) were identified as binding candidates (Figure 3.2). The following six binding candidates raised the T_m between 2.5 and 6°C, P1 (KKK), P2 (MGG), P3 (LGG), P4 (GIINTL), P5[Long] (YLGANGRGGGS), and P6[Brady] (bradykinin, RPPGFSPFR). P1[KKK] was one of the initial peptides discovered to bind OppA, and peptides P1[KKK] and P6[Brady] were first crystallized bound to seOppA and llOppA, respectively (103,175,193). Additionally, ecOppA has also been shown to have a preference for positively charged peptides with approximately half of co-purified peptides having at least one arginine, histidine or lysine (177). The identified binding candidates indicate peptide specificity of nthiOppA is not limited to 3-5 amino acids peptides. NthiOppA can bind positive and hydrophobic peptides as well as longer peptides similar to Gram-positive OppA homologs.

The novel binding candidate peptides were co-crystallized with nthiOppA. Chemically denatured and refolded nthiOppA co-crystallized with P2[MGG], P3[LGG], and P4[GIINTL] in the same condition as natively purified nthiOppA with similar crystal morphology and diffraction quality. However, P5[Long] co-crystallization produced poorly formed and cracked crystals that reduced diffraction to 9 Å. For the endogenous peptide bound to the natively purified nthiOppA, a four-residue peptide backbone was built and refined in the electron density. The observed electron density of the second residue of the co-purified peptide is large enough to fit a bulky side chain. However, the density for the side chains cannot be easily interpreted to confidently identify residue assignments, which is likely caused by a heterogeneous mixture of co-purified peptides

bound to nthiOppA (Figure 3.2H). Hydrophobic peptides P2^{MGG}, P3^{LGG}, and P4^{GIINTL} have well-resolved electron density representing the bound peptides (Figure 3.2, C-E). The overall structure of nthiOppA does not change dramatically between the different bound peptides with RMSD values from 0.07 to 0.33 Å compared to the co-purified peptide complex. While maintaining the protein-peptide interactions, the flexible binding cavity can accommodate longer peptides.

Bound peptide was successfully removed by chemically denaturing and refolding nthiOppA. Refolded nthiOppA co-crystallized with P2^{MGG}, P3^{LGG}, and P4^{GIINTL} in the same optimized crystallization condition as natively purified nthiOppA. Additional co-crystallization of refolded nthiOppA with P1^{KKK} was not successful and P6^{Brady} produced spherulites. Without added peptide, refolded nthiOppA did not crystallize in the optimized crystallization condition. P1^{KKK}, P5^{Long}, and P6^{Brady} were co-crystallized with natively purified nthiOppA in the optimized crystallization condition and fragmented electron density of the side chains indicates partial exchange of bound peptides (Figure 3.2, B, F, and G). The electron density for P1^{KKK}, P5^{Long}, and P6^{Brady} indicate the N-terminal end of these peptides is in the same location as P2^{MGG}, P3^{LGG} and P4^{GIITNL}. The C-terminal end of P5^{Long} and P6^{Brady} are unresolved in the electron density and likely flexible.

Broad substrate specificity of OppA is mainly regulated through hydrogen bonds to the peptide backbone, with few peptide side chain interactions (177,194). In all of the nthiOppA complexes, the N-terminal end of the bound peptide is secured by a salt bridge (Figure 3.3). In addition to the salt bridge, four hydrogen bonds secure the first residue of peptides in the substrate-binding pocket (Tyr130, two from His441, and Asp443). A second salt bridge also contributes to the binding of the C-terminal ends of the tripeptides. For P2^{MGG}, P3^{LGG}, and the co-purified peptide, hydrogen bonds to both amino and carboxyl groups of the remaining
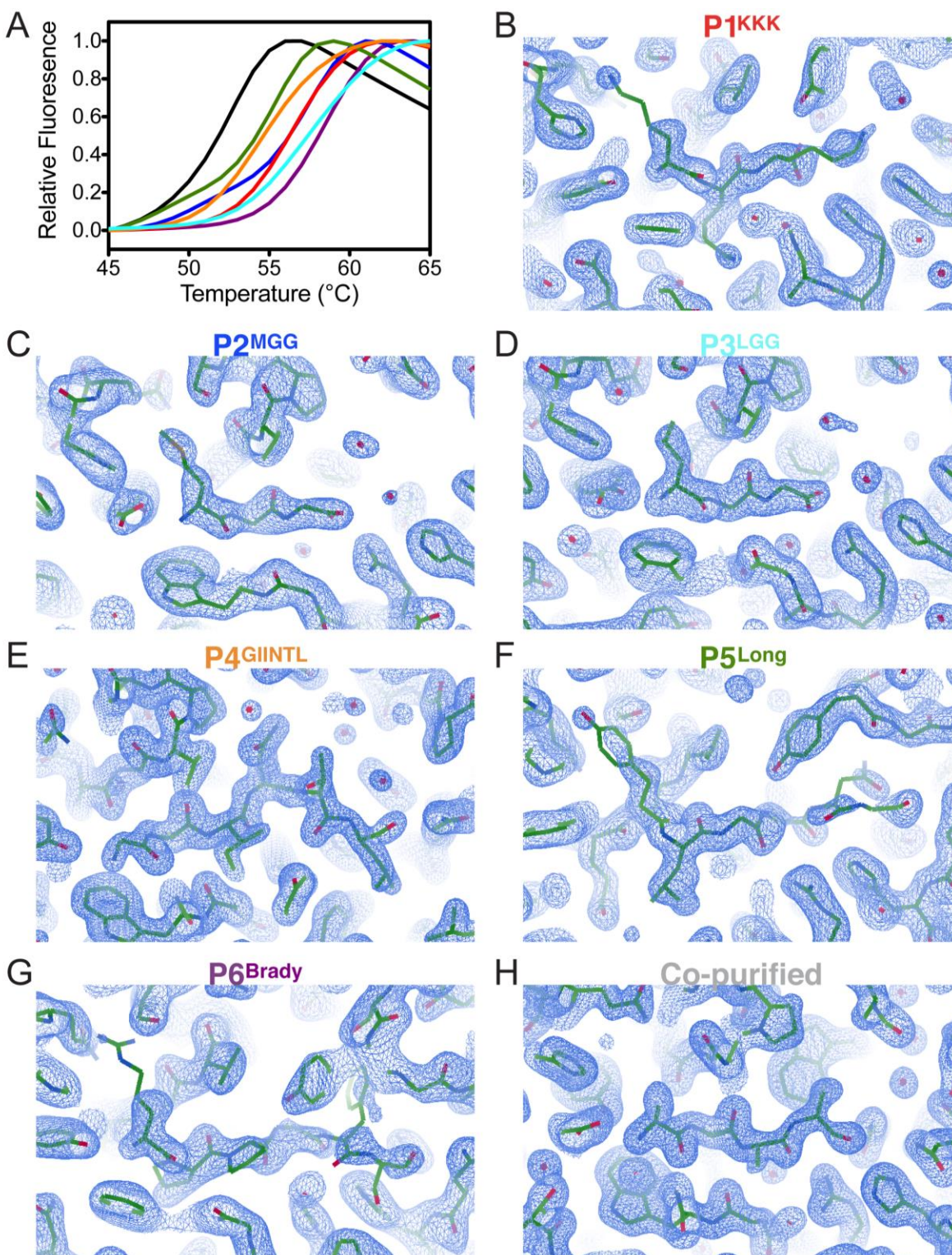
Figure 3.2. Peptide binding and selectivity of the substrate-binding pocket of nthiOppA.

(A) Peptide binding increases the thermal stability of nthiOppA. Refolded nthiOppA is

represented by the black line, and each peptide is represented by the color corresponding to the label above the peptide electron density. A $2F_o-F_c$ omit map was calculated for each of the peptides bound to nthiOppA. (B) P1^{KKK}, (C) P2^{MGG}, (D) P3^{LGG}, (E) P4^{GIINTL}, (F) P5^{Long}, (G) P6^{Brady}, and (H) co-purified peptide share a binding site in the substrate-binding pocket of nthiOppA. The density for the ligand is shown at a contour of 1σ.

residues secure the substrate in the binding pocket. P4$^{\text{GIINTL}}$ has the most peptide-backbone hydrogen bonds involving an additional eight residues Glu52, Val54, Asn388, Asn392, two from Arg437, Gly439, and Tyr509 (Figure 3.3D). The P4$^{\text{GIINTL}}$ complex shows nthiOppA-peptide interactions occur with at least the first six residues of a peptide, providing a platform for nthiOppA to bind longer peptides such as P5$^{\text{Long}}$ and P6$^{\text{Brady}}$. Like the tripeptide complexes, the amino and carbonyl groups of the first three P4$^{\text{GIINTL}}$ residues form hydrogen bonds in the binding cavity, and only the carbonyl groups of the remaining peptide residues hydrogen bond with nthiOppA. With extensive peptide backbone interactions, a salt bridge is not required to stabilize the charged C-terminal end of the hexapeptide.

3.3.3. *Flexible Binding Cavity Accommodates Bulky Ligands*

In the ligand-bound closed conformation, several Gram-positive OppA homologs have flexible substrate-binding pockets that vary in size. The binding cavities efPrgZ, bsAppA, and llOppA range in volume even when bound to long peptides, 1600 Å^3, 2500 Å^3, and 4900 Å^3, respectively (180). Alignment of heptapeptide-bound efPrgZ with the P4$^{\text{GIINTL}}$ complex (RMSD = 1.30 Å) shows a conserved salt bridge and hydrogen bonds to the N-terminal residue of the peptide (Figure 3.4). Similar to other Gram-positive OppA homologs, the P4$^{\text{GIINTL}}$ complex demonstrates the flexibility of the Gram-negative OppA binding cavity by expanding to accommodate a larger substrate and maintaining the peptide interactions in the substrate-binding pocket. Comparing the P2$^{\text{MGG}}$ and the P4$^{\text{GIINTL}}$ complexes, rearrangement of backbone loops and side chains in the substrate-binding pocket widen the binding cavity to prevent steric clashes with the side chains of residues 4 and 5 of P4$^{\text{GIINTL}}$. The side chains of Tyr267 and His441 adopt different rotamer conformations by rotating 89° and 88°, respectively, creating a larger binding
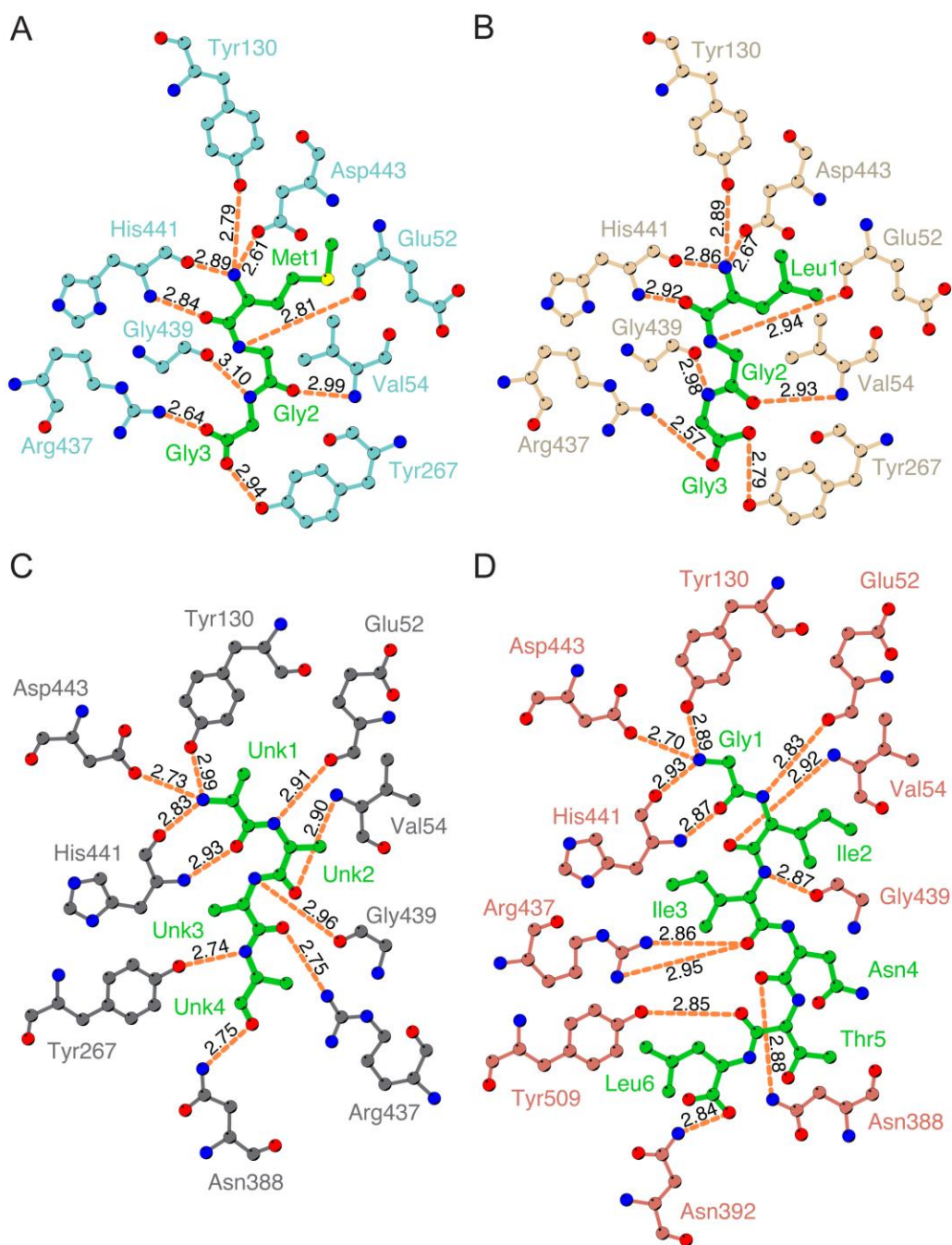
Figure 3.3. Protein-peptide backbone hydrogen bonds are independent of peptide side chains. The hydrogen bond interactions of (A) P2$^{\text{MGG}}$, (B) P3$^{\text{LGG}}$, (C) co-purified peptide, and (D) P4$^{\text{GIITNL}}$ with nthiOppA are represented by orange dashed lines. The bound peptide is shown in green. Hydrogen bond lengths calculated in LigPlot+.
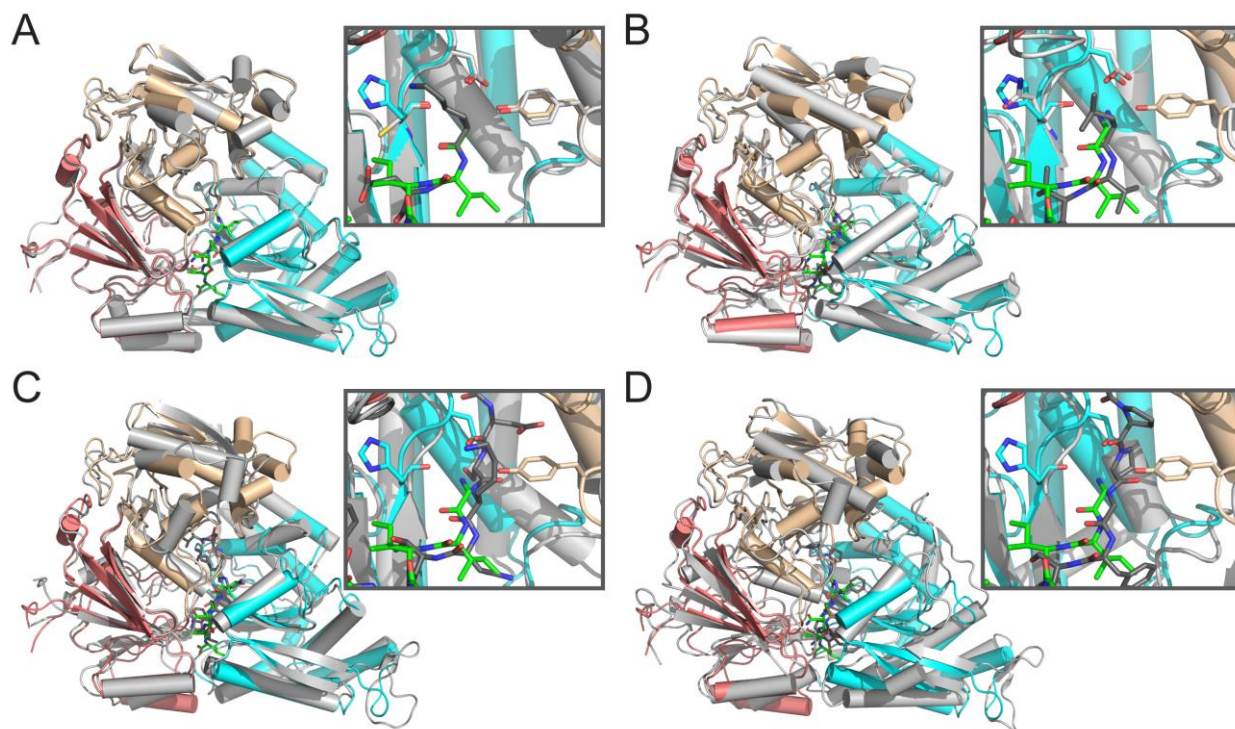
Figure 3.4. Structural alignment of peptide-bound OppA homologs. The peptide-binding site of the P4^{GIINTL} nthiOppA complex is conserved among OppA homologs. The following ligand-bound OppA homologs (light gray) were aligned with nthiOppA (I$_A$, salmon; I$_B$, wheat; II, cyan) bound to P4^{GIINTL} (A) KGE bound ecOppA (PDB code 3TCG, RMSD = 0.72 Å), (B) LVTLVFV bound efPrgZ (PDB code 4FAJ, RMSD = 1.30 Å), (C) VDSKNTSSW bound bsAppA (PDB code 1XOC, RMSD = 2.03 Å), and (D) bradykinin bound llOppA (PDB code 3DRG, RMSD = 3.43 Å). Each inset depicts the N-terminal end of the bound peptides in the substrate-binding pocket with the OppA homolog bound peptide in dark gray and P4^{GIINTL} in green.

pocket for the bound peptide (Figure 3.5).

Additional co-crystallization of nthiOppA with heme was attempted in the optimized crystallization condition and screened for in a new crystallization conditions, but no heme co-crystals were obtained. Therefore, *in silico* heme binding studies of nthiOppA and two other solved Cluster C structures, gpHbpA and ecNikA were used. ROSIE ligand-docking program was used to predict the most likely interactions between the co-purified peptide bound nthiOppA complex and heme. Representative top-ranked solutions for the SBPs show a similar location and ligand position of heme in each protein (Figure 3.6). Based on the docking solutions, movement of backbone loops and side chains in the binding cavities of all three SBPs allows for the docking of heme near the canonical substrate-binding sites. The top-ranked solutions for nthiOppA indicate the substrate-binding pocket could be large enough to accommodate both heme and peptide (Figure 3.6A). The docked heme demonstrates the substrate-binding pocket extends into domain I and is adjacent to the peptide-binding site (Figure 3.7B). Interestingly, the rotations of side chains Tyr267 and His441 in the top-scoring heme docking model of nthiOppA are similar to those observed in the P4^{GIINTL} complex (Figure 3.6D). This model suggests heme binding of nthiOppA does not conflict with peptide-protein interactions and the possibility of a heme-specific cleft in the substrate-binding pocket.

3.3.4. *Accommodating Heme and Peptide in NthiOppA Substrate-Binding Pocket*

To further elucidate the multisubstrate specificity of nthiOppA, the heme and peptide interactions with the substrate-binding pocket were compared. An SPR assay was used to measure the competitive binding between heme and peptide by injecting either ligand alone or together over immobilized nthiOppA. The sum of the individual responses of heme and peptide
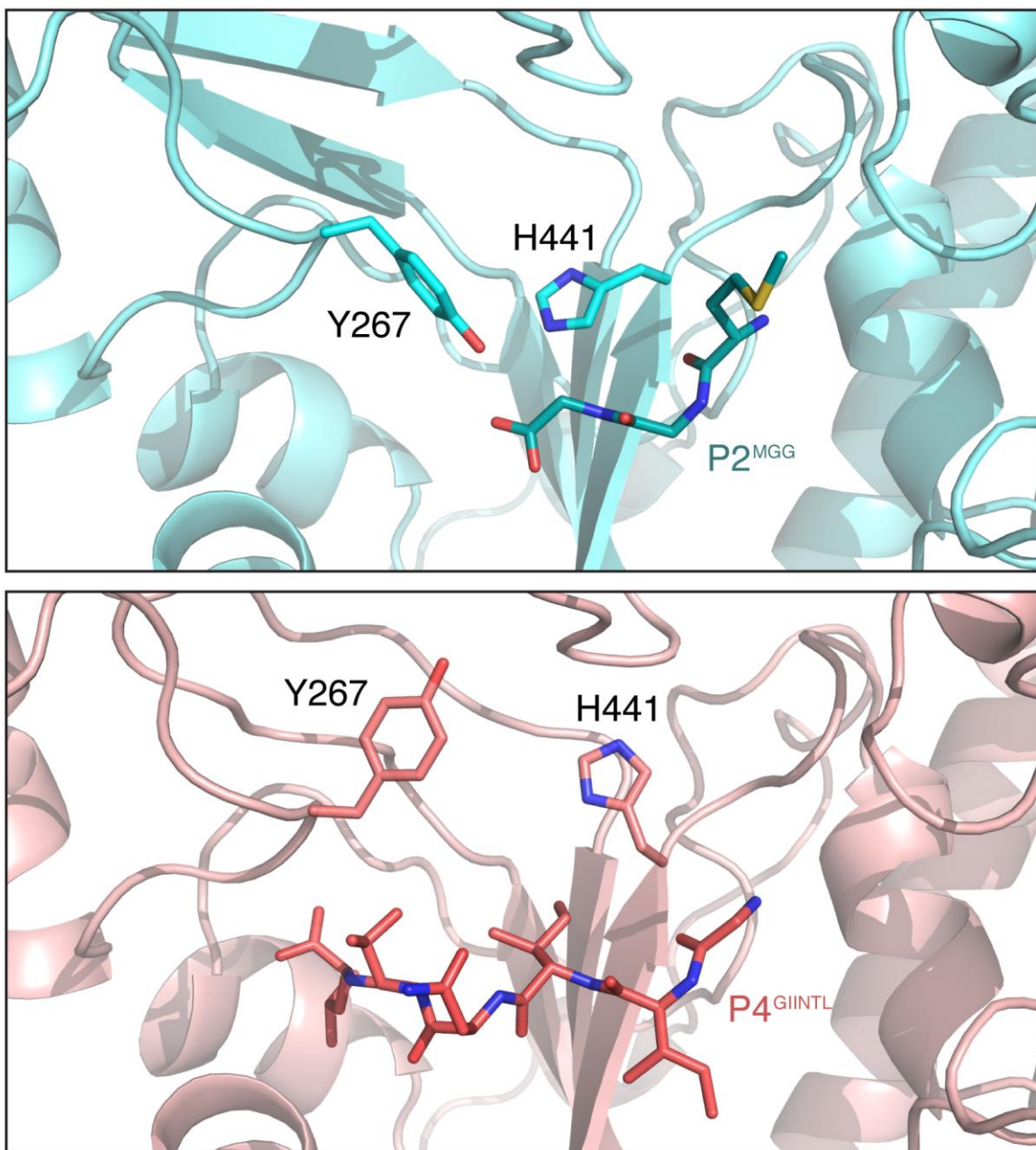
Figure 3.5. Flexible residues allow the substrate-binding pocket to expand and accommodate bulky hydrophobic side chains of bound peptide. Two binding pocket residues, Tyr267 and His441, adopt different rotamer conformations enlarging the binding cavity in the P4$^{\text{GIINTL}}$ complex. The P2$^{\text{MGG}}$ and P4$^{\text{GIINTL}}$ complexes are shown in cyan and salmon, respectively.
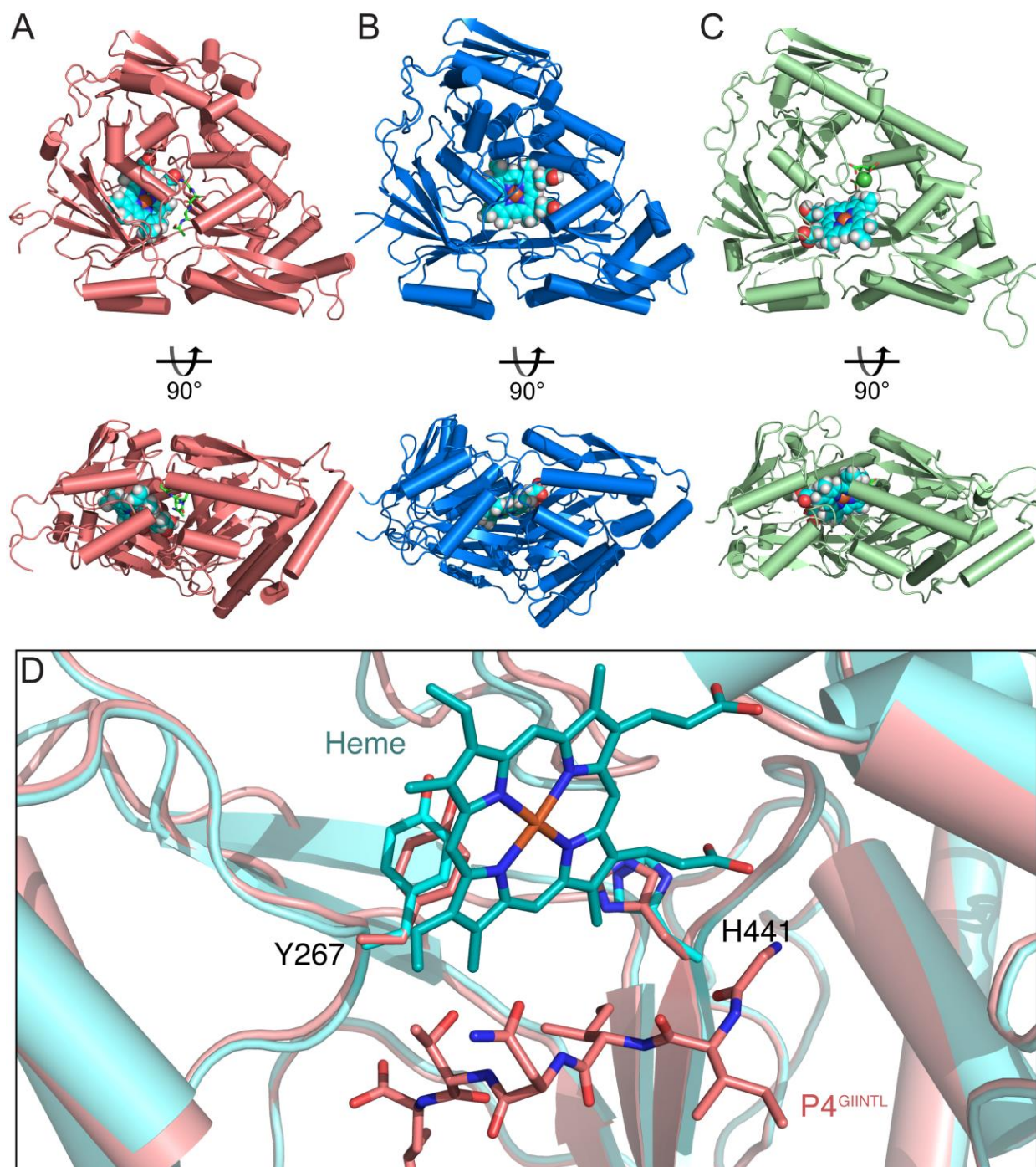
Figure 3.6. Comparing heme docking studies of multiple Cluster C SBPs shows conserved heme-specific cleft in the substrate-binding pocket. Independent of canonical ligand size of these SBPs, structural conservation of Cluster C proteins creates flexible substrate-binding

pockets large enough to accommodate heme binding. (A) A top-scoring model of heme docked in a heme-specific cleft of substrate-binding pocket of nthiOppA. The nthiOppA substrate-binding pocket is large enough to fit two substrates, heme and the co-purified peptide, shown in cyan and green, respectively. The docking model shows both ligands are fully enclosed and buried in the binding pocket. (B) A top-scoring model of gpHbpA (PDB code 3M8U) shows the docked heme in a relatively similar location in binding pocket. (C) A top-scoring heme docked model for ecNikA (PDB code 3DP8) also shows the substrate binding pocket accommodates both heme and butane-1,2,4-tricarboxylate-chelated nickel, shown in green. (D) In the nthiOppA heme docked model shown in cyan, Tyr267 and His441 adopt similar rotamer conformations as the P4$^{\text{GIINTL}}$ complex shown in salmon.
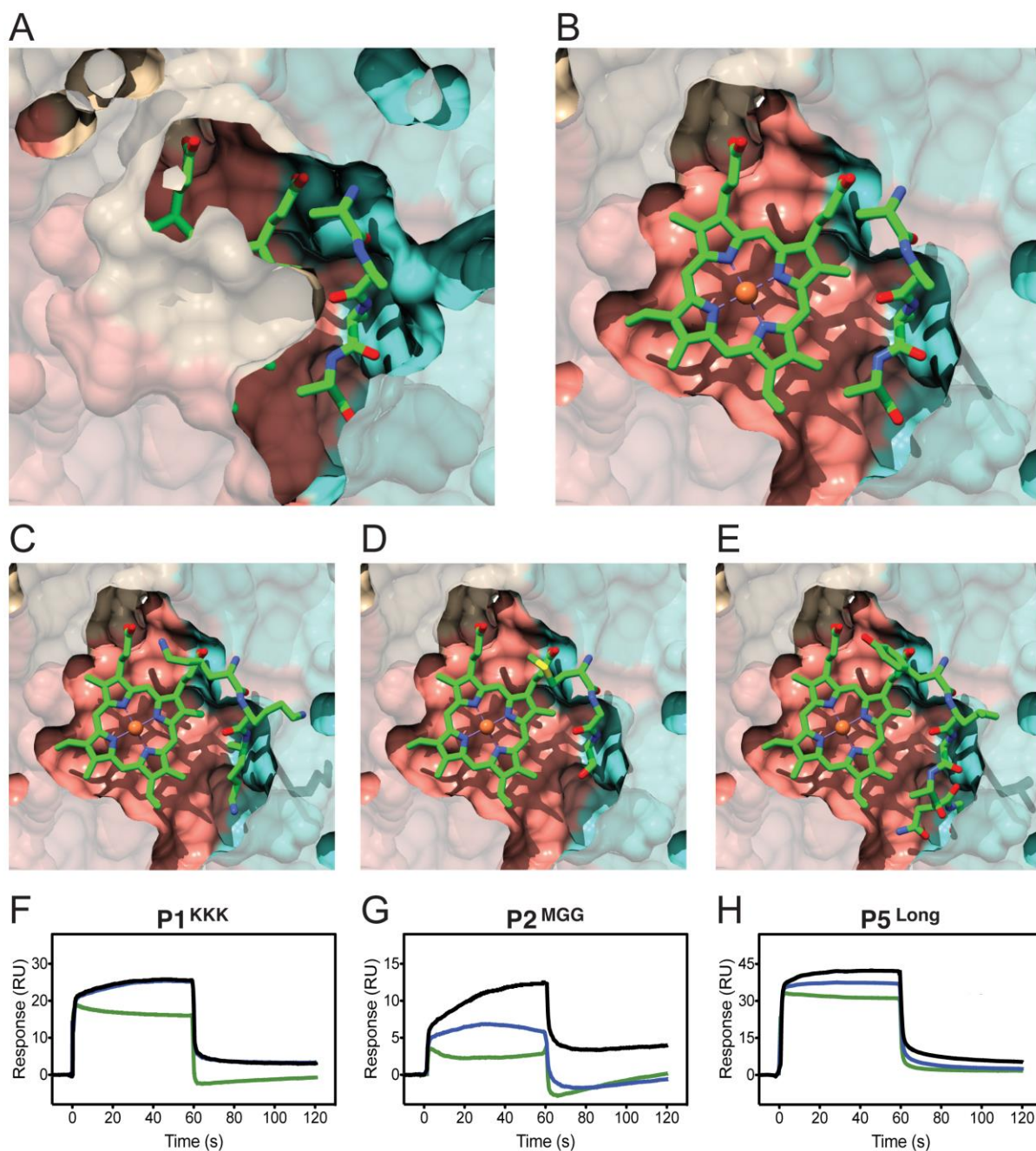
Figure 3.7. Heme-specific binding cleft is independent of bound peptide in the nthiOppA substrate-binding pocket. Cutaway surface representations of the top-scoring ROSIE docking nthiOppA model shows the heme-specific binding cleft does not overlap with the bound peptide. (A) The co-purified peptide discovered in the nthiOppA structure is buried in the peptide-binding

site formed by a majority of hydrogen bonds with domain II. (B) The flexible binding cavity allows for a heme-specific cleft adjacent to the peptide-binding site. Models of (C) P1^{KKK}, (D) P2^{MGG} and (E) P5^{Long} aligned with the heme docking model. A competitive SPR assay was used to measure the ability of heme to bind nthiOppA in the presence of (F) P1^{KKK}, (G) P2^{MGG} or (H) P5^{Long}. The sensograms display the response of peptide binding to nthiOppA, the combined injection of heme and peptide and the theoretical sum model of the individual heme and peptide injections in green, blue and black lines, respectively.

were used to determine the theoretical response of both heme and peptide binding to the substrate pocket simultaneously. In the case of heme binding independent of peptide binding, we would expect the observed SPR response of the combined ligands to correspond to the theoretical sum of the independent heme and the peptide responses. For competitive binding of heme, we would expect a reduction of the observed SPR response of an injection with both ligands in comparison to the theoretical sum of the individual responses of heme and peptide. The SPR competition assay probes the availability of a heme-specific cleft in the presence of bound peptide in the substrate-binding pocket.

Using this experimental design, P1^{KKK}, P2^{MGG}, and P5^{Long} were injected at a high concentration to load the peptide-specific site of the nthiOppA binding pocket. The SPR sensograms of the individual peptide response and the combined heme and peptide response were collected for each peptide. The theoretical sum of the individual peptide and heme responses were calculated and compared to the observed combined heme and peptide response for each peptide (Figure 3.7). The observed SPR response of the combined heme and P1^{KKK} injection matched the theoretical sum of the responses for both ligands. For P1^{KKK}, heme does not compete for binding at the peptide-specific binding site, and heme binding is independent of bound peptide (Figure 3.7F). This is evidence of a heme-specific cleft in the substrate-binding pocket and corresponds with the heme docking studies that predict bound peptide does not exclude heme binding. The combined heme and peptide injections of P2^{MGG} and P5^{Long} are lower than the theoretical sum of the individual responses. In these cases, the presence of peptide does limit, but does not abolish heme binding (Figure 3.7, G and H). In the ligand-bound closed conformation of P2^{MGG} and P5^{Long} complexes, steric hindrance of the bulky and rigid side chains or occlusion of the channel to the heme-specific binding cleft reduces heme binding. These

competition assays show heme does not directly compete with peptide binding and disruptions in heme and peptide binding are likely influenced by a heme-specific binding cleft in close proximity to the peptide binding site.

3.3.5. *Differential Substrate Binding of NthiOppA Domains*

To further expand our knowledge of nthiOppA substrate binding, the individual domains of nthiOppA, nthiOppA$_{1A1B}$ and nthiOppA$_2$ were expressed and purified (Figure 3.8, A and B). Using SPR, I determined nthiOppA$_{1A1B}$ has about four-fold higher affinity for heme than nthiOppA$_2$ with K_D values of 577 nM and 2.46 μM, respectively (Figure 3.8, C and D). NthiOppA$_{1A1B}$ binds heme with a similar affinity to nthiOppA. This corresponds with the heme docking studies, which identified domain I as playing a major role in the formation of a heme-specific cleft in the binding cavity. An intrinsic tryptophan fluorescence quenching assay was used to test the ability of the individual OppA domains to bind the hexapeptide. This assay determined P4^{GIINTL} binds nthiOppA$_2$ with a K_D value of 172 nM, and nthiOppA$_{1A1B}$ has a weaker affinity with a K_D value of 11.7 μM (Figure 3.8, E and F). Peptide binding of nthiOppA is largely mediated through interactions with domain II, and nthiOppA$_2$ has a similar heme affinity as nthiOppA with a K_D value of 754 nM (Figure 3.9). Notably, there are two hydrogen bonds and a salt bridge between residues in domain II and the N-terminal residue of the bound peptide. Based on these binding studies, each domain plays a differential role in binding both substrates with domain I directing heme binding and domain II driving P4^{GIINTL} binding of nthiOppA.
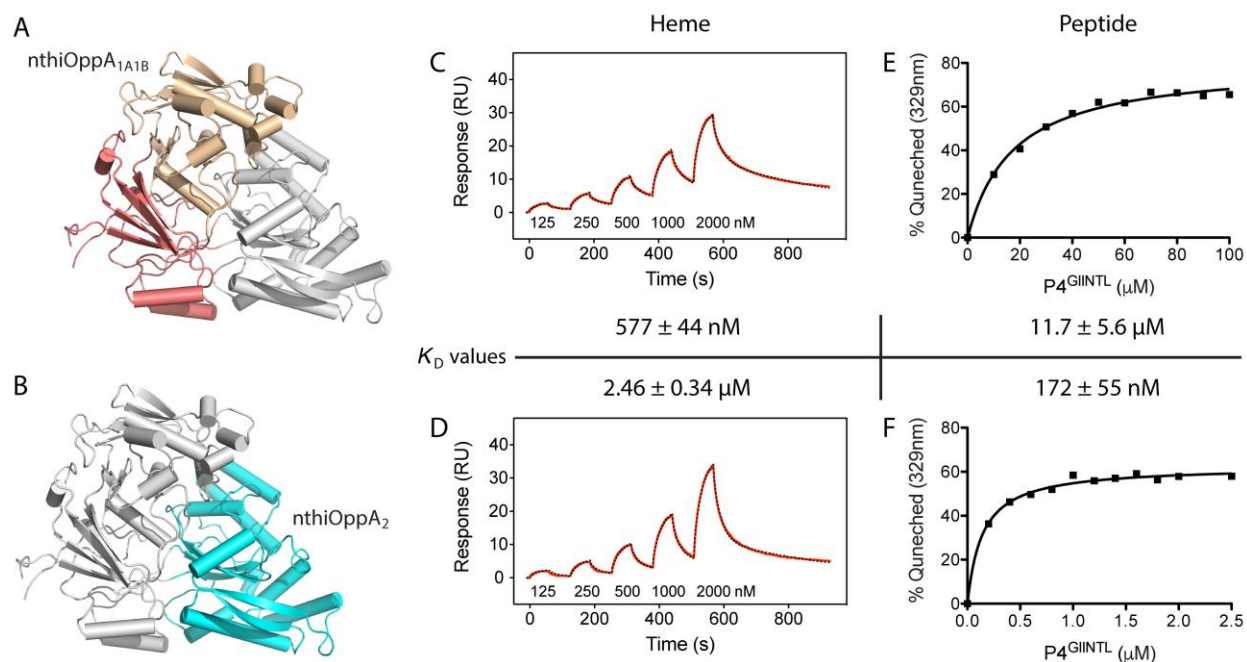
Figure 3.8. NthiOppA_{1A1B} and nthiOppA_2 differentially bind heme and peptide substrates. Cartoon represntations of individual nthiOppA domains, (A) nthiOppA_{1A1B} and (B) nthiOppA_2 are highlighted in salmon/wheat and cyan, respectively. Single-cycle kinetic analysis of (C) nthiOppA_{1A1B} and (D) nthiOppA_2 heme binding. Each sensogram depicts representative data fit to a 1:1 two-state reaction model, shown in red and dashed black lines, respectively. Calculated kinetic constants shown in Table 3.3. The tryptophan fluorescence quenching of (E) nthiOppA_{1A1B} and (F) nthiOppA_2 upon P4^{GIINTL} binding. Representative data shown fit to a one-site binding model.

Table 3.3. Heme kinetic constants of nthiOppA domains.

	k_{a1} $M^{-1}s^{-1}$	k_{d1} s^{-1}	k_{a2} s^{-1}	k_{d2} s^{-1}
nthiOppA 1A1B	1.23 (0.04) x 10^4	2.66 (0.12) x 10^{-2}	6.88 (0.30) x 10^{-3}	2.50 (0.10) x 10^{-3}
nthiOppA 2	5.78 (0.54) x 10^3	3.72 (0.07) x 10^{-2}	4.65 (0.06) x 10^{-3}	2.84 (0.10) x 10^{-3}

* Standard deviation shown in parentheses
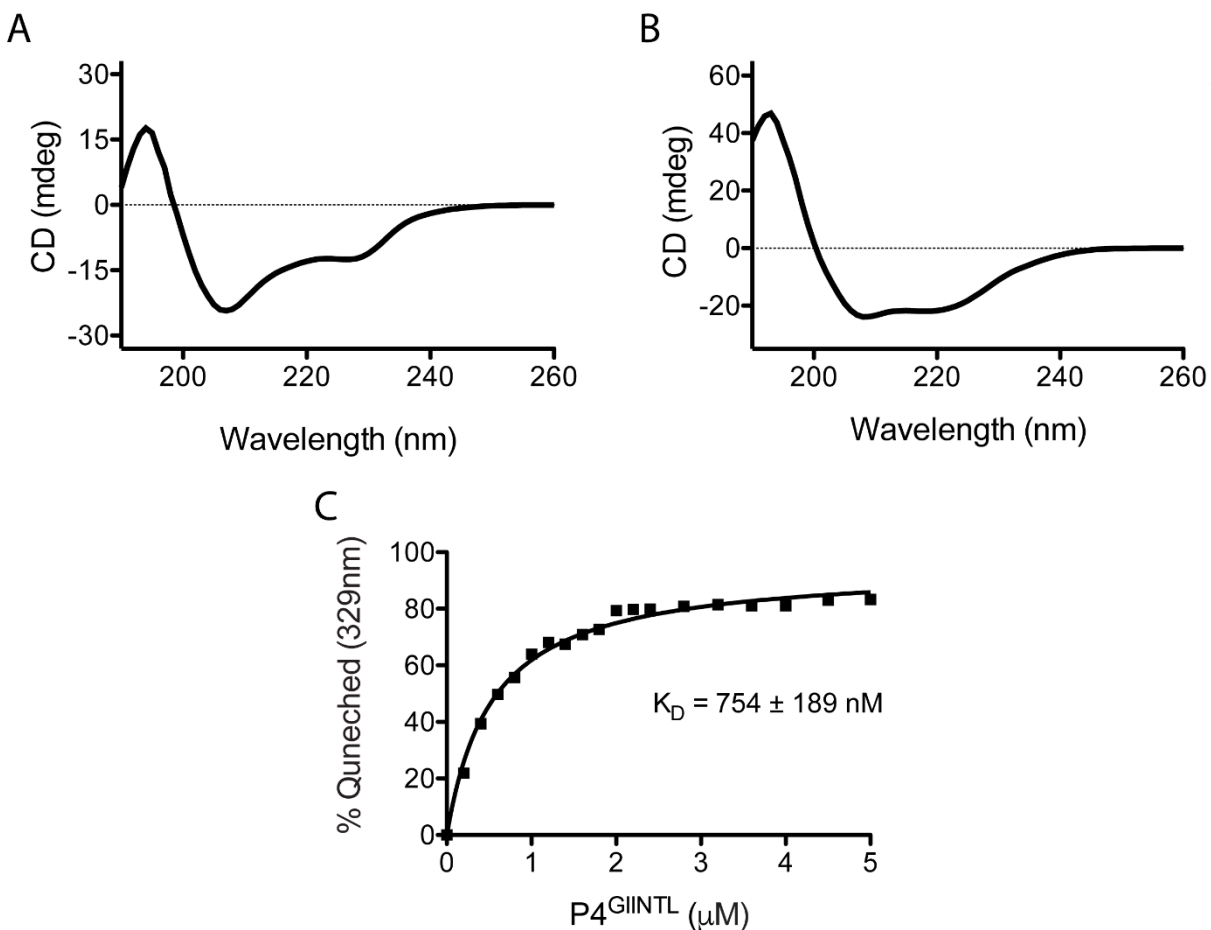
Figure 3.9. Domain truncation does not disrupt the overall structure of the individual nthiOppA domains. The far UV CD spectra of the (A) nthiOppA$_{1A1B}$ and (B) nthiOppA$_2$ correspond to the anticipated secondary structure content of the individual domains. The α/β–domain of nthiOppA$_2$ consists of several α–helical structures surrounding the β–sheet, and the secondary structure properties of nthiOppA$_{1A1B}$ contain a higher proportion of flexible loops connecting domains I$_A$ and I$_B$. (C) The quenching of nthiOppA tryptophan fluorescence with the titration of P4^{GIINTL}. NthiOppA was used as a control to compare nthiOppA$_{IAIB}$ and nthiOppA$_{II}$ peptide binding affinities. Representative data shown fit to a one-site binding model.

3.4. Discussion

NTHi employs Cluster C SBPs to scavenge essential nutrients and adapt to rapidly changing microenvironments in the host. In Gram-negative *M. catarrhalis, oppA* is necessary for invasion of human respiratory epithelial cells and persistence during infection (84). Both mcOppA and its transporter are capable of binding and importing peptides up to 10 amino acids which is comparable to the binding capacity of other Gram-positive OppA homologs (104). In addition to nutrient uptake, Gram-negative OppA plays a role in proteostasis of the periplasm. To aid in protein folding, ecOppA acts as a protein chaperone in the periplasm (195,196). OppA can assist in the recycling of misfolded periplasmic proteins by transporting protease-degraded peptides into the cytoplasm for reuse as a nutrient source.

Broadening our understanding of Gram-negative OppA peptide specificity is important for determining peptide utilization for essential nutrients and signaling pathways. Prior to this work, peptide specificity of Gram-negative OppA homologs was believed to be limited to tri- and tetrapeptide substrates. This data shows nthiOppA bound to a longer peptide than previously observed in other Gram-negative OppA structures. The protein-peptide hydrogen bond interactions of the tripeptide bound nthiOppA structures are maintained in the novel hexapeptide bound complex and demonstrate peptide recognition of this SBP is independent of the length and amino acid composition of these peptides. The P4$^{\text{GIINTL}}$ nthiOppA structure highlights the flexibility of the binding cavity that expands to accommodate the hexapeptide. These findings bridge the peptide specificity of Gram-negative and Gram-positive OppA proteins and highlight the similarities of these SBPs.

The binding studies presented in this work have identified heme as a novel substrate for nthiOppA. The SPR competition assays observed a distinct heme-specific binding cleft separate

from the peptide-binding site of nthiOppA and determined heme binding is not completely inhibited by bound peptide. This demonstrates the substrate-binding pocket of nthiOppA is capable of expanding to accommodate larger peptides, and that heme and peptide substrates can coexist in the binding pocket. The substrate-binding pocket is formed at the interface of the nthiOppA domains with each domain playing a differential role in substrate binding, heme binding is managed by domain I and peptide binding in controlled by domain II.

We suspect the multifunctional role of OppA helps NTHi survive in the hostile host environment. The ligand-specific sites in the binding cavity allow nthiOppA to accommodate both heme and peptide for the uptake of these essential nutrients. The cooperation and competition between substrates in the binding cavities of Cluster C SBPs will determine which substrates are delivered to ABC importers for transport. Next, we turn our attention to another multisubstrate NTHi SBP that binds heme in addition to its canonical substrate to understand how these proteins can recognize a few unique substrates with high affinity. In Chapter 4, we will explore the canonical substrate binding of another Cluster C SBP by characterizing the ability of nthiSapA to recognize AMPs.

CHAPTER 4:

Structural and Mechanistic Studies of the Sensitivity to Antimicrobial Peptides (Sap)

System

4.1. Introduction

4.1.1. Antimicrobial peptides (AMPs) in Immune Defense

The focus of this chapter was to understand how the ability of the SBPs to recognize distinct substrates plays a role in the bacterial response to the host immune defense. A major component of the host innate immune response is the production of small cationic AMPs, conserved from plants to humans, with antimicrobial activity against a variety of viruses, bacteria, fungi and parasites (197-199). Two major families of AMPs peptides are cathelicidins and defensins that act as effector molecules in host-pathogen interactions. These positively charged amphipathic peptides range in size from about 20 to 50 amino acids and selectively target microbial cell membranes. The general bactericidal mechanism of these AMPs is that the peptides collect on the surface of bacteria causing perturbation of the lipid membrane and this leads to rapid cell death (200).

AMPs are derived from inactive propeptide precursors, and proteolytic cleavage of the C-terminal antimicrobial domain activates the AMPs. The human cathelicidin propeptide hCAP-18 is processed to create α-helical AMP hLL-37. Cathelicidin is produced by many cells in the body but large amounts of this AMP precursor are localized in neutrophil granules (201). Once activated, hLL-37 stimulates host defense pathways by inducing ROS production and phagocytosis by neutrophils (202). Cathelicidin moderates overreaction of the inflammatory response to bacterial infection by preventing activated neutrophils and macrophages from stimulating proinflammatory mechanisms and reducing the harmful effects of endotoxin (203).

In the human airway, α-defensins are packaged in neutrophil granules and epithelial cells produce β-defensins (204,205). Defensins are cysteine-rich AMPs with three intramolecular disulfide bridges, a conserved structural characteristic called a γ-core motif (206). Even with a

high level of sequence diversity, defensins share a common secondary structure signature with a β-hairpin in a three-strand antiparallel β-sheet. The two main subfamilies are classified by their conserved disulfide bond motifs, α-defensins (C_1-C_6, C_2-C_4, C_3-C_5) and β-defensins (C_1-C_5, C_2-C_4, C_3-C_6). In addition to antimicrobial activity, defensins can inhibit bacterial toxins, act as a chemoattractant for macrophages, and effector molecules in inflammation, immune activation and wound healing (207-209).

4.1.2. *Host Response to NTHi Infection*

In a healthy state in the nasopharynx, the host and bacteria maintain homeostasis by balancing the NTHi-induced AMP immune response. When this balance is lost, NTHi spreads to the middle ear causing OM infections. Middle ear epithelial cells detect bacteria through pathogen-associated molecular patterns (PAMPs). NTHi is recognized by Toll-like receptor 2 (TLR2) signaling the mitogen activated protein kinase (MAPK) pathway to mobilize the immune response (210). Defensins including α-defensin 1 (hNP1), hBD2, and hBD3 are likely to be the most potent AMPs in response to NTHi infections (211-213). HNP1 has a positive net charge +3 and has 30 amino acids. The β-defensins, hBD2 and hBD3, are larger with 41 and 45 amino acids and net charges of +6 and +11, respectively. When hBD3 homolog cBD1 is used as an intranasal treatment in the OM infection animal model, NTHi colonization of the chinchilla nasopharynx was drastically reduced (214). Additionally, coinfection with respiratory syncytial virus (RSV) lead to the decrease in expression of the hBD3 homolog in the chinchilla animal model and allowed NTHi to flourish in the upper respiratory tract (215). Quantification of defensins during OM infection in the middle ear fluid of patients has not yet been evaluated.

4.1.3. *Sap Importer Required for Heme Uptake and AMP Resistance*

NTHi has developed protective mechanisms to evade the host-mediated response, including biofilm formation, alterations to the cellular membrane, inhibiting neutrophil chemotaxis, invasion of host cells, avoiding phagocytosis, and AMP resistance (141,216-219). The Sap transport system mediates NTHi-host interactions through nutrient uptake and AMP resistance, and the *sap* gene cluster is up-regulated during OM infection (109). In addition to nthiSapA, the NTHi *sap* gene cluster includes two TMDs nthiSapB and nthiSapC, followed by two NBDs nthiSapD and nthiSapF, and putative membrane protein nthiSapZ. NthiSapZ is not widely conserved in the *sap* operon and has only been identified in *E. coli*, *N. meningitidis*, *Pasteurella multocida*, *P. aeruginosa*, *S. enterica*, and *S.* Typhimurium gene clusters (109). Multiple components of the Sap transport system are known to be essential for NTHi colonization and virulence. Mutations in nthiSapA, nthiSapD, and nthiSapF have similar phenotypes in OM infection models with attenuated survival in the nasopharynx and middle ear of chinchillas compared to the parent strain (109,115,153). The role of TMD components in colonization and virulence of NTHi has not been published. However, the TMDs are needed for formation of a functional Sap transporter and, similar to the NBDs, are also likely necessary for NTHi survival.

The individual Sap components contribute to the distinct functional roles of the Sap transporter in the nutrient uptake and antimicrobial resistance. NthiSapA is necessary for survival after heme starvation and evading the bactericidal activity of AMPs (109,110). In NTHi, the role of the TMDs in heme uptake has focused on the combined function of nthiSapB and nthiSapC. A mutant strain lacking both TMDs, *sapB* and *sapC*, was unable to efficiently transport heme across the inner membrane of NTHi (110). Unlike the NTHi parent strain that

prevents AMPs from building up on the cell membrane, hBD3 and hLL-37 accumulate on the cell surface of a double mutant *sapB sapC* strain and are not transported to the cytoplasm for degradation (113). The individual NBD genes play differential roles in nutrient uptake and AMP resistance. NthiSapF is essential for NTHi survival in heme-starved growth conditions (153). However, nthiSapD is not thought to play a role in heme uptake but has been shown to be necessary for potassium uptake through the Trk system (115,220). NTHi parent and *sapF* mutant strains are resistant to AMPs hBD3 and hLL-37. However, the mutant *sapD* strain is susceptible to both AMPs (153). NthiSapD is also necessary for NTHi resistance against cBD1 (115).

A better understanding of how nthiSapA selects substrates for delivery to the Sap transporter will help to elucidate the multifunctional role this system plays in heme uptake and antimicrobial resistance. Functional and structural studies were used to better understand substrate recognition of nthiSapA. In comparison to other peptide SBPs such as DppA and OppA, nthiSapA is capable of binding more complex and larger peptides. Our collaborator Kevin Mason identified nthiSapA mediates antimicrobial activity of hNP1, hBD2 and hBD3. SPR was used to investigate the binding affinity of nthiSapA for these defensin AMPs. Simplified AMP peptides containing the loop region of hNP1, hBD2, and hBD3 were synthesized to determine the role of the conserved γ-core motif 3D structure in nthiSapA specificity and binding. NthiSapA recognizes the loop region of all three defensin AMPs with similar affinity as the full-length peptides. Additionally, AMP recognition and binding affinity of nthiSapA is not dependent on the structure of the loop region. This work highlights the ability of nthiSapA to bind hNP1, hBD2 and hBD3 with high affinity, despite their differences in peptide sequence, length and net charge.

4.2. Experimental Procedures

4.2.1. Materials

Recombinant hNP1, hBD2, hBD3, and hLL-37 were purchased from PeproTech. Synthetic hNP1 and hBD2 were purchased from Peptide International. Custom peptides hNP1$_{loop}$, hBD2$_{loop}$ and hBD3$_{loop}$ (>95% pure) were purchased from GenScript. All peptides were solubilized according to manufacture recommendations.

4.2.2. Expression Vectors and Initial Expression Trials of Sap Transporter Components

Sap transporter components, nthiSapB, nthiSapC, nthiSapD, and nthiSapF, were amplified from the genomic DNA of a clinical strain of NTHi 86-028NP. Multiple protein tags were tested to optimize solubility of the Sap transporter components, and dual expression vectors were trialed to improve assembly of the Sap transporter components. Constructs were designed with ligation independent cloning (LIC) primers. For N-terminal tag expression vectors the following primers were used, forward primer TACTTCCAATCCAATGCA and reverse primer TTATCCACTTCCAATGTTA, and for C-terminal tag expression vectors the following forward primer GTCTCTCCCATG and reverse primer GGTTCTCCCCAGC were used. Using the LIC technique, Sap transporter components were cloned into MSCG vectors with various tags, summarized in Table 4.1. All plasmids were verified by sequencing (ACGT Inc.).

Sap transporter components were transformed in BL21(DE3), C41(DE3), and C43(DE3) strains for expression testing. The initial Sap transporter component constructs and the results of the expression trials with different protein tags are summarized in Table 4.1. In brief, cells were cultured in Terrific Broth media with the appropriate antibiotics. Cultures were grown at 37°C to an OD$_{600}$ of 0.4, and then the incubator was then cooled to 16°C. Cells were induced with 400

Table 4.1. Sap transporter components construct design and expression trials.

	TOPO100D 1st position	TOPO100D 2nd position	TOPO100D 3rd position	MCSG7 1st position	MCSG7 2nd position	MCSG8 1st postion	MCSG8 2nd position	MCSG12 1st promoter	MCSG12 2nd promoter	MCSG21 1st promoter	MCSG21 2nd promoter	MCSG28 One postion	pET22b 1st position	pET22b 2nd position
Tag location	N-term tag											C-term tag		
Promoter	One promoter							Two promoters				One promoter		
Vector	TOPO100D ampicillin			MCSG7 ampicillin		MCSG8 ampicillin		MCSG12 kanamycin		MCSG21 spectomycin		MCSG28 ampicillin	pET22b ampicillin	
Gene position	1st position	2nd position	3rd position	1st position	2nd position	1st postion	2nd position	1st promoter	2nd promoter	1st promoter	2nd promoter	One postion	1st position	2nd position
Cloning site	RE, cloned operon			RE	LIC	RE	LIC	RE	LIC	RE	LIC	LIC	RE, operon	
Gene tag	His	No tag	No tag	His	His	His	Sloop	His	Sloop	His	His	His	FLAG	His
SapB	XOS				Xn		Xn				XO	Xn		
SapC	XOS				XOS		XO				XOS	Xn		
SapD					XPS		XO		XOS		XP	XOS		
SapF					XPS		XO		XOS		XP	XOS		
SapBCD	XOS	Xn	Xn											
SapBC										XnN	XnM			
SapBD	XOS	Xn						XnN	XOM	XnN	XOM			
SapBF								Xn	XO	Xn	XOS			
SapCD	XOS	Xn						XnN	XOM	Xn	XO			
SapCF								Xn	XOS	Xn	XOS			
SapDF								Xn	XOS	Xn	XOS			
SapFD								Xn	XOS	Xn	XO			
SapDB										Xn	Xn		XnN	XN (His false +)
SapFB										XOS	Xn		XOM	XN (His false +)
SapDC										Xn	Xn		XOM	XN (His false +)
SapFC										XOS	XOS		XOM	XN (His false +)
SapZ					Xn		Xn	Xn		Xn				

Cloned by Mason Lab   Cloned by M. Lab

X = Cloned
O = Expression via western
P = Expression in Pellet via western
n = No expression via western
M = Expression in Membrane via western
N = No expression in Membrane via western
S = Purified and soluble

μM IPTG at an OD_{600} of 0.8. Samples were taken at 0 h, 2 h, 6 h, and ON, and an anti-His western blot of the expression time points were used to determine protein expression levels. Expression vectors with different antibiotic markers were cotransformed in an *E. coli* strain for coexpression of multiple Sap transporter components at one time (Table 4.2). In addition to the expression conditions mentioned above, coexpression was also tested using cells grown in Luria Broth media with the appropriate antibiotics at 37°C. Cells were induced with 400 μM IPTG at an OD_{600} of 0.6. Samples were taking at 0 h, 1 h, 2 h and 3 h to determine the level of protein expression.

4.2.3. *Expression and Purification of NthiSapC, NthiSapD and NthiSapF*

Individual Sap transporter components were expressed under the following optimized conditions. To express TMD nthiSapC, an overnight culture of nthiSapC MCSG7 in BL21(DE3) was diluted 1:1000 into 1 L Terrific Broth media supplemented with 100 μg/mL ampicillin. For expression of nthiSapD, an overnight culture of nthiSapD MCSG12 in BL21(DE3) was diluted 1:1000 into 1 L Terrific Broth media supplemented with 34 μg/mL chloramphenicol. The same expression conditions were used for nthiSapC and nthiSapF. Cells were grown at 37°C to OD_{600} of 0.4 and then the incubator was cooled to 16°C. At an OD_{600} of 0.8, cells were induced with 400 μM IPTG. Protein was expressed overnight. A shorter expression time and warmer temperature were used for nthiSapF expression. An overnight culture of nthiSapF MCSG7 in BL21(DE3) was diluted 1:1000 into 1 L Luria Broth media supplemented with 100 μg/mL ampicillin. Cells were grown at 37°C to OD_{600} of 0.6 and induced with 400 μM IPTG. Protein was expressed for 3 h at 37°C. After protein expression, cells were harvested by centrifugation at 5000 rpm and cell pellets were stored at -80°C.

Table 4.2. Dual expression trials of Sap transporter component.

Tag location	N-term tag			
Promoter	One promoter		Two promoters	
Vector	TOPO100D AMP	MCSG7 AMP	MCSG12 CAM	MCSG21 SPEC
Gene position	1st position	2nd position (LIC site)	2nd promoter (LIC site)	2nd promoter (LIC site)
Gene tag	His	His	Sloop	His
SapB_D	SapB O = BL21 LB 37C 3h		SapD P = BL21 LB 37C 3h	
			SapD n = BL21 LB 37C 3h n = BL21 TB 16C ON n = C41 TB 16C ON n = C43 TB 16C ON n = C41 LB 37C 3h n = C43 LB 37C 3h	SapB n = BL21 LB 37C 3h n = BL21 TB 16C ON n = C41 TB 16C ON n = C43 TB 16C ON O = C41 LB 37C 3h O = C43 LB 37C 3h
SapB_F	SapB O = BL21 LB 37C 3h		SapF O = BL21 LB 37C 3h	
			SapF n = BL21 LB 37C 3h n = BL21 TB 16C ON nN = C41 TB 16C ON n = C43 TB 16C ON O = C41 LB 37C 3h n = C43 LB 37C 3h	SapB n = BL21 LB 37C 3h O = BL21 TB 16C ON OMV = C41 TB 16C ON O = C43 TB 16C ON O = C41 LB 37C 3h O = C43 LB 37C 3h
SapC_D		SapC OM = C41 LB 37C 3h O = C43 LB 37C 3h	SapD PN = C41 LB 37C 3h P = C43 LB 37C 3h	
			SapD n = BL21 LB 37C 3h n = BL21 TB 16C ON P = C41 TB 16C ON P = C43 TB 16C ON	SapC n = BL21 LB 37C 3h n = BL21 TB 16C ON O = C41 TB 16C ON O = C43 TB 16C ON
SapC_F		SapC OMV = C41 LB 37C 3h O = C43 LB 37C 3h	SapF OMV = C41 LB 37C 3h O = C43 LB 37C 3h	
			SapF n = BL21 LB 37C 3h O = BL21 TB 16C ON O = C41 TB 16C ON O = C43 TB 16C ON	SapC n = BL21 LB 37C 3h O = BL21 TB 16C ON O = C41 TB 16C ON O = C43 TB 16C ON
SapD_F			SapD n = BL21 LB 37C 3h	SapF O = BL21 LB 37C 3h
SapDC				SapD 1st promoter His SapC 2nd promoter His O = BL21 TB 16C ON
SapFC				SapF 1st promoter His SapC 2nd promoter His OMV=BL21 TB 16C ON

SapFD			SapF 1st promoter His SapD 2nd promoter Sloop O = BL21 TB 16C ON	SapF 1st promoter His SapD 2nd promoter His O = BL21 TB 16C ON
SapDB				SapD 1st promoter His SapB 2nd promoter His n = BL21 TB 16C ON
SapFB				SapF 1st promoter His SapB 2nd promoter His O(F) = BL21 TB 16C ON
SapBC				SapB 1st promoter His SapC 2nd promoter His O(C) = BL21 TB 16C ON
SapFC_B		SapB O = C41 LB 37C 3h ? = C43 LB 37C 3h		SapFC n = C41 LB 37C 3h ? = C43 LB 37C 3h
SapFC_D		SapD O = C41 LB 37C 3h ? = C43 LB 37C 3h		SapFC O = C41 LB 37C 3h ? = C43 LB 37C 3h
			SapD n = C41 LB 37C 3h ? = C43 LB 37C 3h	SapFC O = C41 LB 37C 3h ? = C43 LB 37C 3h
SapFC_Z		SapZ n = C41 LB 37C 3h ? = C43 LB 37C 3h		SapFC O = C41 LB 37C 3h ? = C43 LB 37C 3h
SapFD_B		SapB O = C41 LB 37C 3h ? = C43 LB 37C 3h	SapFD On = C41 LB 37C 3h ? = C43 LB 37C 3h	
SapFD_C		SapC O = C41 LB 37C 3h ? = C43 LB 37C 3h	SapFD OP = C41 LB 37C 3h ? = C43 LB 37C 3h	
SapFD_Z		SapZ n = C41 LB 37C 3h ? = C43 LB 37C 3h	SapFD n = C41 LB 37C 3h ? = C43 LB 37C 3h	
SapFC_B_D		SapB n = C41 LB 37C 3h ? = C43 LB 37C 3h	SapD n = C41 LB 37C 3h ? = C43 LB 37C 3h	SapFC nO = C41 LB 37C 3h ? = C43 LB 37C 3h
SapFD_B_C		SapC O = C41 LB 37C 3h ? = C43 LB 37C 3h	SapFD nn = C41 LB 37C 3h ? = C43 LB 37C 3h	SapB n = C41 LB 37C 3h ? = C43 LB 37C 3h

O = Expression via western
P = Expression in pellet via western
n = No expression via western
M = Expression in membrane via western
N = No expression in membrane via western
V = Purified and soluble

Coexpression
Coexpression but SapD insoluable
Single expression
No expression

The following is a general purification protocol for Sap transporter components. See Table 4.3 for specific purification conditions for each Sap transporter component. The cell pellet was resuspended in sonication buffer and the cells were lysed using S-4000 sonicator. If detergent was used in the purification, the protein was solubilized by stirring for 1 h at 4°C. The cellular debris was centrifuged at 17,000 rpm for 30 min at 4°C. The supernatant was applied to an equilibrated Ni-NTA affinity chromatography column and washed with 10 column volumes of wash buffer. The protein was eluted with 10 column volumes of elution buffer and fractions (determined by SDS-PAGE to be >95% pure) were pooled. To cleave the protein tag, TEV protease was added to the protein during overnight dialysis at 4°C. A second Ni-NTA affinity chromatography column was used to remove the protein tag and TEV protease from the sample. The sample was passed over the second nickel column twice and washed with 5 column volumes of equilibration buffer. To verify TEV protease and tagged protein were separated from the cleaved protein, the column was wash with 5 column volumes of wash buffer and then 10 column volumes of elution buffer. The flow through and the equilibration fractions (determined by SDS-PAGE to be >95% pure) were pooled. The cleaved sample was concentrated in a 30 kDa Amicon concentrator (15 mL) for 15 min at 2500 rpm. The concentrated sample was applied to an equilibrated HiLoad 16/600 Superdex 200 size-exclusion chromatography column. The sample was concentrated to 10-20 mg/mL and stored at -80°C.

The focus of the Sap transporter component project was to express and purify the Sap transporter for functional and structural studies. Crystal structures of the Sap transporter could reveal the assembly of Sap components for complex formation and conformational changes induced by NBD regulatory domains. ATPase hydrolysis and transport assays could be used to characterize the roles of Sap components complex assembly, nthiSapA, and substrates in the

Table 4.3 Purification conditions for Sap components.

	SapC	SapD	SapF
Cell pellet	20 g	10 g	5 g
Resuspension vol.	200 mL	100 mL	100 mL
Sonicate	90 amp	90 amp	90 amp
total time	3 min	2 min	1 min
on/off time	1 s/9 s	1 s	1 s
1st column CV	2 mL	2 mL	2 mL
2nd column CV	5 mL	5 mL	5 mL
Sonication buffer	25 mM Tris pH 7.5 500 mM NaCl 15 mM Imidazole 1% DDM 100 µM PMSF	25 mM Tris pH 7.5 450 mM NaCl 50 mM $MgCl_2$ 15 mM Imidazole 10% glycerol 1% Triton-X 100 µM PMSF	25 mM Tris pH 7.5 500 mM NaCl 15 mM Imidazole 100 µM PMSF
Equilibration buffer	25 mM Tris pH 7.5 500 mM NaCl 15 mM Imidazole 0.025% DDM	25 mM Tris pH 7.5 450 mM NaCl 50 mM MgCl2 15 mM Imidazole 10% glycerol 0.025% DDM	25 mM Tris pH 7.5 500 mM NaCl 15 mM Imidazole
Wash buffer	25 mM Tris pH 7.5 500 mM NaCl 60 mM Imidazole 0.025% DDM	25 mM Tris pH 7.5 450 mM NaCl 50 mM MgCl2 10% glycerol 0.025% DDM	25 mM Tris pH 7.5 500 mM NaCl 60 mM Imidazole
Elution buffer	25 mM Tris pH 7.5 500 mM NaCl 250 mM Imidazole 0.025% DDM	25 mM Tris pH 7.5 450 mM NaCl 50 mM MgCl2 250 mM Imidazole 10% glycerol 0.025% DDM	25 mM Tris pH 7.5 500 mM NaCl 250 mM Imidazole
Dialysis buffer	25 mM Tris pH 7.5 500 mM NaCl 0.025% DDM 0.5 mM EDTA 1 mM DTT	25 mM Tris pH 7.5 450 mM NaCl 50 mM MgCl2 10% glycerol 0.025% DDM 0.5 mM EDTA 1 mM DTT	25 mM Tris pH 7.5 500 mM NaCl 0.5 mM EDTA 1 mM DTT
Running buffer	25 mM Tris pH 7.5 500 mM NaCl 0.025% DDM	25 mM Tris pH 7.5 450 mM NaCl 50 mM MgCl2 0.025% DDM	25 mM Tris pH 7.5 500 mM NaCl

activity of the Sap transporter. Unfortunately, the expression of nthiSapB was too low for purification. Purification of nthiSapC and nthiSapD were successful but size-exclusion chromatography demonstrated the components were heterogeneous (Figure 4.1). The purification of nthiSapF yielded monomer protein with high purity (Figure 4.2), which led to the successfully crystallization and structure determination of nthiSapF.

4.2.4. Expression and Purification of NthiSapA

NthiSapA construct and expression conditions were used as previously described in Chapter 2 Experimental Procedures. For purification of nthiSapA, a 20 g cell pellet was resuspended in 200 mL of buffer A (25 mM Tris pH 7.5, 500 mM NaCl, 15 mM imidazole pH 7.4) and sonicated on ice for 2.5 min with pulses of 1 s on and 9 s off (S-4000, Misonix Sonicators). The lysate was centrifuged at 17,000 rpm for 1 h and the supernatant was loaded on to a 5 mL Ni-NTA affinity chromatography column. The column was rinsed with 10 column volumes of buffer A, followed by 5 column volumes of buffer B (25 mM Tris pH 7.5, 500 mM NaCl, 60 mM imidazole pH 7.4) and the protein was eluted with 8 column volumes of buffer C (25 mM Tris pH 7.5, 500 mM NaCl, 250 mM imidazole pH 7.4). The protein was dialyzed overnight in buffer D (25 mM Tris pH 7.5, 500 mM NaCl). The protein was concentrated with a 50 kDa Amicon Ultra concentrator (15 mL) for 10 min at 4000 rpm and injected on an equilibrated HiLoad 16/600 Superdex 200 size-exclusion chromatography column (GE Healthcare). For peptide SPR, nthiSapA was dialyzed in 25 mM HEPES pH 7.5, 500 mM NaCl. Protein concentration was determined using a nanodrop spectrophotometer (NanoDrop-1000, Thermo Fisher Scientific). The protein is stable for months at 4°C, even at high concentrations and can be stored at -80°C without effecting its ability to crystallize.
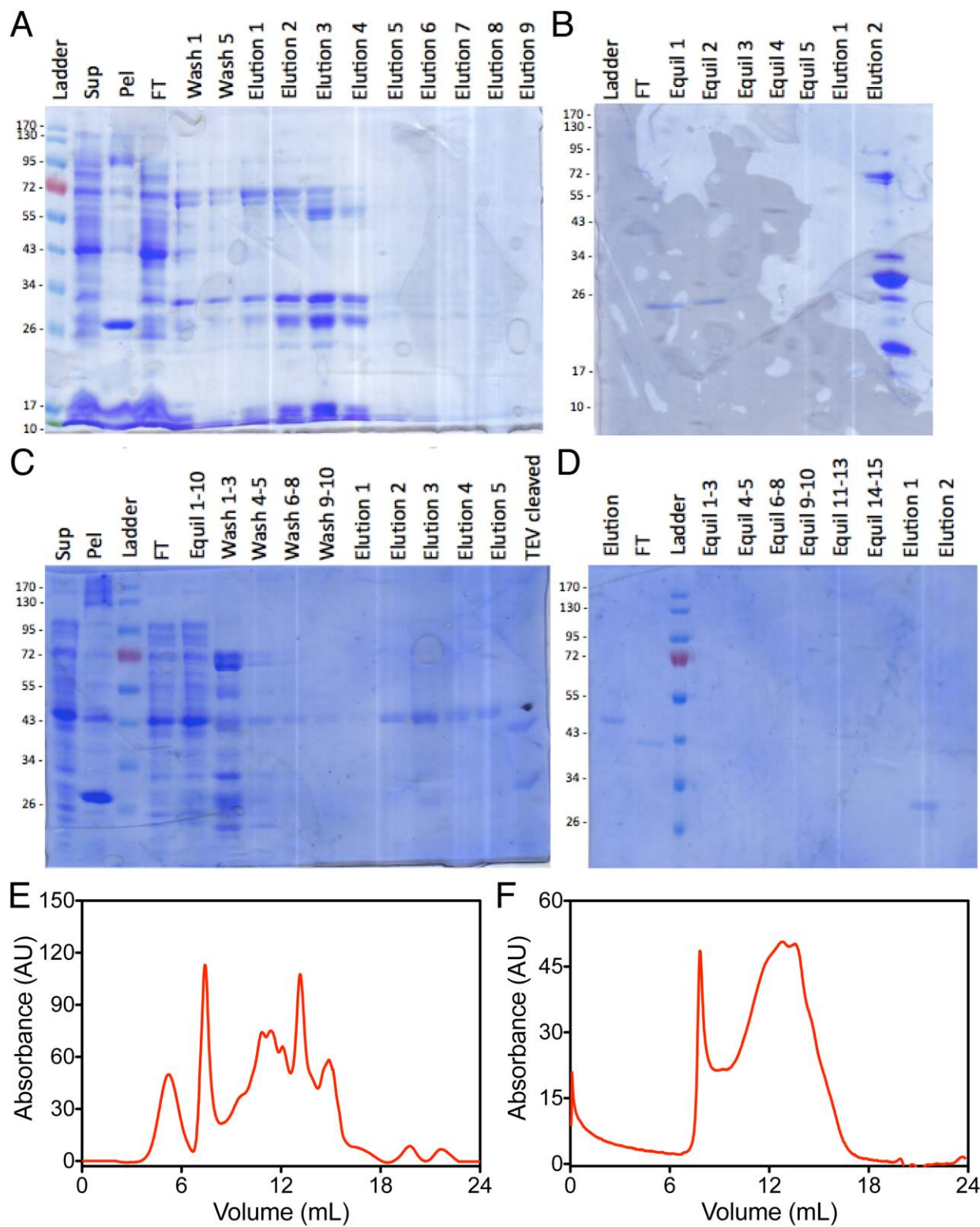
Figure 4.1. Protein purification of nthiSapC and nthiSapD. During the nthiSapC purification

process, SDS-PAGE images of (A) the first nickel affinity column and (B) the second nickel

affinity column after TEV protease cleavage were used to monitor the sample quality. The

purification of nthiSapD was evaluated by SDS images of (C) the first nickel affinity column and

(D) the second nickel affinity column after TEV protease cleavage. The expected size of

nthiSapC and nthiSapD is 33 kDa and 40 kDa, respectively. Size-exclusion chromatographs of

(E) nthiSapC and (F) nthiSapD were collected at 280 nm.
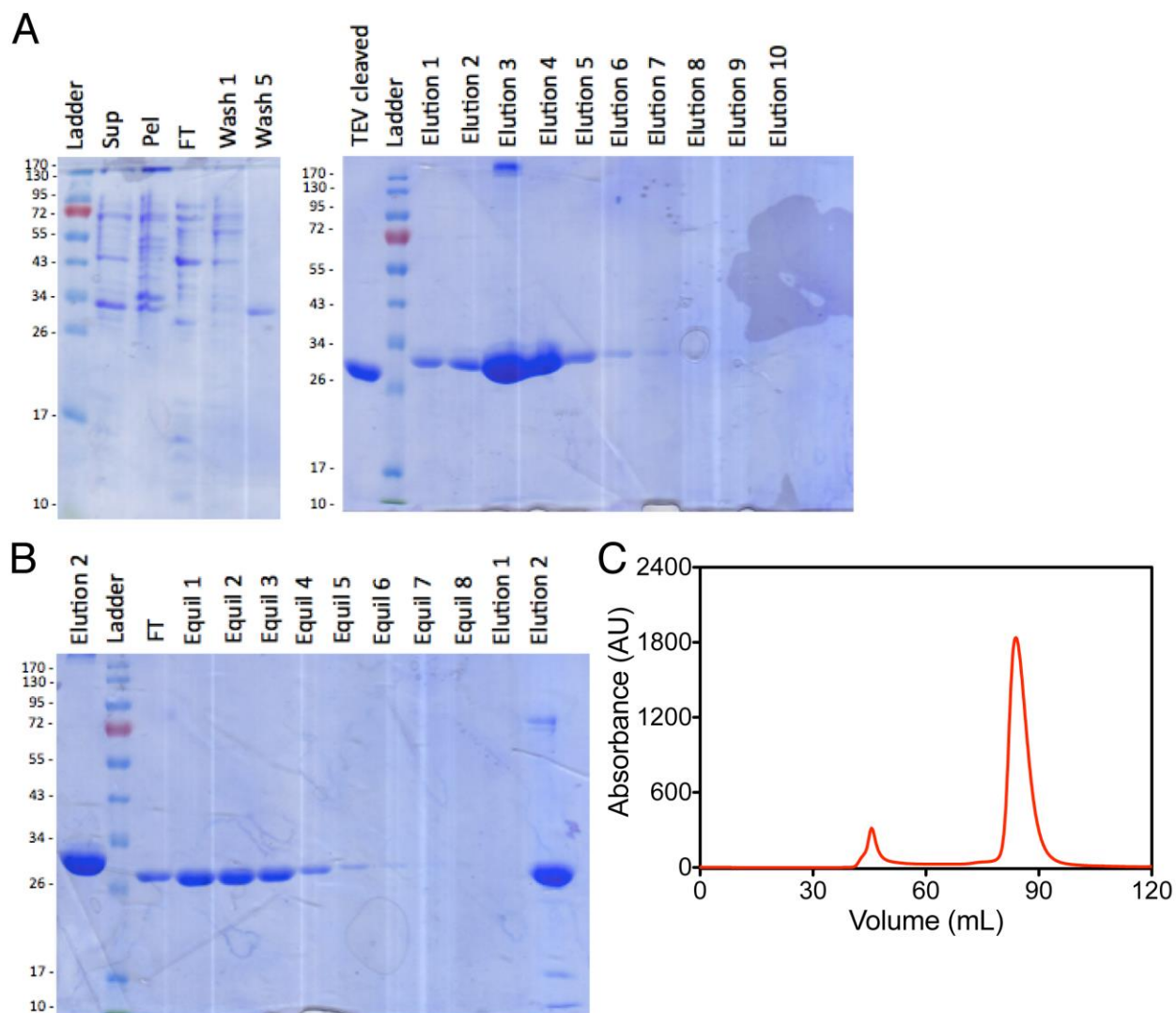
Figure 4.2. Protein purification of nthiSapF. SDS-PAGE images of the nthiSapF purification process depicting (A) the first nickel affinity column and (B) the second nickel affinity column after TEV protease cleavage. The expected size of nthiSapF is 30 kDa. (C) The size-exclusion chromatograph of nthiSapF was collected at 280 nm.

4.2.5. *Protein Crystallization of NthiSapF*

Crystallization trials of nthiSapF were performed using the sparse-matrix method. Initial nthiSapF hits were found in commercial screens summarized in Table 4.4. Based on the initial hits, high salt conditions were used to optimize nthiSapF crystals. NthiSapF crystals grew well in optimized conditions of 50-55% Tacsimate pH 7 and diffracted to 2.8-3.0 Å. The best diffracting nthiSapF crystals were found in the optimized condition containing 0.1 M MES pH 6, 1.25 M ammonium citrate pH 7. Sitting drop trays were set up using a ratio of 1:1 with 11 mg/mL protein to crystallization condition at 22°C. The crystal morphology of nthiSapF crystals was usually hexagonal prism, and the crystals grew overnight. The crystals were harvested and flash-cooled in liquid nitrogen.

4.2.6. *Protein Crystallization of NthiSapA*

Sitting-drop vapor diffusion and sparse-matrix methods were used to identify potential crystallization conditions for nthiSapA. An initial hit was found in 0.1 M HEPES pH 7.5, 1.3 M ammonium sulfate at 22°C. An additive screen (Hampton Research, Cat. No. HR2-428) was used to optimize the initial nthiSapA hit. Using the 2 M sodium thiocyanate additive improved nthiSapA crystal formation, and diffraction quality bipyramidal crystals were grown overnight at 22°C. Crystals typically measured about 50 x 50 x 100 μm.

For the final optimized condition, nthiSapA was chemically denatured and refolded as described in Chapter 3 Experimental Procedures, Ligand-Free Protein Purification. Drops were set up with 1 μL nthiSapA (15 mg/mL, 25mM Tris pH 9.5, 150 mM NaCl), 1 μL crystallization condition (0.1 M Tris pH 9.4, 1.5 M ammonium phosphate) and 0.2 μL additive condition (2 M sodium thiocyanate) and equilibrated against 500 μL of the crystallization condition in the

Table 4.4. Initial crystallization conditions for nthiSapF crystals.

Screen	Conditions	Hit
Hampton Research Index 5	0.1 M HEPES pH 7.5, 2.0 M Ammonium sulfate	Brush-like crystals
Hampton Research Index 29	60% v/v Tacsimate pH 7.0	Small crystals
Qiagen JCSG+ 49	1 M tri-sodium citrate, 0.1 M sodium cacodylate pH 6.5	Small crystals
Wizard I 14	1.0 M sodium citrate, 0.1 M sodium cacodylate pH 6.5	Small crystals
Wizard II 16	1.0 M sodium citrate, 0.1 M CHES pH 9.5	Brush-like crystals

reservoir. Crystals were briefly soaked in cryoprotectant (0.1 M Tris pH 9.4, 1.8 M ammonium phosphate, 15% v/v glycerol) and flash-cooled in liquid nitrogen. The crystals were subject to radiation damage, and data were obtained using two crystals from the same drop to collect a complete data set in the outer shell.

Co-crystallization of nthiSapA with AMPs was attempted with AMP fragment peptides (Table 4.5). Co-crystallization drops set with AMP peptides only produced apo nthiSapA crystals. Many different crystallization variables were trialed to optimize for peptide bound nthiSapA. While conditions for peptide bound nthiSapA crystals were not identified, the range of conditions for apo nthiSapA crystallization was expanded. NthiSapA crystallizes using a variety of high salt conditions, condition 1 (0.1 M Tris pH 9.4, 0.8-1.1 M sodium/potassium tartrate), condition 2 (0.1 M Tris pH 9.4, 1.3-1.8 M ammonium phosphate), condition 3 (0.8-1.4 M potassium phosphate dibasic), and condition 4 (0.1 M HEPES pH 7.5, 1.3-1.5 M ammonium phosphate). NthiSapA protein concentration can be varied from 2-20 mg/mL, but 10-20 mg/mL produces higher diffraction quality crystals. Three different protein purification buffers were used to crystallize nthiSapA, buffer 1 (25mM Tris pH 9.5, 150 mM NaCl), buffer 2 (25mM Tris pH 7.5, 500 mM NaCl), and buffer 3 (25mM HEPES pH 7.5, 500 mM NaCl). The amount of additive added to the drop can vary from 0.05-0.2 µL, but apo nthiSapA will not crystallize without it. Refolded nthiSapA was used to eliminate the possibility of co-purified peptides bound to the SBP. However, natively purified nthiSapA crystallizes in the same conditions as refolded nthiSapA and the electron density from both types of crystals looks similar.

Interesting, nthiSapA crystals with a new morphology were discovered when a protein buffer containing glycerol (25 mM HEPES pH 7.5, 125 mM NaCl, 10% glycerol) was used to set up crystal trays. Slender rod shaped nthiSapA crystals were grown using this protein buffer. The

Table 4.5. Custom defensin AMP fragments.

	Sequence
hBD3_Nterm_6	GIINTL
hBD3_Mid_8	KSSTRGRK
hBD3_Cterm_4	RRKK
hNP1_loop	CRIPAGIAGERRCGGGGSPAPAK, C1-C13
hBD2_loop	CHPVFGPRRYKQCGGGGSPAPAK, C1-C13
hBD3_loop	CAVLSGLPKEEQCGGGGSPAPAK, C1-C13
hNP1_linear	SRIPAGIAGERRSGGGGSPAPAK
hBD2_linear	HPVFGPRRYKQ
hBD3_linear	AVLSGLPKEEQ
biotin_hBD3_11	RIPAGIAGERR
biotin_hBD3_8	SGLPKEEQ
biotin_AAA_11	SAAAGAAGSSS

best diffracting crystals were grown in 0.1 M Tris pH 8.5, 1.8 M ammonium sulfate, 18% glycerol. Sitting drop trays were set up using a ratio of 1:1:0.2 with 6.25 mg/mL protein to crystallization condition to additive (2 M sodium thiocyanate) at 22°C. Crystals were briefly soaked in cryoprotectant (0.1 M Tris pH 8.5, 1.6 M ammonium sulfate, 25% v/v glycerol) and flash-cooled in liquid nitrogen.

4.2.7.   *Structure Determination of NthiSapA and NthiSapF*

Crystal diffraction data for nthiSapA and nthiSapF was collected at the Advanced Photon Source (Argonne, IL). For nthiSapA crystals, LS-CAT beamline 21-ID-G with a MX300 CCD detector (Rayonix, LLC) was used to collect data. Data for nthiSapF was collected at LS-CAT beamline 21-ID-D with an Eiger X 9M detector (DECTRIS AG). The data were integrated using XDS (181) and scaled with AIMLESS, from the CCP4 suite (182). Molecular replacement pipeline Balbes was used to build the initial models of nthiSapA and nthiSapF (183). NthiSapA model building was improved with ARP/warp from the online CCP4 platform (184). The final nthiSapA and nthiSapF models were edited in Coot (185) and refined with REFMAC (186). The cartoon representations of solved protein structures and protein alignments were created in PyMOL v2.0 (Schrödinger, LLC). The Dali server was used to identify structures similar to nthiSapA (221). Data collection and refinement statistics of nthiSapA and nthiSapF structures are summarized in Table 4.6. As of September 2018, Saemee Song is continuing to optimize SapF crystallization and structure determination.

4.2.8.   *NthiSapA Peptide Binding Affinity using SPR*

Single-cycle kinetic experiments were used to determine defensin AMP binding affinity of

Table 4.6. Data collection and refinement statistics of nthiSapA and nthiSapF.

Statistics	nthiSapA	nthiSapF
Space group	$P4_1 2_1 2$	$P6\,2\,2$
Data Collection		
Unit cell Dimensions, Å		
a	119.76	121.13
b	119.76	121.13
c	129.59	148.54
Unit Cell Angles, °		
α	90.0	90.0
β	90.0	90.0
γ	90.0	120.0
Resolution, Å	43.97-2.25	44.78-2.60
	(2.32-2.25)	(2.72-2.60)
Wavelength, Å	0.9786	1.1020
Completeness, %	99.9 (100)	99.9 (100)
R_{merge}	0.088 (0.702)	0.134 (1.347)
Average $I/\sigma I$	16.1 (4.3)	19.7 (3.6)
Redundancy	19.2	21.9
Total reflections	869659	773708
Unique reflections	45307	20421
Refinement		
R_{work}/R_{free}	0.1998/0.2316	0.2865/0.3380
Number of atoms		
All atoms	4374	
Protein	4250	
Water	124	
Average B-factor, Å2		
All atoms	59.6	
Protein	59.7	
Water	53.3	
Rmsd		
Bond lengths, Å	0.011	0.008
Bond angles, °	1.809	1.898
Ramachandran statistics		
Favored, %	96.0	
Allowed, %	3.4	
Outliers, %	0.6	

*Data for the highest-resolution shell are given in parentheses.

nthiSapA. Defensin AMPs were coupled via a standard amine-coupling method in flow channels 2, 3, and 4 on a CM5 sensor chip (GE Healthcare); 300-1000 RU of each AMP was immobilized. Flow channel 1 was designated the control channel. The surface of the chip was equilibrated in running buffer (25 mM HEPES pH 7.5, 150 mM NaCl, 0.1% Tween 20) at a flow rate of 30 μL/min for at least 3 h. Analyte injections of nthiSapA were prepared by 2-fold serial dilution. The analyte samples of increasing concentrations were consecutively injected over all four channels followed by a final dissociation step. Experiments were run at a flow rate of 30 μL/min at 25°C. The sensor surface was regenerated after each experiment with four 30 s injections of running buffer, supplemented with 0.1% SDS, at a flow rate of 50 μL/min.

AMP loop peptides were amine-coupled using the method described above with 300-400 RU of each peptide immobilized. The samples were treated with the same conditions as previously mentioned with one exception, two injections were used to regenerate the sensor surface instead of four. After collecting data under oxidizing conditions, the chip was equilibrated with reducing buffer (25 mM HEPES pH 7.5, 150 mM NaCl, 0.1% Tween 20, 2 mM TCEP) for at least 4 h. The nthiSapA analyte injections were than repeated under reducing conditions.

Data were obtained in triplicate. All experiments were performed with the Biacore T200 instrument (GE Healthcare) according to the manufacturer's instructions. Kinetic rate constants and equilibrium dissociation constants were determined by fitting the data globally to the 1:1 two-state reaction model using the Biacore T200 evaluation software v3.0 (GE Healthcare).

4.3. Results

4.3.1. Crystal Structure of Sap Transporter Component NthiSapF

NBD dimerization is necessary for ATP hydrolysis to drive the conformational changes of the TMDs for the translocation of the substrate. However, nthiSapF appears to be a monomer in solution. The nthiSapF protein peak on the size-exclusion column correlates with the size of nthiSapF monomer (Figure 4.2C). NthiSapF was crystallized with the hope of capturing the NBD in the dimer conformation. The structure of nthiSapF was solved by molecular replacement with a resolution of 2.6 Å and space group *P*6 2 2 (Figure 4.3A). Unfortunately, nthiSapF did not crystallize as a dimer but has two monomers in the asymmetric unit.

In the SapF model, residues 9-253 were built in the electron density. The N-terminal and C-terminal ends of the protein and a loop from residues 176-182 were not visible in the electron density. Despite low sequence identity, NBDs of ABC transporters have a highly conserved 3D structure with specific ATP binding motifs, the Walker A, the Walker B, and the signature sequence. All these features are found in the nthiSapF structure. The structure of nthiSapF was aligned with the NBDs of Type I importer *Archaeoglobus fulgidus* ModABC (PDB code 2ONK, RMSD = 2.11 Å), which is expected to have a similar overall structure as the Sap transporter (Figure 4.3B). Some Type I importers have NBDs with regulatory domains that can inactivate the transporter by adapting an inhibitory conformation to prevent NBD dimerization. However, nthiSapF lacks a regulatory domain as illustrated by the structural alignment with *Thermoanaerobacter tengcongensis* DppD (PDB code 4FWI, RMSD of 1.94 Å), a homolog of nthiSapD (Figure 4.1C).
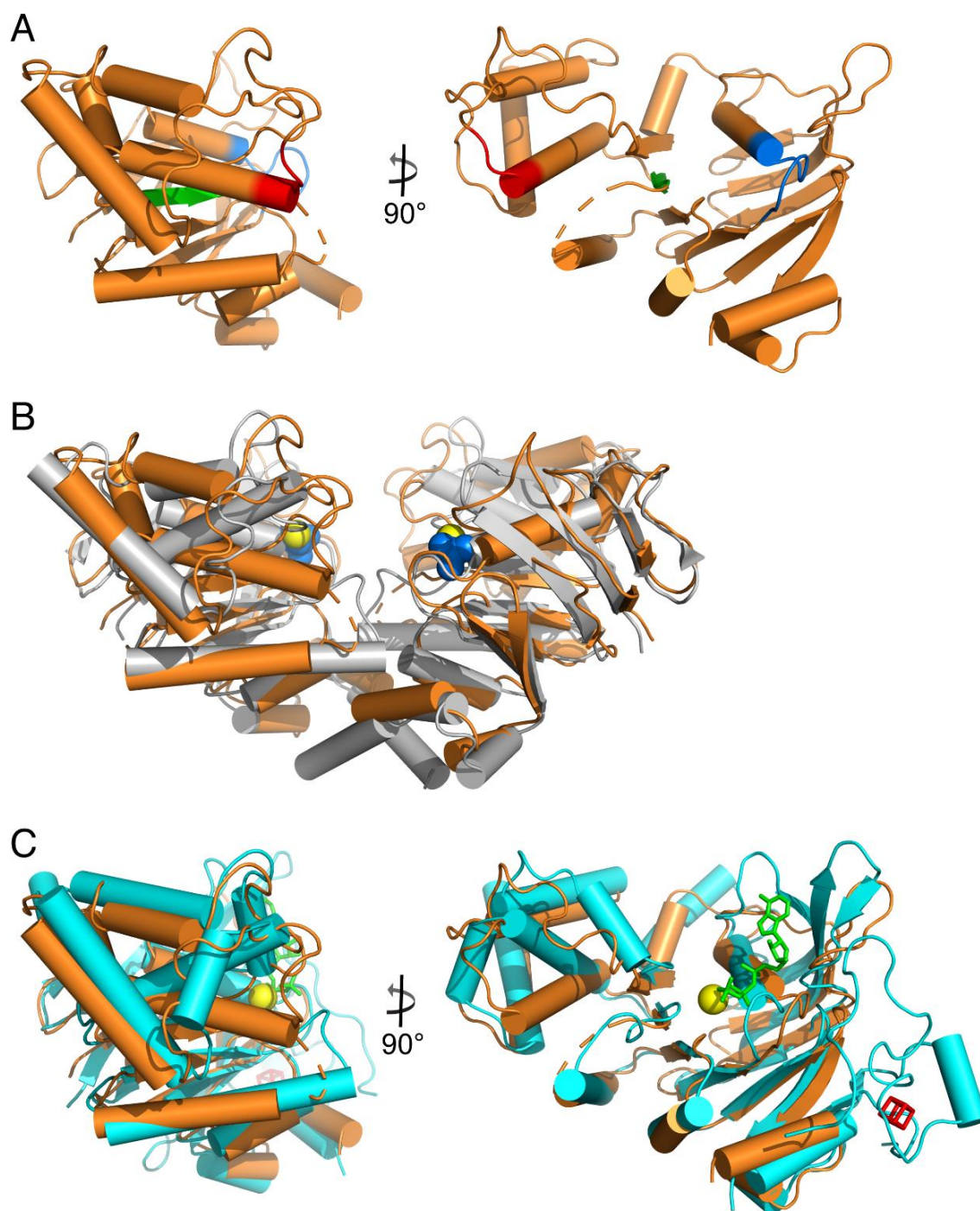
Figure 4.3. The 3D structure of Sap transporter component nthiSapF. (A) Cartoon representation with two views of nthiSapF shown in orange. The conserved Walker A, Walker B and ABC signature motifs are shown in blue, green and red, respectively. The missing loop from

residues 176-182 is represented by a dashed line. (B) Two nthiSapF monomers aligned with afModC dimer shown in gray (PDB code, 2ONK). Ligands bound at the dimer interface, Mg^{2+} and P_i, are shown in yellow and blue, respectively. (C) Alignment of nthiSapF with nthiSapD homolog ttDppD shown in cyan (PDB code, 4FWI). ATP and Mg^{2+} are bound in the active site of ttDppD, represented in green and yellow respectively. A 4Fe-4S iron-sulfur cluster, shown in red, is bound at the C-terminal end of the ttDppD and may play a regulatory role in substrate transport.

4.3.2. *Crystal Structure of Unbound NthiSapA*

NthiSapA is an AMP-specific peptide SBP in comparison to more indiscriminate peptide SBPs including OppA and DppA. Many Cluster C SBPs have been co-purified and crystallized with their canonical substrates. As mentioned in Chapter 3, the structure of natively purified nthiOppA was solved with co-purified endogenous peptide. However, endogenous peptides do not appear to be bound to nthiSapA during the expression and purification process. This highlights the specialized role nthiSapA peptide binding. The crystal structure of nthiSapA was solved to resolution of 2.3 Å by molecular replacement (Figure 4.4A). The first 10 residues are not visible in the electron density with the refined model starting at Thr32.

Overall the structure of nthiSapA contains two globular α/β domains that are connected by a hinge region at the interface of the domains to form the substrate-binding pocket. One unique feature of Cluster C SBPs is an additional sub-domain, I_B, which for nthiSapA includes residues 46-235. Domain I_A spans residues 24-45, 236-313 and 532-564 and domain II contains residues 314-531. Given the limited sequence identity of nthiSapA to other Cluster C SBPs, the Dali server was used to perform a search of Protein Data Bank for structures similar to nthiSapA. The search identified *G. parasuis* HbpA2 (PDB code 3TPA) in an open unbound conformation as most similar to nthiSapA (RMSD 1.625 Å). In comparison, structural alignment of nthiSapA with the ligand-bound structure of gpHbpA (PDB code 3M8U) indicates a conformational change between the structures (RMSD 3.048 Å). These structure comparisons suggest nthiSapA crystallized in an open unbound conformation (Figure 4.4B).

4.3.3. *NthiSapA Mediates α- and β-Defensins Killing of NTHi*

NTHi sensitivity to defensin AMPs has previously only focused on the antimicrobial
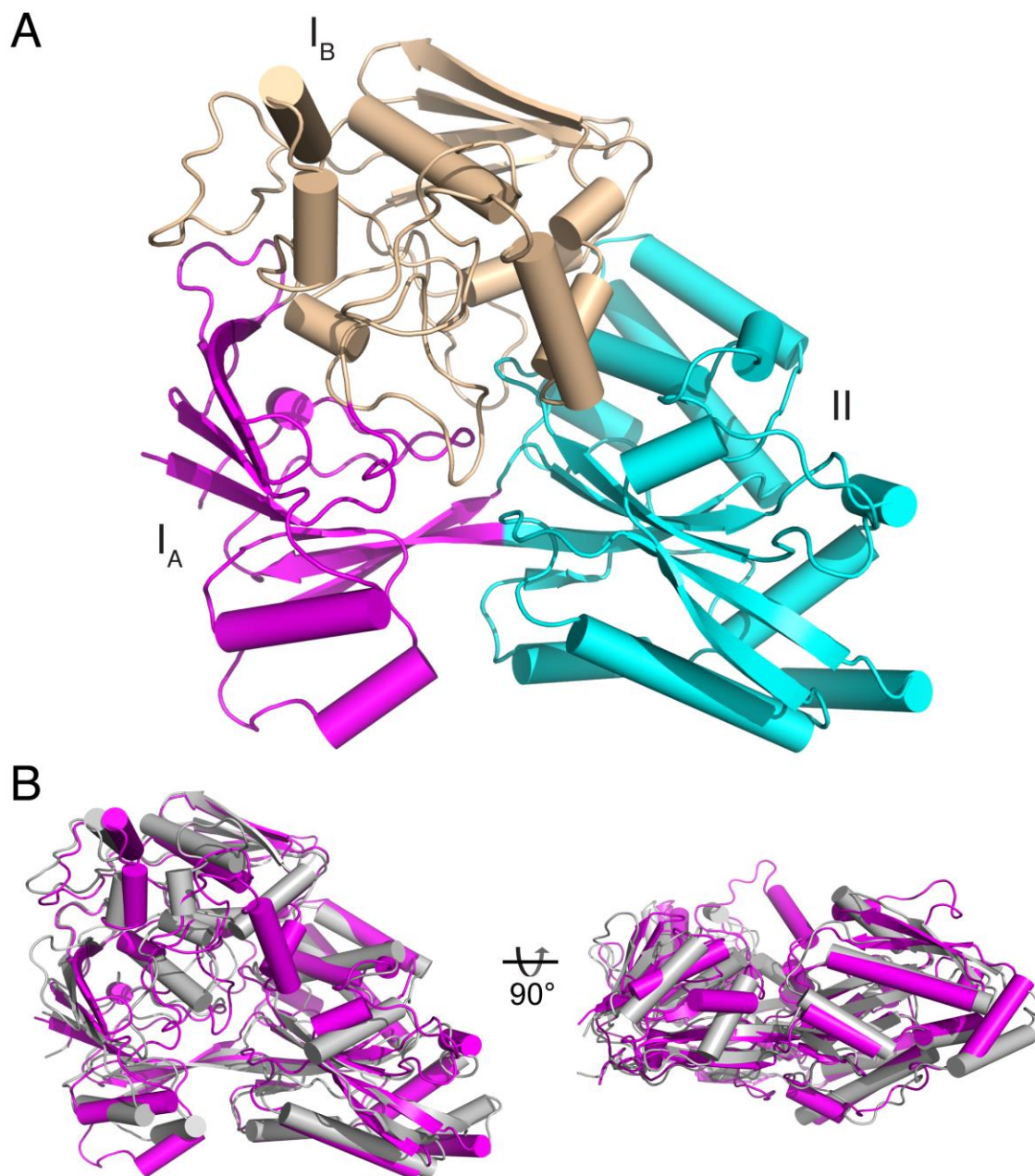
Figure 4.4. Structure of unbound nthiSapA in the open conformation. (A) Cartoon representation of crystal structure of unbound nthiSapA with I_A, I_B and II domains highlighted in purple, wheat and cyan, respectively. (B) Structural alignment of nthiSapA in purple with gpHbpA2 in gray (PDB code 3TPA) shows nthiSapA has adopted the open conformation in this structure.

activity of hBD3 and cBD1 (109,115). Our collaborator, Kevin Mason expanded this to include hNP1 and hBD2 and determined nthiSapA mediates the resistance of NTHi for all these defensin AMPs. The sapA mutant strain was more sensitive to the antimicrobial activity of hBD2 than the parent strain, and hBD2 is comparable to hBD3 at similar concentrations (personal communication from Kevin Mason). Antimicrobial activity of hNP1 is slightly different from the other defensin AMPs. At up to 5 µg/mL of hNP1, the NTHi parent strain was not sensitive to the defensin AMP. However, the *sapA* mutant strain was sensitive to hNP1 and sensitivity was independent of AMP concentration (personal communication from Kevin Mason).

4.3.4. *NthiSapA Binds Defensin AMPs with High Affinity*

SapA-mediated antimicrobial activity of hNP1, hBD2, and hBD3 was investigated using SPR to characterize the binding between nthiSapA and AMPs. NthiSapA binds all three defensin AMPs with high affinity (Figure 4.5). NthiSapA has the tightest affinity for hNP1 with a K_D value of 4.0 nM. The affinity of nthiSapA for the other two defensin AMPs was slightly weaker with K_D values of 10.5 nM and 17.5 nM for hBD3 and hBD2, respectively. The kinetic and equilibrium dissociation constants are summarized in Table 4.7. NthiOppA and ecNikA showed no binding specificity for any of the defensin AMPs (data not shown). Similar to other peptide binding SBPs, peptide specificity of nthiSapA is independent of peptide sequence. The physical properties of the three defensin AMPs vary in peptide length, sequence, and net charge (Figure 4.6B). The six-cysteine motif is the only conserved feature of the defensin AMPs. Despite these distinct characteristics of the defensin AMPs, there is a high degree of similarity in nthiSapA binding affinity for these AMPs.

Tertiary structure analysis of hNP1, hBD2, and hBD3 shows the conserved γ-core domain
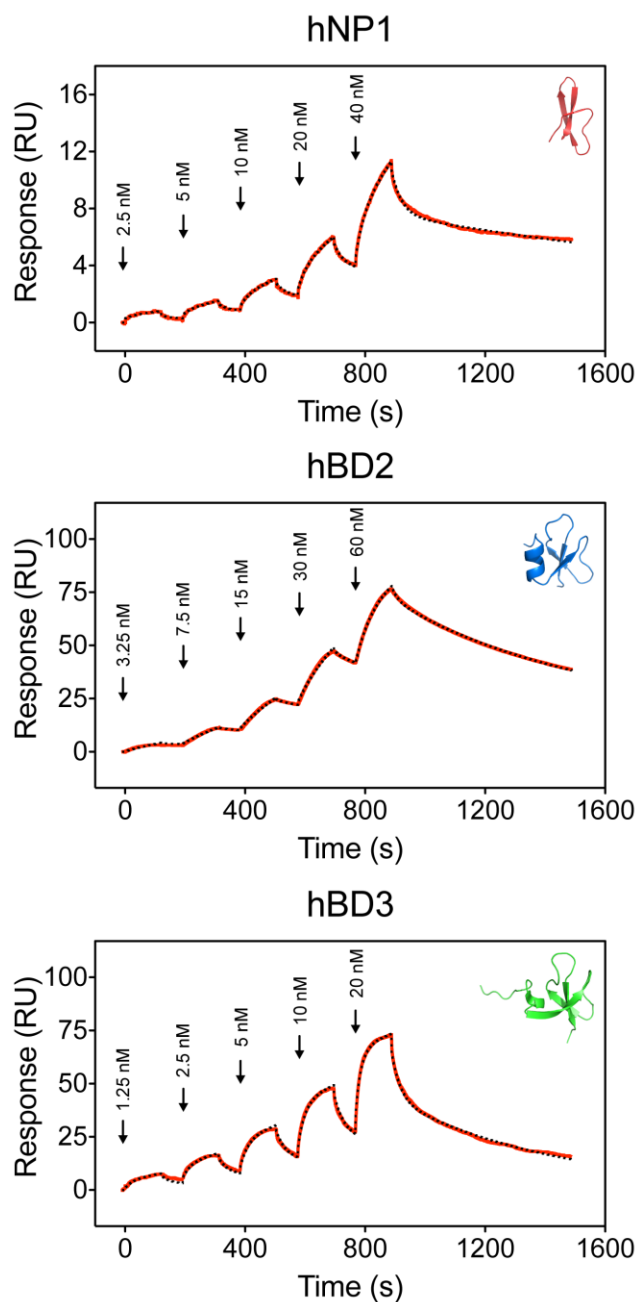
Figure 4.5. Single cycle kinetic SPR characterization of nthiSapA binding of AMPs. Kinetic analysis was performed with five analyte injections at increasing concentrations of nthiSapA, noted on the sensogram, over immobilized AMPs. For the association phase, each analyte sample was injected in series, with a final dissociation phase. Representative sensogram data shown in red and fitted model drawn in black.

Table 4.7. NthiSapA kinetic and equilibrium dissociation constants for defensin AMPs.

	k_{a1} ($M^{-1}s^{-1}$)	k_{d1} (s^{-1})	k_{a2} (s^{-1})	k_{d2} (s^{-1})	K_D (nM)
hNP1	3.6 (1.5) x 10^5	1.2 (0.3) x 10^{-2}	6.1 (1.9) x 10^{-3}	6.9 (1.6) x 10^{-4}	4.0 (1.1)
hBD2	6.3 (9.6) x 10^5	4.7 (7.1) x 10^{-2}	1.3 (0.8) x 10^{-2}	2.6 (0.1) x 10^{-3}	17.5 (10.1)
hBD3	7.1 (5.4) x 10^5	1.9 (1.2) x 10^{-2}	5.9 (1.4) x 10^{-3}	2.2 (0.3) x 10^{-3}	10.5 (5.3)

A
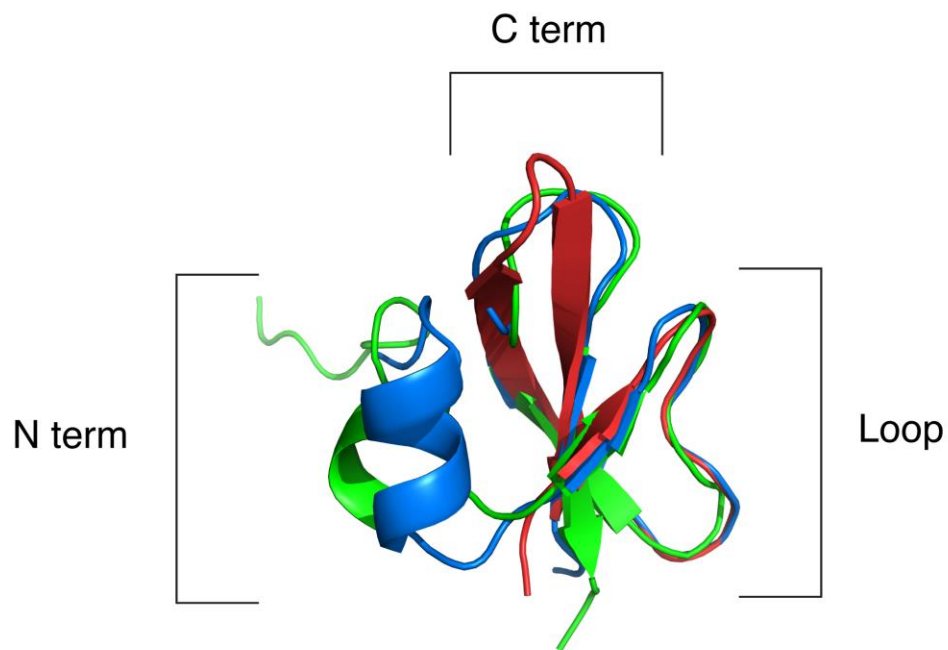
B

	N term	Loop	C term	

```
hNP1              ACYCRIPACIAGERRYGTCIYQGRLWAFCC   +3
hBD2        GIGDPVTCLKSGAICHPVFCPRRYKQIGTCGLPGTKCCKKP   +6
hBD3  GIINTLQKYYCRVRGGRCAVLSCLPKEEQIGKCSTRGRKCCRRKK  +11
```

Figure 4.6. The γ-core domain is conserved among the 3D structures of defensin AMPs. (A) Cartoon representations of hNP1, hBD2 and hBD3 shown in red, blue, and green, respectively. (B) Individual sequences of defensin AMPs with conserved cysteine residues of the γ-core domain are highlighted in orange.

of these AMPs and highlights the differences in the termini of the peptides (Figure 4.6A). The N- and C-terminal regions vary in length and the number of residues between the conserved cysteine residues in the γ-core domain differs between the defensin AMPs. Both hBD2 and hBD3 have an additional small N-terminal helix in comparison to hNP1. As the smallest defensin, hNP1 has no C-terminal residues after the γ-core domain. HBD2 and hBD3 have two and four positive residues on the C-terminal end of the domain, respectively. Additionally, the number and arrangement of charged residues on the exterior of the peptides differs among all three defensin AMPs.

4.3.5. *Loop Region of Defensin AMPs Recognized by NthiSapA*

To determine the role of the conserved 3D structure of the defensin AMPs in nthiSapA recognition, the γ-core domain was simplified to include only the loop region of hNP1, hBD2, and hBD3 (Figure 4.6B). Peptides hNP1$_{loop}$, hBD2$_{loop}$, and hBD3$_{loop}$ were synthesized with a disulfide bond connecting the termini of each 13-residue fragment to replicate the shape of the loop region in the defensin AMPs, and a C-terminal linker was added for peptide accessibility after SPR immobilization (Figure 4.7A). The loop regions of hNP1, hBD2 and hBD3 are sufficient to maintain recognition of nthiSapA (Figure 4.7B, C and D). The nthiSapA binding affinities for hNP1$_{loop}$, hBD2$_{loop}$, and hBD3$_{loop}$ are very similar to the full length defensin AMPs with the K_D values of 17.1 nM, 9.5 nM, and 17.2 nM (Table 4.8). To determine if nthiSapA binding was dependent on loop structure, a reducing agent was added to the SPR running buffer (Figure 4.7E, F and G). Interestingly, nthiSapA has a slightly higher affinity, increasing about 5- to 20-fold, for the AMP loop peptides under reducing conditions with K_D values 3.8 nM, 0.9 nM, and 0.9 nM for hNP1$_{loop}$, hBD2$_{loop}$ and hBD3$_{loop}$ peptides, respectively (Table 4.8). NthiSapA
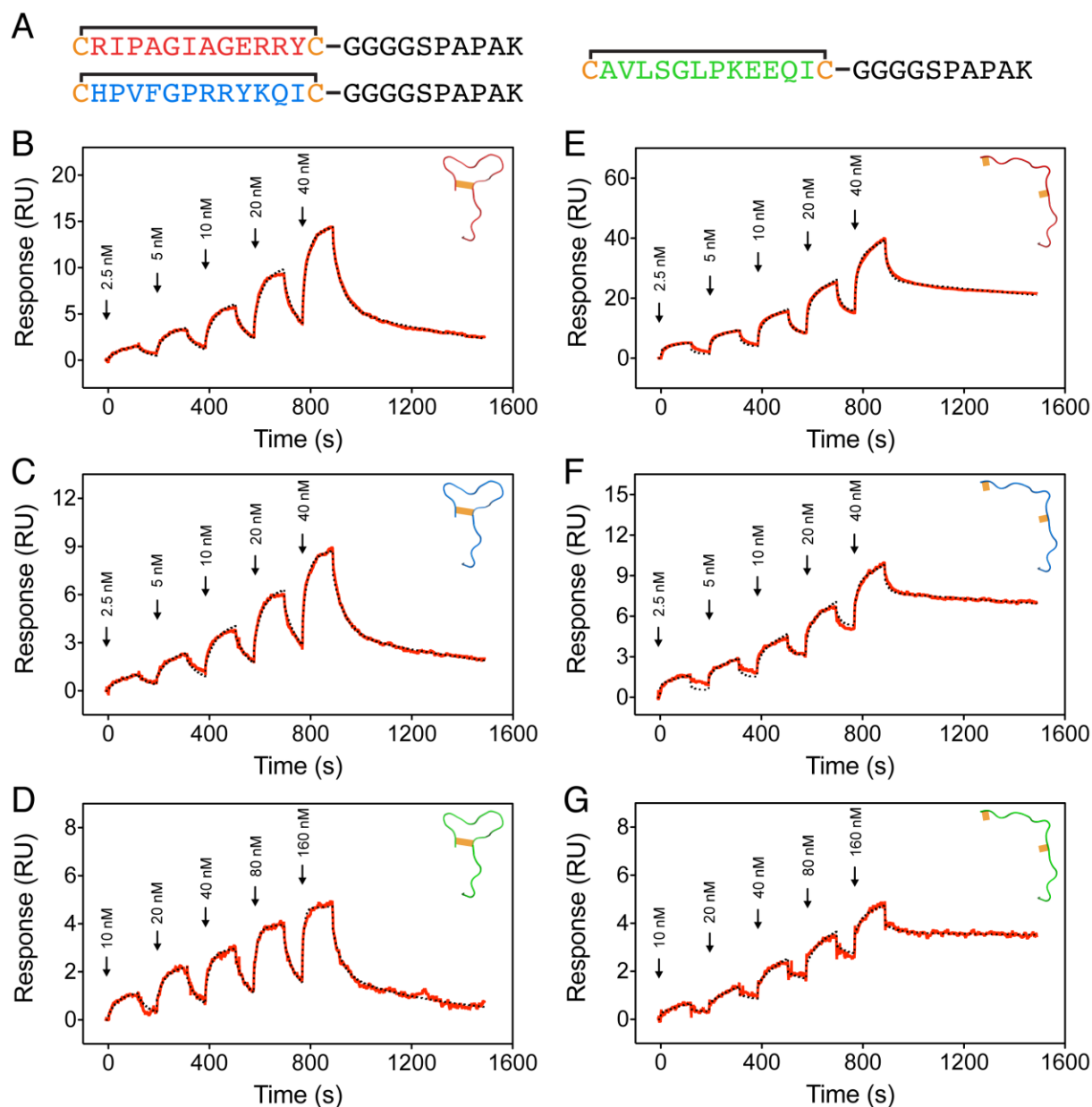
Figure 4.7. NthiSapA maintains high binding affinity for loop region of defensin AMPs. (A) The sequences of the synthetic AMP loop peptides, hNP1$_{loop}$, hBD2$_{loop}$, and hBD3$_{loop}$, produced are shown in red, blue and green, respectively. SPR sensograms of AMP loop peptides (B) hNP1$_{loop}$, (C) hBD2$_{loop}$, and (D) hBD3$_{loop}$ demonstrate the ability of nthiSapA to bind the loop region of defensin AMPs. Under reducing conditions to break the disulfide bond, nthiSapA maintains specificity for AMP loop peptides (E) hNP1$_{loop}$, (F) hBD2$_{loop}$ and (G) hBD3$_{loop}$.

Table 4.8. AMP loop peptides kinetic and equilibrium dissociation constants.

	k_{a1} (M^{-1}s^{-1})	k_{d1} (s^{-1})	k_{a2} (s^{-1})	k_{d2} (s^{-1})	K_D (nM)
Oxidized – disulfide bridge					
hNP1 loop	6.0 (1.0) x 10^5	2.3 (0.1) x 10^{-2}	2.6 (0.3) x 10^{-3}	1.9 (0.2) x 10^{-3}	17.1 (4.4)
hBD2 loop	7.5 (1.1) x 10^5	1.9 (0.1) x 10^{-2}	2.4 (0.2) x 10^{-3}	1.4 (0.2) x 10^{-3}	9.5 (2.0)
hBD3 loop	1.0 (0.6) x 10^6	3.3 (0.9) x 10^{-2}	4.0 (1.6) x 10^{-3}	3.0 (2.1) x 10^{-3}	17.2 (12.0)
Reduced – two cysteine residues					
hNP1 loop	8.8 (2.1) x 10^5	5.0 (0.3) x 10^{-2}	6.4 (0.8) x 10^{-3}	4.5 (0.5) x 10^{-4}	3.8 (0.1)
hBD2 loop	7.6 (1.1) x 10^5	3.4 (0.1) x 10^{-2}	9.5 (0.2) x 10^{-3}	2.4 (0.2) x 10^{-4}	0.9 (0.2)
hBD3 loop	2.8 (1.4) x 10^5	2.8 (2.0) x 10^{-2}	1.2 (0.4) x 10^{-2}	1.2 (0.4) x 10^{-4}	0.9 (0.3)

Representative sensogram data shown in red and fitted model drawn in black.

maintains high affinity for $hNP1_{loop}$, $hBD2_{loop}$ and $hBD3_{loop}$ peptides with net charges of +2, +3, and -1, respectively. Additionally, nthiSapA recognizes AMP peptide substrates without discrimination for the peptide loop structure.

4.4. Discussion

The Sap transport system is essential for NTHi colonization and pathogenesis in the host environment. NTHi utilizes the Sap system for heme uptake to meet essential metabolic requirements. Under stress from host immune response, the Sap system is crucial for evading the antimicrobial activity of AMPs. As AMPs accumulate on the outer membrane, they are recognized by nthiSapA and shuttled to the Sap TMDs for import into the cytoplasm (Figure 4.8). Cytoplasmic proteases degrade the AMPs and neutralize the bactericidal activity of the peptides (110). NthiSapA provides the first layer of substrate specificity for the transport system. The individual Sap transporter components coordinate an additional layer of specificity for import of substrates. Our collaborators in the Mason lab have detailed the functionally independent roles of nthiSapD and nthiSapF in AMP resistance and heme uptake, respectively (115,153). Future studies will expand on our structure of SapF to include the other Sap components and understand how the complex formation of Sap components determines the substrate specificity of the Sap transporter for heme and AMPs.

The work presented in this chapter suggests the molecular bases for this multifunctional substrate binding of nthiSapA. NthiSapA has about an order of magnitude higher affinity for defensin AMPs than for heme. This suggests a substrate hierarchy where nthiSapA preferential binds AMPs to prevent the immune response from clearing the NTHi infection.

Antimicrobial activity of AMPs is largely dependent on peptide concentration. Defensins
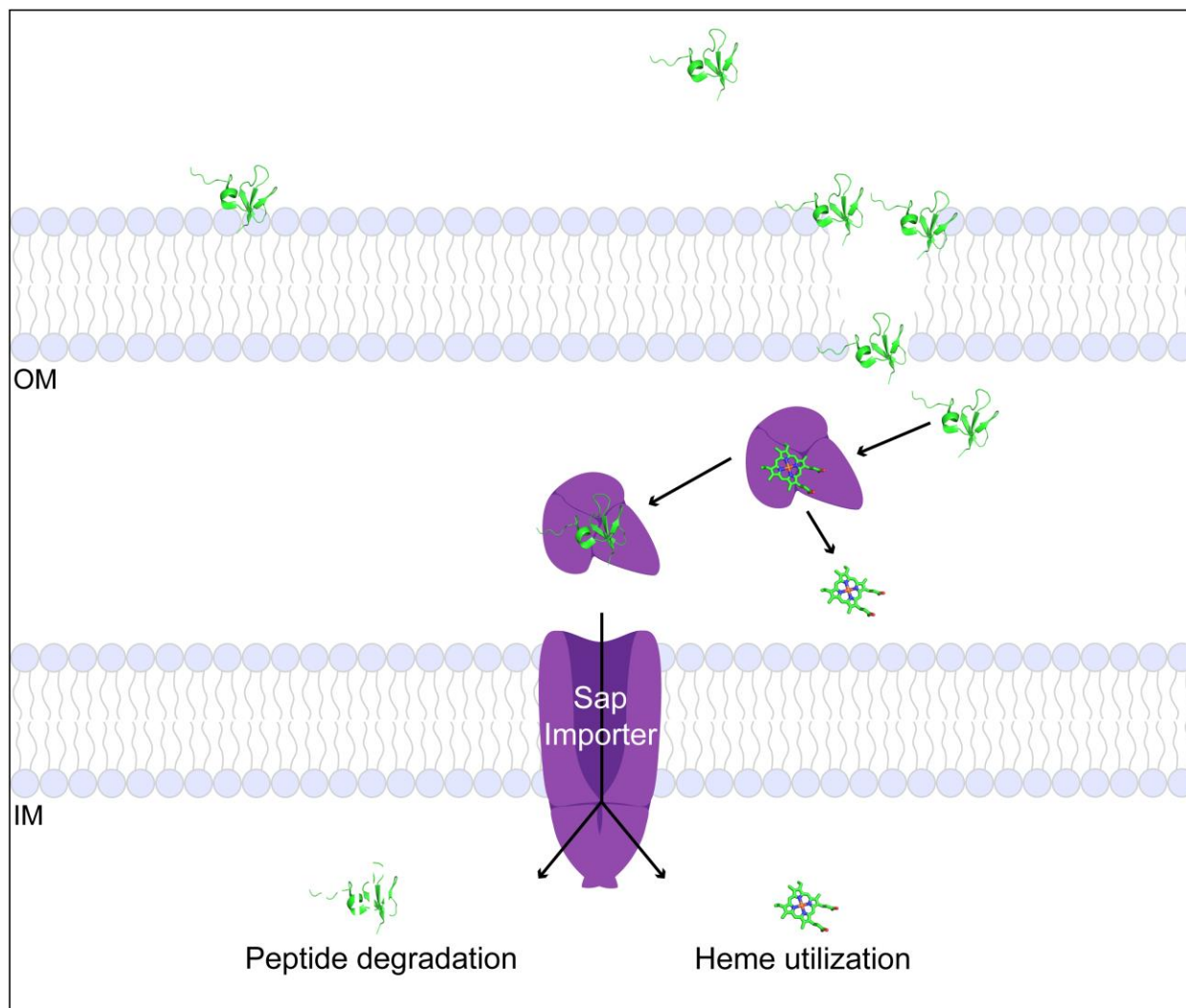
Figure 4.8. The Sap system in heme uptake and AMP resistance. The Sap importer plays an essential role in heme uptake after heme starvation. After defensin AMPs disrupt the bacterial membrane, nthiSapA binds the peptides and delivers them to the Sap TMDs for import into the cell. Once the defensin AMPs are in the cytoplasm, the peptides are degraded and their antimicrobial activity is neutralized.

have high membrane partitioning for model bacterial membranes. Despite the low concentrations of AMPs needed for antimicrobial activity, membrane partitioning dramatically increases the local AMP concentration on the surface of the model bacterial membrane, ranging from 10^3- to 10^6-fold (222-224). This amplification of AMP concentration on the cell surface is necessary for membrane permeability. After hNP1 localizes on the membrane, a 1:20 ratio of peptide:lipid is needed for the AMP to penetrate the phospholipid bilayer of a model membrane (225). A comparison study showed hBD2 and hBD3 have similar membrane permeabilization activity as a hNP1 homolog, hNP3 (226). While it is difficult to determine the exact peptide:lipid ratio needed for AMPs to perturb the outer membrane of bacteria, there is a high local AMP concentration at the site where the peptides successfully break through the cell surface. Negatively charged phospholipids could compete with nthiSapA for AMP binding but the affinity of AMPs for the bacterial membrane has not yet been characterized. However, relatively weak interactions of hNP1 (binding affinity of 2.19 µM) and hBD3 with cell wall precursor lipid II have been observed (227,228). The high binding affinity of nthiSapA for defensin AMPs likely helps the SBP prevent these peptides from reaching the critical concentration for membrane permeabilization and outcompete individual phospholipids for AMP binding.

Defensins are defined by their γ-core motif. Interestingly, these disulfide bonds are not essential to AMP activity. Defensin AMP analogs with a reduced number of disulfide bonds, different disulfide bond patterns, or had all the disulfide bonds eliminated maintain antimicrobial activity (229-231). Additionally, truncations of defensin AMPs, including an hBD3 analog of the loop region, also retain antimicrobial activity (231-234). Theses analogs demonstrate the antimicrobial activity of defensin AMPs is not dependent on the overall 3D structure of the γ-core motif. Upon insertion into the membrane, hNP1 preserves its dimerization and overall 3D

structure (235). However, changes to the overall structure of hBD2 and hBD3 after membrane binding are not yet known. Possible conformational changes of the AMPs during membrane perturbation likely do not disrupt nthiSapA recognition, which binds independent of the peptide loop structure. It is difficult to identify the shared characteristics between $hNP1_{loop}$, $hBD2_{loop}$, and $hBD3_{loop}$ that would activate nthiSapA recognition, and future studies should focus on a more comprehensive understanding nthiSapA AMP specificity.

Many avenues of research promote defensins as a natural blueprint to improve the design of therapeutics against pathogens. The defensin analogs are promising candidates for peptide-based antibiotics or the development of peptide-mimic compounds or (236,237). This work shows antimicrobial activity of hNP1, hBD2 and hBD3 is mediated by nthiSapA, and the SBP binds these defensin AMPs with high affinity. Additionally, nthiSapA binds the loop region of the defensin AMPs and recognition is independent of the loop structure. This highlights the need to better understand AMP specificity of the nthiSapA and the Sap transporter for mediating NTHi sensitivity to AMPs.

CHAPTER 5:

Conclusions

5.1. The Overlapping Function of SBPs in Heme Uptake

As a heme auxotroph, NTHi relies on host hemoproteins as a source of the essential nutrient during infection. The work presented in this thesis reveals that the four Cluster C SBPs that have been identified in NTHi all have specificity for heme. The additional six Cluster C proteins from *E. coli* also all bound heme. Surprisingly, heme specificity was conserved among all Cluster C SBPs despite the variation in their canonical substrates. While heme binding of some Cluster C SBPs had previously been demonstrated, the heme binding affinity of most SBPs had not been measured with analytical methods. The affinity SPR experiments show all four NTHi SBPs, which ranges from about 200 nM to 1 μM, nthiOppA < nthiHbpA < NTHI0310 < nthiSapA. This is an important step in understanding the concerted effort of overlapping transport systems to maintain heme levels in a challenging and dynamic host environment.

Our data show that heme can be transported by Cluster C SBPs in NTHi. In other nutrient uptake systems, SBPs acquire substrate through interactions with other components of the transport system including metallochaperones and the receptor/TonB complex (238-241). Possible mechanisms for heme acquisition of NTHi Cluster C SBPs in the periplasm are depicted in Figure 5.1. The SBPs directly receive imported heme from the outer membrane receptors, a periplasmic heme chaperone protein loads the SBPs with heme, or the TonB complex recruits SBPs to pick up heme from the outer membrane receptor. In the zinc uptake pathway, SBPs AtzC and ZnuA acquire zinc from periplasmic metallochaperones, AtzD and ZinT, respectively (238,239). In other nutrient uptake pathways, the interaction between the outer membrane receptor and TonB complex acts as a scaffold to position SBPs, FhuD and BtuF, near their cognate receptors for delivery of iron-chelated siderophores and vitamin B12, respectively (240,241).
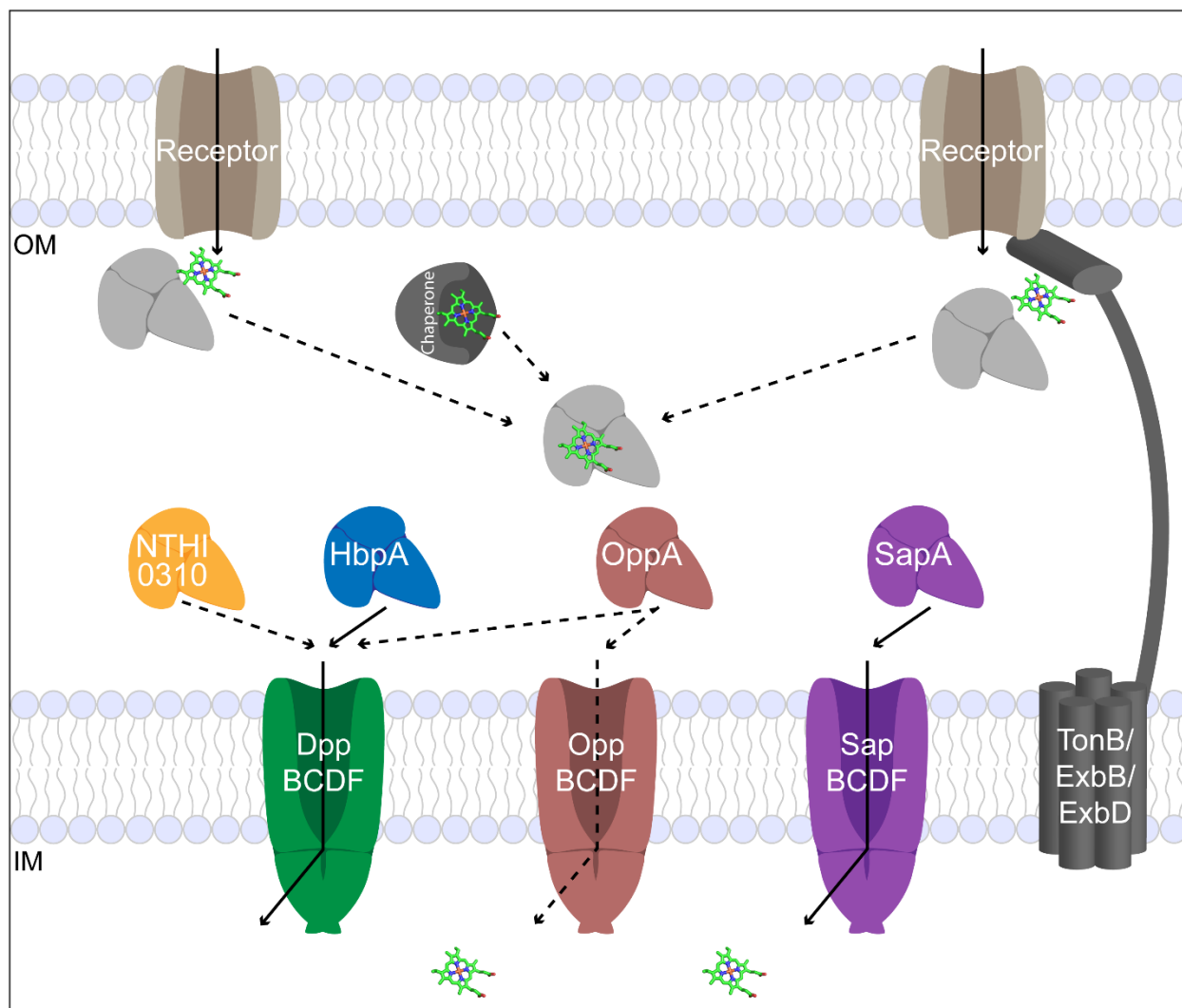
Figure 5.1. Cluster C SBPs have an important role in the NTHi heme uptake pathway. Cluster C SBPs acquire substrate from other components of the transport system, including metallochaperones or the receptor/TonB complex, and deliver it to one of the PepT importers for import into the cell.

Probing the interaction between the SBPs and heme led us to the discovery that the individual nthiOppA domains differentially contribute to substrate binding with domain I playing a dominant role in heme binding. The results presented in this thesis demonstrate all of the Cluster C SBPs have the potential to transport heme and highlight the importance of scrutinizing the functional overlap between these proteins when studying the heme uptake pathway.

A crystal structure of a Cluster C SBP heme complex could reveal the specific protein interactions responsible heme binding. However, the low solubility of heme in aqueous buffers and low pH crystallization conditions have made it difficult to obtain SBP heme co-crystals. Further studies of heme binding by Cluster C proteins are needed to discover the conserved heme-binding motif, how the SBPs prioritize heme binding, and the formation of ABC importer complexes for heme uptake.

5.2. Ligand-Specific Sites in the SBP Binding Cavity

The structure and functional studies of nthiOppA revealed two interesting findings: the novel nthiOppA hexapeptide complex demonstrated the flexibility of the binding cavity to expand and accommodate the longer peptide and ligand-specific sites in the individual nthiOppA domains play a dominant role in heme or peptide binding. These discoveries demonstrate the complexity of Cluster C SBPs binding cavities to accommodate and coordinate multisubstrate specificity for their roles in nutrient uptake and AMP resistance. The significance of the work presented in this thesis demonstrates the SBPs do not always have to choose one substrate over another and can accommodate canonical and heme substrates at the same time. The multifunctional roles of Cluster C SBPs make this a unique class of proteins in the ABC importer family yet it is one of the least understood aspects of the transporter mechanism.

As with shared heme specificity of Cluster C SBPs, the mechanism for heme and canonical substrate binding of nthiOppA is likely conserved in at least some of these SBPs. Interestingly, ecNikA has an oversized binding pocket even though it has a small canonical ligand. Simultaneous binding of canonical and heme substrates has been observed in an ecNikA competition assay were Ni^{2+} binding did not interfere with heme binding (162). Like nthiOppA, the heme binding cleft of peptide SBPs, ecDppA and ecMppA, is in close proximity to the peptide binding site. Excess canonical peptide in the growth media reduced heme utilization of ecDppA or ecMppA deletion mutants and demonstrated competition between canonical substrates and heme for these Cluster C SBPs (164). These SBPs have similar binding cavity features with ligand-specific sites for canonical substrates and heme as nthiOppA. To uncover the mechanisms regulating which substrates are delivered to ABC importers for transport, further understanding of how Cluster C SBPs accommodate canonical substrates and heme in their binding cavities and the determinants of substrate hierarchy for transport are needed.

5.3. Sap Mediated Defensin AMP Sensitivity

AMPs are a critical component of the host immune response to prevent bacterial infections. NthiSapA mediates antimicrobial resistance of NTHi defensin AMPs hNP1, hBD2, and hBD3. The data presented in this thesis demonstrates nthiSapA has high binding affinity for these defensin AMPs. The conserved loop regions of hNP1, hBD2 and hBD3 were sufficient for recognition of nthiSapA and binding was independent of the peptide loop structure. NthiSapA recognizes AMPs independent of peptide sequence. Overall, this work has broadened our understanding of how nthiSapA and the Sap system mediate NTHi sensitivity to AMPs.

Our collaborator Kevin Mason has shown that some AMPs can displace heme bound to

nthiSapA (110). The nthiSapA AMP complex structure would answer outstanding questions about nthiSapA AMP specificity and competition between heme and AMPs. Unfortunately, there are many difficulties to overcome for co-crystallization of the complex, the heterogeneity of the AMP sample, the low solubility of AMPs in salt buffer and the instability of nthiSapA in low salt buffer at crystallization concentrations. Future crystallization trials should explore nthiSapA in complex with fused fragments of defensin AMPs. Using a linker, target peptides could be covalently attached to nthiSapA, leading to a homogeneous sample for crystallization. With their high binding affinity, the loop regions of defensin AMPs are promising candidates to help solve the structure of nthiSapA bound defensin AMPs. Additionally, nthiSapA recognition of other AMPs, such as helical AMP cathelicidin, should be characterized to better understand AMP specificity of the nthiSapA.

Characterizing nthiSapA recognition of AMPs is important for designing new therapeutics to mimic the antimicrobial activity of these peptides without activating the Sap transport system or inhibit the SBP to increase the sensitivity of NTHi to AMPs. To identify the mechanisms driving nthiSapA AMP specificity, further peptide binding and structural studies are needed to characterize the protein-peptide interactions that regulate nthiSapA substrate recognition.

5.4. Future Directions to Explore

5.4.1. Regulation of Substrate Transport

As our understanding of substrate specificity for NTHi Cluster C SBPs advances, we can capitalize on this knowledge to uncovering more about the substrate specificity and transport of the PepT importers. The traditional regulatory mechanisms of ABC importers such as expression factors that regulate importer transcription or inactivation of the importer through the regulatory

domains of the NBDs have not been identified for the PepT transport systems (5). Uncovering regulatory mechanisms of the PepT importers will help to elucidate the differential roles nthiSapD and nthiSapF in the Sap transport system for AMP resistance and heme uptake, respectively. While the structure of nthiSapF did not reveal an obvious accessory domain that could serve as a traditional regulatory domain, nthiSapD contains an accessory domain with an iron sulfur cluster motif. It is possible that this accessory domain serves as an iron sensor. This indicates there is an additional possible level of regulation independent of the SBP's ability to select one substrate over another.

The assembly of the multicomponent PepT transporters is another avenue by which substrate transport could be regulated. Complex formation of the importers could influence the substrate specificity of the importer. Further characterization of the homo- and heterodimerization of the TMDs and the NBDs is of interest in determining how this may impact transport of both the canonical and heme substrate. As mentioned in Chapter 2, MppA selects transport systems based on its bound substrates and delivers peptides to the Opp system and heme to the Dpp system (164). More work is needed to determine whether all PepT transporters are involved in heme uptake or how substrate binding of SBPs can direct noncognate ABC importer complex formation. Answering some of the questions will expand our knowledge of the multifunctional roles of the Cluster C SBPs and PepT importers.

5.4.2.   SBPs are Promising Therapeutic Targets

Although in its infancy, the use of ABC importers as potential targets to thwart pathogenic bacteria has proven to be promising for the development of new therapies. While the approaches differ from mimics to inhibitors, the most promising cases capitalize on substrate recognition of

the SBP or complex formation between the SBP and transporter (242). In these cases, the loss of substrate binding or selective transport of substrates results in an inability of the bacteria to acquire necessary nutrients to support pathogenesis. Targeting biological systems essential for nutrient acquisition provides a viable alternative to therapeutics directed at cell surface proteins, which may be prone to antigenic variability or phase variation. Ultimately, therapeutics that target ABC importer functions have the potential to disrupt the virulence pathways of bacteria (243).

Targeting the SBP is a promising avenue for the design of therapeutics to restrict nutrient uptake by pathogens, thereby leading to the potential decrease in pathogen virulence. The zinc uptake pathway has proven the SBP is a promising target for new antimicrobial drugs to inhibit substrate binding (125). Additional therapeutics could target the translocation pathway of the TMDs and ATP-hydrolysis of the NBDs to prevent transport of nutrients and limit bacterial pathogenesis. Recent studies of other transporters, including AcrB and TAP, have identified inhibitors that lock the conformation of transporter and prevent substrate translocation (244,245). Although more work is still needed, many ABC importers have been identified as essential virulence factors for pathogens (242). These findings highlight the many vital cellular functions that can be exploited to fight bacterial infections and emphasize the promise of targeting these transport systems for the design of therapeutics.

There are many possible compounds with antimicrobial activity that might be potential therapeutics that exploit these SBP's roles in the uptake of the essential nutrient heme and resistance (Figure 5.2). Heme analog, gallium protoporphyrin IX, is recognized by the heme uptake pathway in bacteria and has antimicrobial activity against Gram-negative and Gram-positive bacteria (246-248). Additionally, many expect AMP-inspired compounds to be the next
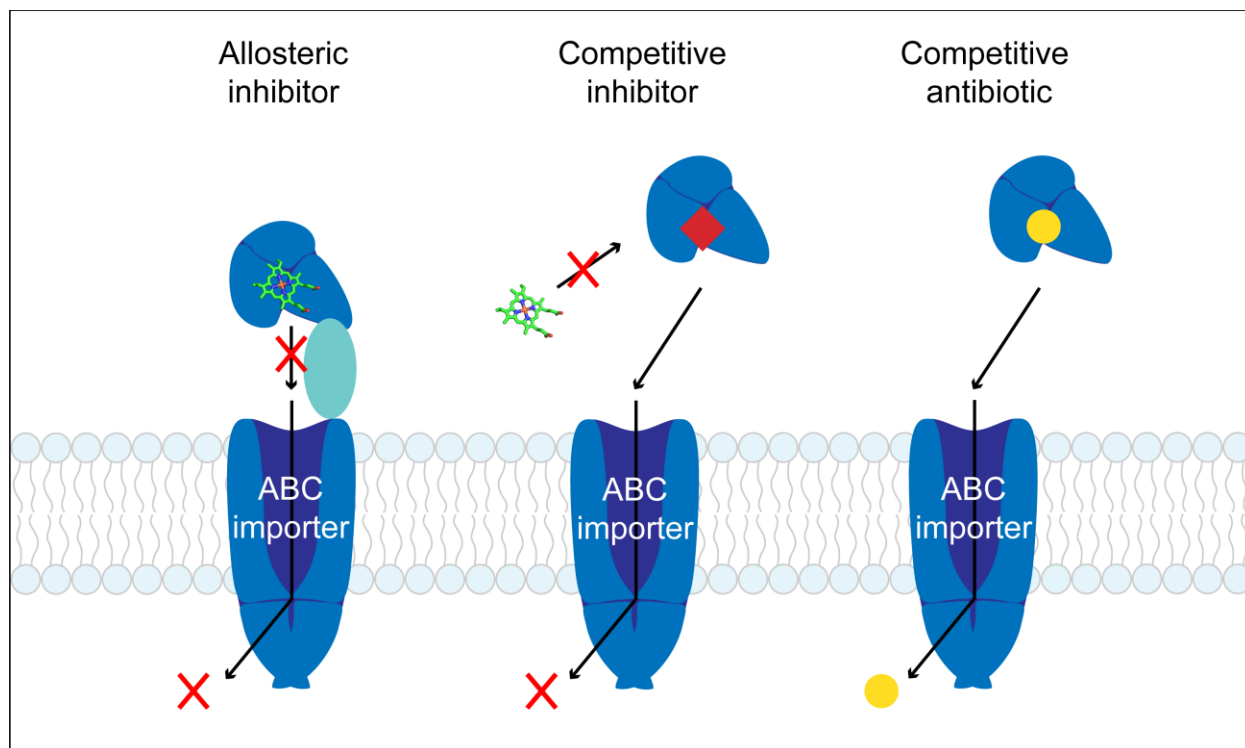
Figure 5.2. Therapeutics targeting SBPs to disrupt substrate transport. Allosteric inhibitors can prevent the SBP from binding substrates or the transfer of the substrate from the SBP to the TMDs. Competitive inhibitors can obstruct the binding cavity and block substrates from binding the SBP. Antibiotics that mimic SBP substrates can exploit nutrient uptake pathways to be imported into the cell.

generation of antimicrobial drugs (249). Some of the current challenges for peptides as novel antimicrobial agents are degradation by proteases, bioavailability at the infection site, and high production costs. Antibiotics, polymers, DNA, salts, phenolic derivatives, and gold nanoparticles are possible AMP-conjugates to amplify the effectiveness of AMPs through mechanisms of action that include increasing membrane permeability, reducing antigenicity, or transporting drugs across the bacterial membrane (236,250). Nano drug delivery systems can increase the biostability of AMPs, reduce off-target toxicity, and improve delivery of AMP to the target site (236).

Currently, there is one AMP synthetic analog approved for use by the FDA, Cancidas®, and many others in advanced stages of clinical trials including, iseganan, omiganan, Brilacidin®, and Novexatin® (237). Interestingly, Brilacidin®, and Novexatin® are both derivatives of defensin AMPs (249,251). Substrate mimetics and analogs have the potential to effectively exploit or inhibit the NTHi Cluster C SBPs for the development of therapeutic treatments for OM. This work highlights the need for a better understanding of the natural defense mechanisms bacteria have developed to evade the host immune response and emphasizes that these defense strategies must be considered in the design of new therapeutics.

CHAPTER 6:

Appendix

6.1. Controlling Drug Resistance: Functional Studies of Pleotropic Drug Resistance (PDR) Transcription Factors

6.1.1. Introduction

A wide range of antibiotics and antifungal medications has been developed to treat infections. Drug resistance is a major challenge in the ever-escalating fight against pathogens and is quickly rendering many of these drugs ineffective. Patients with compromised immune systems, the elderly, and infants are the most susceptible to fungal infections. Primary and opportunistic fungal pathogens have developed mechanisms to circumvent antifungal drugs. One mechanism known as the pleiotropic drug resistance (PDR) pathway utilizes a network of proteins to confer drug resistance against a wide range of diverse xenobiotics. Studying the PDR pathway in *Saccharomyces cerevisiae* will lead to a better understanding of homologous pathways identified in pathogenic species, such as *Canadida albicans*, *Canadida galbrata* and *Aspergillus fumigatus* (252-255). In vertebrates, this pathway is known as multi-drug resistance (MDR) and utilizes nuclear xenobiotic receptors, such as pregnane X receptor (PXR), to detect xenobiotics (256). The PDR pathway employs ABC transporters, major facilitators superfamily (MFS) transporters, sphingolipid biosynthesis proteins and zinc cluster transcription factors to identify and expel xenobiotics from the cell (257-259). The PDR response is controlled by several transcription factors including two major regulators, Pdr1 and Pdr3 (260,261). Transcriptional regulation of drug resistance ABC transporters by Pdr1 and Pdr3 has been well-characterized (262). Uncovering the DNA-recognition mechanisms of Pdr1 and Pdr3 will lead to a better understanding of xenobiotic-activated transcription of drug ABC transporters.

6.1.1.1. *Pdr1 and Pdr3 — Regulators of the PDR pathway*

The PDR pathway utilizes a sensor/effector regulatory mechanism to detect toxic molecules with a range of diversity including detergents, cancer drugs, antibiotics, and fungicides through ligand-binding transcription factors. In response to xenobiotics, Prd1 and Pdr3 activate the expression of PDR genes. These genes include ABC and MFS transporters to export xenobiotics out of the cell and enzymes that can manipulate the lipid composition of the membrane to disrupt diffusion of xenobiotics into the cell (Figure 6.1). Together, Pdr1 and Pdr3 regulate all known PDR genes, including positive autoregulation of Pdr3 (263,264). Of the known Pdr1 and Pdr3 target genes, ABC transporters *pdr5*, *yor1* and *snq2* have broad substrate specificity and are responsible for the efflux of most identified xenobiotics (265-267). Other transcription factors, such as Yrr1 and Stb5 have minor roles in the PDR pathway and only regulate a subset of PDR genes (268,269). Interestingly, hyperactive phenotypes of Pdr1 and Pdr3 have identified gain-of-function mutations that lead to an increase in the transcription of ABC transporters and enhance the drug resistance of cells (270,271).

As functional homologs that share 36% identity, Pdr1 and Pdr3 have overlapping roles in the PDR pathway. Either activator is sufficient for regulating the efflux transporters in the PDR pathway (263). Inactivation of both Pdr1 and Pdr3 is needed for a corresponding decrease in transcriptional levels of target genes, and an absence of both Pdr1 and Pdr3 creates cells that are highly susceptible to a broad range of xenobiotics (272). However, a few independent regulatory roles of Pdr1 and Pdr3 have been identified. Pdr1 activates the expression of *pdr5* for cycloheximide resistance and is necessary for the early PDR response to xenobiotics, benomyl and fluphenazine (273,274). Loss-of-function mutations in Pdr3 reduce resistance to some xenobiotics such as rhodamine 6G and diazaborine despite the presence of functional Pdr1
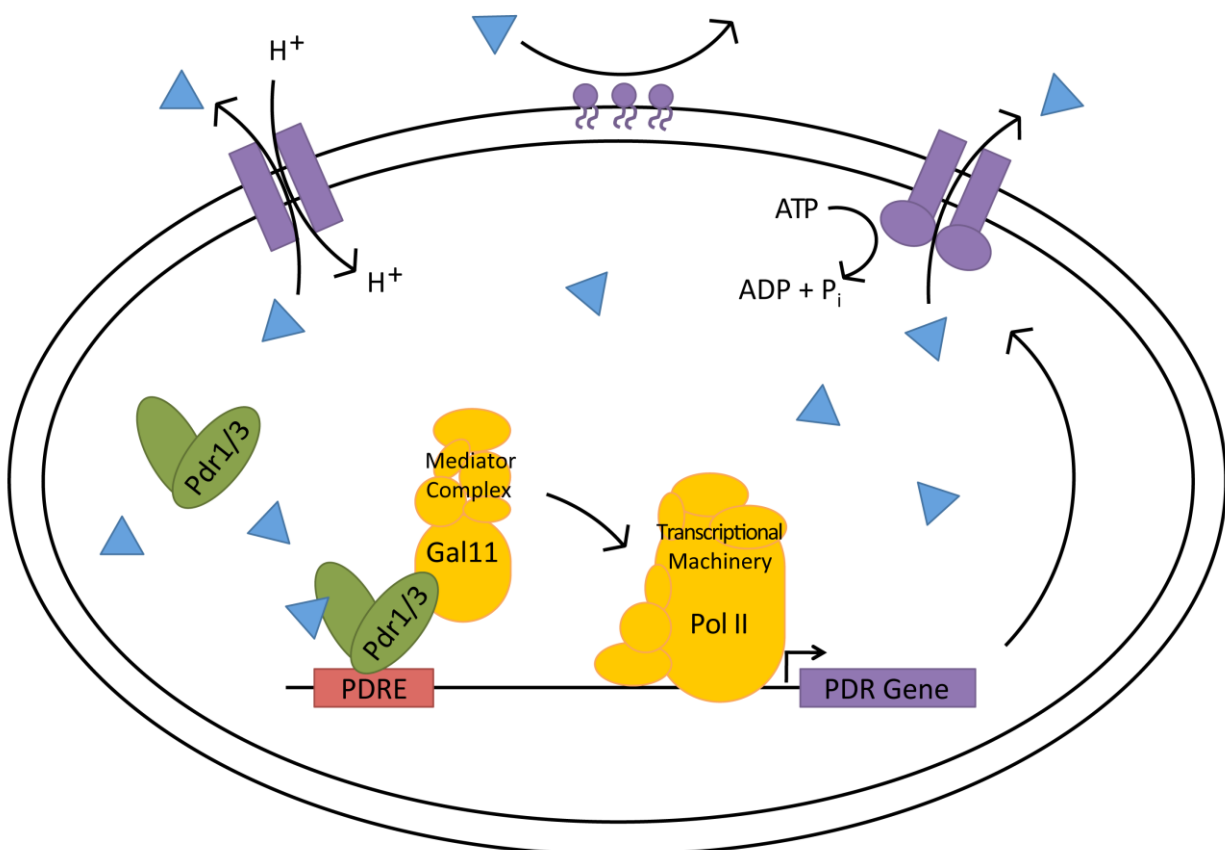
Figure 6.1. Xenobiotic-activated regulation of the pleiotropic drug resistance pathway by Pdr1 and Pdr3. PDR genes including ABC transporters, MFS transporters and sphingolipid biosynthesis proteins are regulated by Pdr1 and Pdr3. Pdr1 and Pdr3 have three regulatory domains: the DBD recognizes the promoter region of PDR genes, the XBD binds xenobiotics, and the TAD targets co-activator Gal11 of the Mediator complex. The Mediator complex recruits Pol II to activate transcription of the target PDR gene. ABC transporters hydrolyze ATP and MFS transporters exchange H^+ to transport xenobiotics out of the cell. Additionally, sphingolipid biosynthesis proteins modify the lipid composition of the membrane to regulate the diffusion of xenobiotics into the cell.

(275,276). The xenobiotic-activated mechanisms of Pdr1 and Pdr3 that lead to transcription of specific PDR genes and the differential response of the transcription factors to specific xenobiotics are unknown.

6.1.1.2. *Pleiotropic Drug Response Elements (PDREs) in Promoters of PDR Genes*

In the PDR pathway, Pdr1 and Pdr3 coordinate the expression of PDR genes by recognizing consensus motifs called pleiotropic drug response elements (PDREs) (267). The canonical PDRE includes 8bps with two everted CGG repeats, TCCGCGGA (277). Interestingly, these transcriptional regulators can tolerate sequence diversity within the binding site and recognize variant PDRE sites. Promoter regions of PDR genes have varying numbers and combinations of canonical and variant PDREs (278). Figure 6.2 depicts the canonical and variant PDREs in the promoter region of the prominent multisubstrate ABC exporter Pdr5. Many studies focus on *pdr5* transcription levels to examine Pdr1 and Pdr3 activity and the resulting drug resistance to a broad range of xenobiotics.

6.1.1.3. *Functional Domains of Pdr1 and Pdr3*

Pdr1 and Pdr3 each have three regulatory domains (Figure 6.3): the DNA-binding domain (DBD), the xenobiotic-binding domain (XBD), and the transactivation domain (TAD) (279-281). The DBD recognizes the PDREs in promoter regions of target PDR genes. Truncation studies have shown the DBDs of Pdr1 and Pdr3 (residues 1-207 and 1-146, respectively) are sufficient for DNA binding (277,279). The XBD is necessary for ligand-binding of Pdr1 and Pdr3 (282), and xenobiotic-activation of Pdr1 and Pdr3 can lead to the targeted up-regulation of specific PDR exporters. Transcription of *pdr5* is preferentially activated in response to cycloheximide,
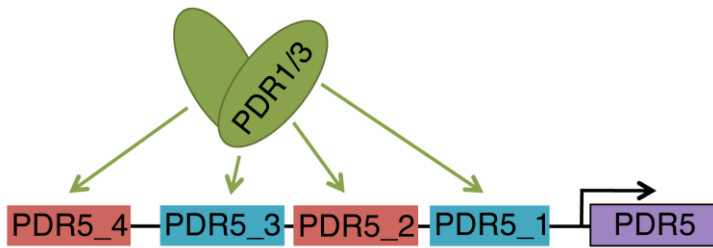
PDR5_1 ATGTC**TCCGCGGA**ACTCT
PDR5_2 GTGAT**TCCGTGGA**AAGGT
PDR5_3 CTCTT**TCCGCGGA**ATCGC
PDR5_4 AAACG**TCCGTGGA**GAACC

Figure 6.2. Multiple canonical and variant PDREs in the promoter region of _pdr5_. PDR5_1 and PDR5_3 are canonical PDREs shown in teal, and PDR5_2 and PDR5_4 are variant PDREs shown in red.

yor1 for oligomycin, and *snq2* for resazurine (272,283). The TAD directly binds co-activator Gal11 in the Mediator complex (282), and gain-of-function or loss-of-function mutations in the TAD alter Gal11 interactions to increase or disrupt transcription of PDR genes, respectively (284,285).

The DBD contains three motifs, the zinc finger, the linker and the dimerization regions (Figure 6.3). Pdr1 and Pdr3 are members of the well-characterized Gal4 zinc cluster transcription factor family. These fungal zinc cluster transcriptional regulators share a conserved $Zn(II)_2Cys_6$ motif for DNA recognition (286). There are two metal-binding sites in the zinc finger unit with each zinc atom coordinated by three cysteine residues (287). Members of the zinc cluster family recognize binding sites that contain direct, inverted, or everted repeats separated by a varying number of nucleotides. The orientation and distance of CGG repeats in the DNA-binding site is important for zinc finger protein specificity. The linker regions provide a rigid scaffold for zinc finger units to bind their targeted DNA motifs (288), and this region provides the specificity for Pdr1 and Pdr3 to bind the tandem everted CGG repeats that are characteristic of PDREs. Pdr1 and Pdr3 form dimers to bind PDREs. The dimerization region consists of a conserved coiled-coil motif and allows Pdr1 and Pdr3 to form homodimers and heterodimers with each other (289).

The goal of this project was to determine the binding affinity of Pdr1 and Pdr3 DBDs for canonical and variant PDREs from the promoter region of *pdr5*. Expression of Pdr1 and Pdr3 DBDs was achieved. However, only Pdr1 was stable and homogeneous after purification. Pdr3 was degraded during expression and purification. I observed the binding of Pdr1 DBD to Alexa488-labeled DNA duplexes and measured the binding affinity of canonical and variant PDREs by fluorescence polarization. DNA footprinting studies determined Pdr3 protects an 18-
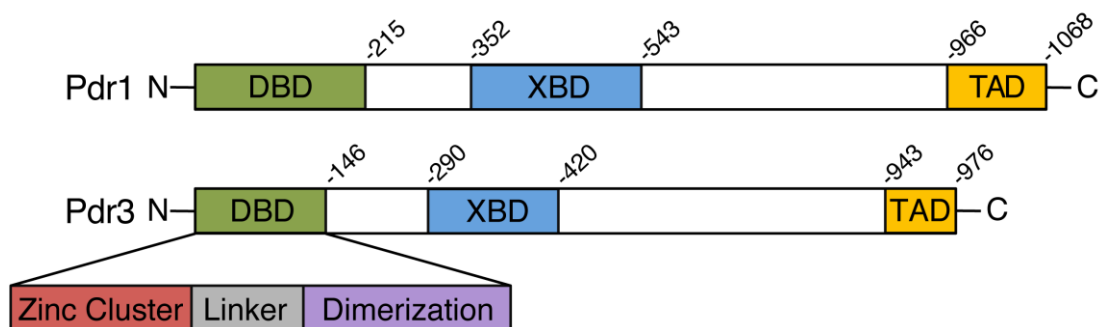
Figure 6.3. Functional domains of Pdr1 and Pdr3. Each transcription factor has an N-terminal DBD that recognizes PDRE binding sites in the promoter regions of PDR genes. The XBD directly binds xenobiotics for the differential regulation of PDR genes. The C-terminal TAD interacts with transcriptional machinery to initiate transcription.

base pair segment of DNA centered on the consensus PDRE sequence (264,290). I included these flanking regions of the PDRE sites and discovered Pdr1 DBD DNA recognition includes more than the consensus PDRE motif.

6.1.2. Experimental Procedures

6.1.2.1. Expression Vectors of Pdr1 and Pdr3

S. cerevisiae Pdr1 and Pdr3 genes were amplified from the yeast cDNA tiling library stored in the Northwestern High Throughput Analysis Laboratory. A domain truncation strategy was used to optimize solubility of Pdr1 and Pdr3 constructs. Domain constructs were designed with ligation independent cloning (LIC) primers, forward primer TACTTCCAATCCAATGCA and reverse primer TTATCCACTTCCAATGTTA, for insertion into a N-terminal tag expression vector. Using the LIC technique, Pdr1 and Pdr3 domains were cloned into the MSCG10 vector to create N-terminal His_6-GST (glutathione-S-transferase) fused constructs with a TEV protease cleavable tag. All plasmids were verified by sequencing (ACGT Inc.).

Constructs were transformed in BL21(DE3), BL21(DE3) pLysS, Rosetta(DE3), and Rosetta(DE3) pLysS strains for expression testing. Table 6.1 summarizes the Pdr1 and Pdr3 domain constructs that were created and the initial expression conditions that were tested. In brief, expression of Pdr1 and Pdr3 constructs were tested in all four strains. Cells were grown in Luria Broth media with the appropriate antibiotics at 37°C. Cells were induced with 400 μM IPTG at an OD_{600} of 0.6. Samples were taking at 0 h and 3 h to evaluate protein expression. Alternatively, expression of some strains was carried out using Terrific Broth media with the appropriate antibiotics. Cells were grown at 37°C to an OD_{600} of 0.4, and then the incubator was then cooled to 16°C. Cells were induced with 400 μM IPTG at an OD_{600} of 0.8. Samples were

taking at 0 h, 2 h, 6 h, and ON to evaluate protein expression. Anti-His western blots of expression time points were used to determine protein expression levels. Pdr1 and Pdr3 constructs with high expression levels were tested for solubility by trial purifications (Table 6.2).

6.1.2.2. *Expression and Purification of Pdr1*

Pdr1 constructs GST_R_1-152 and GST_R_1-168 were expressed in Rosetta(DE3) and Rosetta(DE3) pLysS, respectively. Cultures of 1 L Luria Broth media were inoculated with a dilution of 1:1000 overnight culture and supplemented with 100 μg/mL ampicillin and 34 μg/mL chloramphenicol. Cells were grown at 37°C to OD_{600} of 0.6 and induced with 400 μM IPTG. Cells were cultured for 3 h and harvested by centrifugation at 5000 rpm. Cell pellets were stored at -80°C.

All steps of the purification were kept at 4°C. A 4 g cell pellet was resuspended in 40 mL buffer A (25 mM Tris pH 7.5, 150 mM NaCl, 10 μM zinc acetate, 15 mM imidazole pH 7.4, 10% glycerol) and thawed on ice for 15 min. To prevent protein degradation, 100 μM phenylmethylsulfonyl fluoride (PMSF) was added to the resuspended cell pellet before cell lysis. The homogenizer was used to mix the cells until the solid portions were completely blended into the mixture. In an ice bath, the mixture was lysed for 2 min at amplitude of 40, 2 s on time, and 8 s off time using S-4000 sonicator. The cellular contents were pelleted by centrifugation at 17,000 rpm for 30 min. The supernatant was transferred to an equilibrated 6 mL column volume Ni-NTA affinity chromatography column and allowed to batch on a rotary shaker for 30 min. After passing the supernatant over the column, the flow through was collected and passed over the column a second time. The column was washed with 10 column volume buffer A. To remove bound DNA, the column was washed using a high salt solution with 10 column volume of buffer

Table 6.1. Pdr1 and Pdr3 constructs and trial protein expression.

	Domain	Construct	Vector	Expression Test			
				Bl21 (DE3)	BL21 (DE3) pLysS	Rosetta (DE3)	Rosetta (DE3) pLysS
PDR1	DNA-Binding Domain	R_1-152	MCSG10	pink		green	green
		R_1-168	MCSG10	yellow	pink	yellow	green
		R_1-182	MCSG10	yellow	pink	yellow	pink
		R_1-207	MCSG10	gray	gray	green	green
		R_1-233	MCSG10	gray	gray	pink	green
		R_1-252	MCSG10	green	gray	pink	pink
		R_1-337	MCSG10	gray	gray	green	pink
		R_1-351	MCSG10	gray	gray	yellow	yellow
	Xenobiotic-Binding Domain	R_329-543	MCSG10	gray	gray	pink	green
			MCSG7	orange	gray	orange	orange
			MCSG23	green	x	x	x
			pWaldoD	gray	gray	gray	gray
		R_352-543	MCSG10	gray	orange	blue	green
			MCSG7	orange	gray	blue	orange
			MCSG23	green	x	x	x
			pWaldoD	gray	x	x	x
	Activation Domain	R_544-1068	MCSG10	gray	gray	gray	pink
		R_966-1068	MCSG10	gray	gray	gray	gray
	Multi-Domain Construct	R_1-543	MCSG10	pink	pink	orange	yellow
		R_352-1068	MCSG10	gray	gray	yellow	gray
		R_1-1068	MCSG10	gray	gray	gray	gray
PDR3	DNA-Binding Domain	D_1-134	MCSG10	pink	gray	pink	pink
		TEV_D-1-146	pET19b	green	x	x	x
		D_1-168	MCSG10	blue	green	blue	green
		D_1-198	MCSG10	blue	pink	yellow	green
		D_1-217	MCSG10	pink	yellow	blue	pink
		D_1-290	MCSG10	gray	gray	blue	pink
	Xenobiotic-Binding Domain	D_290-420	MCSG10	gray	gray	gray	pink
			MCSG7	orange	gray	orange	gray
			pWaldoD	gray	gray	gray	gray
		D_298-424	MCSG10	gray	gray	gray	gray
	Activation Domain	D_428-976	MCSG10	gray	gray	gray	gray
		D_762-976	MCSG10	gray	gray	gray	pink
	Multi-Domain Construct	D_1-424	MCSG10	pink	gray	gray	yellow
		D_290-976	MCSG10	gray	gray	gray	pink
		D_1-976	MCSG10	pink	gray	gray	gray

Legend:

- (green) 37C LB = High Expression
- (yellow) 37C LB = Low expression/pellet
- (pink) 37C LB = No expression
- (blue) 16C TB = High expression
- (orange) 16C TB = Low expression/pellet
- (gray) Expression unknown
- x Construct not transformed in strain

Table 6.2. Trial purifications of Pdr1 and Pdr3 constructs.

	Domain	Construct	Vector	Trial Purification		Notes
				Rosetta(DE3)	Rosetta(DE3) pLysS	
PDR1	DNA-Binding Domain	R_1-152	MCSG10	37C LB = soluble	37C LB = soluble	
		R_1-168	MCSG10		37C LB = soluble	
		R_1-182	MCSG10			
		R_1-207	MCSG10	37C LB = soluble		
		R_1-233	MCSG10			
		R_1-252	MCSG10			
		R_1-337	MCSG10	37C LB = slightly soluble		
		R_1-351	MCSG10			
	Xenobiotic-Binding Domain	R_329-543	MCSG10	37C LB = pellet		
			MCSG7		16C TB = slightly soluble	
			MCSG23			
			pWaldoD			
		R_352-543	MCSG10	16C TB = slightly soluble 37C LB = pellet		
			MCSG7	16C TB = slightly soluble	16C TB = slightly soluble	
			MCSG23			
			pWaldoD			
	Activation Domain	R_544-1068	MCSG10			
		R_966-1068	MCSG10			
	Multi-Domain Construct	R_1-543	MCSG10	16C TB = pellet		
		R_352-1068	MCSG10	37C LB = pellet		
		R_1-1068	MCSG10			
PDR3	DNA-Binding Domain	D_1-134	MCSG10			
		TEV_D-1-146	pET19b			
		D_1-168	MCSG10	16C TB = soluble	37C LB = soluble	Degraded products
		D_1-198	MCSG10		37C LB = soluble	Degraded products
		D_1-217	MCSG10	16C TB = slightly soluble		
		D_1-290	MCSG10			
	Xenobiotic-Binding Domain	D_290-420	MCSG10			
			MCSG7			
			pWaldoD			
		D_298-424	MCSG10			
	Activation Domain	D_428-976	MCSG10			
		D_762-976	MCSG10			
	Multi-Domain Construct	D_1-424	MCSG10			
		D_290-976	MCSG10			
		D_1-976	MCSG10			

B (buffer A supplemented to 1 M NaCl and 50 mM imidazole pH 7.4). The protein was eluted with 10 column volume of buffer C (buffer A supplemented to 300 mM imidazole pH 7.4). For the first couple of elution fractions the resin was stirred and incubated for 5 to 10 min in buffer C. The eluted protein (determined by SDS-PAGE to be >95% pure) was dialyzed with TEV protease in buffer D (25 mM Tris pH 7.5, 150 mM NaCl, 10 μM zinc acetate, 1 mM DTT) for at least 4 h. The DTT was removed by overnight dialysis in buffer E (25 mM Tris pH 7.5, 150 mM NaCl, 10 μM zinc acetate).

TEV protease was removed from the sample using an equilibrated 12 mL column volume Ni-NTA affinity chromatography column. The dialyzed protein was transferred onto the nickel column and the column was batched on a rotary shaker for 30 min. After the dialyzed protein was allowed to flow through the column, it was collected and passed over the column a second time. The flow through contained the TEV cleaved protein sample. The column was washed with 10 column volume buffer A, and 10 column volume of buffer F (buffer A supplemented to 50 mM imidazole pH 7.4). The TEV protease and protein tag was eluted with 10 column volume of buffer C. The flow through and equilibration fractions (determined by SDS-PAGE to be >95% pure) were immediately concentrated to 1.2 mL using a 10 kDa Amicon concentrator. Pdr1 constructs may have stability issues while sitting for prolonged periods of time. Immediately after concentration, the protein was applied to a HiLoad 16/600 Superdex 200 size-exclusion chromatography column in buffer E. The protein fractions were pooled and concentrated. The sample quality of R_1-152 (Figure 6.4) and R_1-168 (Figure 6.5) were evaluated by purification SDS-PAGE images and size-exclusion chromatograms at each step of the purification process.
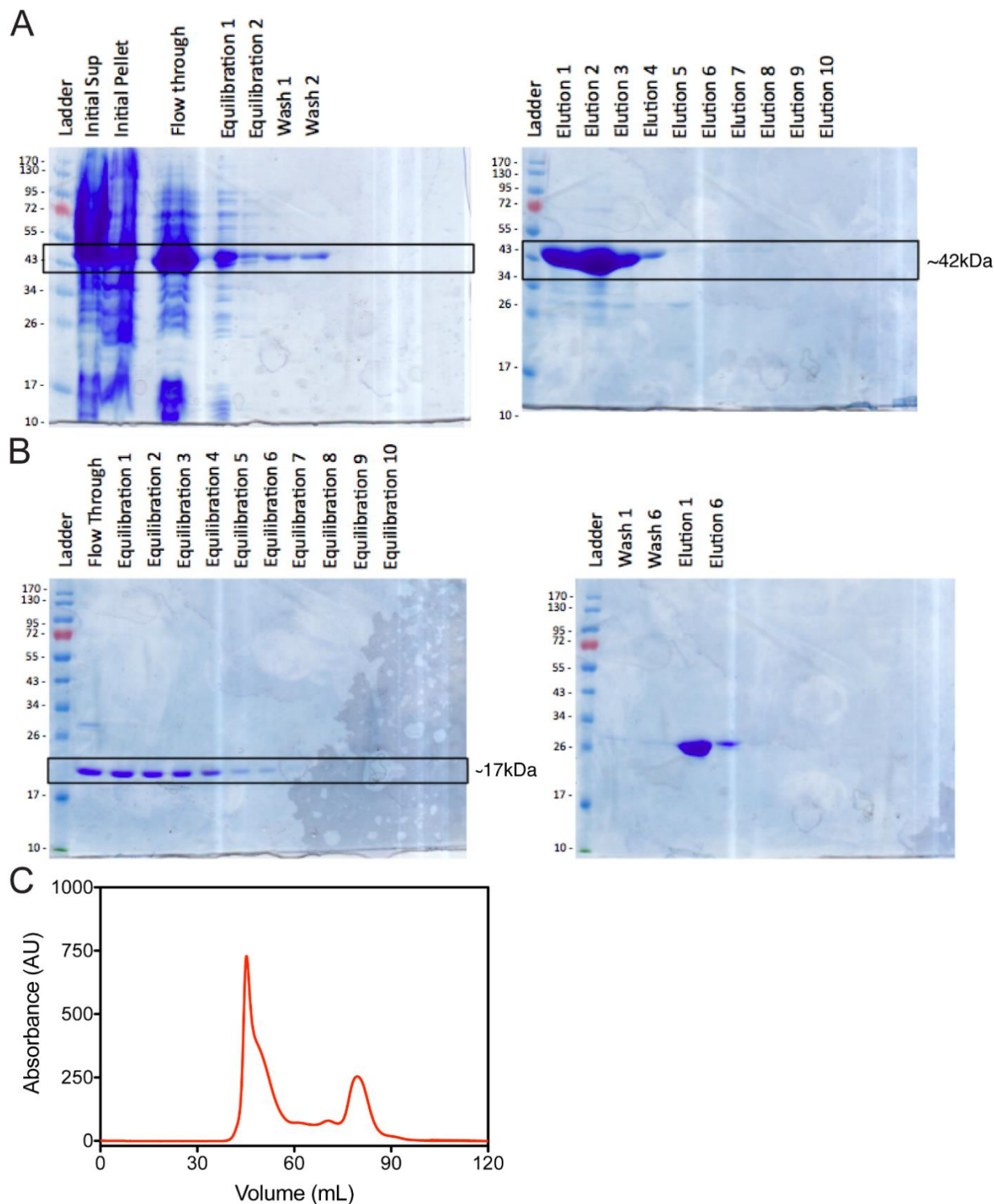
Figure 6.4. Protein purification of R_1-152. SDS-PAGE images of (A) the first nickel affinity column and (B) the second nickel affinity column after TEV protease cleavage of R_1-152. (C) Size-exclusion chromatograph of R_1-152.
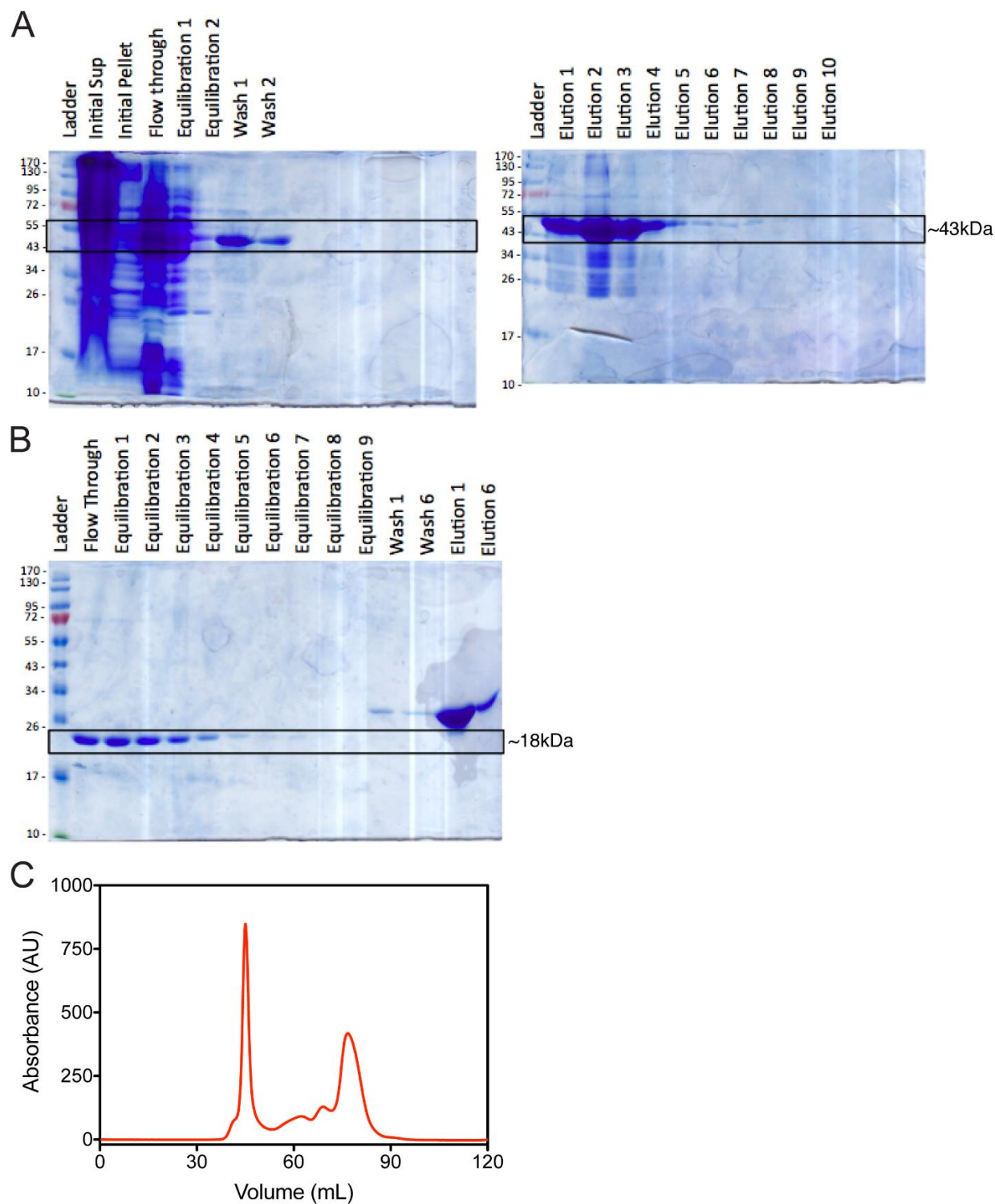
Figure 6.5. Protein purification of R_1-168. SDS-PAGE images of (A) the first nickel affinity column and (B) the second nickel affinity column after TEV protease cleavage of R_1-168. (C) Size-exclusion chromatograph of R_1-168.

6.1.2.3. DNA Annealing

Oligonucleotides are listed in Table 6.3. Alexa488-labeled ssDNA fragments were obtained from IDT Inc. The lyophilized ssDNA was resuspened in ddH2O to make a 1 mM stock solution. Complimentary ssDNA was combined in equal volumes and diluted with 2x annealing buffer (10 mM Tris pH 7.5, 50 mM NaCl) for a final stock concentration of 250 μM. The sample was then heated at 95°C for 5 min. The sample was allowed to gently cool to RT overnight. The annealed DNA was stored at -20°C.

6.1.2.4. *Fluorescence Polarization Assay*

The dsDNA probe was prepared in binding buffer (50 mM Tris pH 7.5, 45 mM NaCl, 5 mM $MgCl_2$, 10 μM zinc acetate). Purified Pdr1 from 1 nM to 10 μM (1.5-fold serial dilution) in binding buffer was incubated with 2 nM probe for 1 h at 4°C. All fluorescence polarization experiments were performed on a Synergy4 (Biotek) at 25°C with excitation and emission filters 485/20 and 528/20, respectively. Measurements were collected in triplicate using a 384-well plate (Greiner Bio-one, Cat. No. 781076). The data were fit with a one-site binding model using GraphPad Prism 6.0.

6.1.3. *Results*

6.1.3.1. DNA Recognition of Pdr1 DBD Includes Flanking Regions of PDREs

Fluorescence polarization was used to characterize the DNA-protein interactions of PDRE and Pdr1 DBD complex formation (Figure 6.6). All four PDREs from the promoter region of *pdr5* were synthesized with a fluorescent Alexa488 label on the 5' end of ssDNA and annealed together to create a duplex. Each 18bp DNA duplex was designed to include the 5bp

Table 6.3. Alexa488-labeled oligonucleotides.

	Labeled DNA strand	Complimentary DNA strand
PDR5_1	Alexa488-ATGTCTCCGCGGAACTCT	AGAGTTCCGCGGAGACAT
PDR5_2	Alexa488-GTGATTCCGTGGAAAGGT	ACCTTTCCACGGAATCAC
PDR5_3	Alexa488-CTCTTTCCGCGGAATCGC	GCGATTCCGCGGAAAGAG
PDR5_4	Alexa488-AAACGTCCGTGGAGAACC	GGTTCTCCACGGACGTTT

flanking regions on either side of the 8bp PDRE.

Table 6.4 summarizes the PDRE binding affinities for the Pdr1 DBD constructs. For R_1-152, the canonical PDR5_3 has the highest affinity, K_D value of 71 nM. Interestingly, the flanking regions are a major determining factor for Pdr1 DBD DNA binding affinity. Pdr1 DBD has higher binding affinity for variant PDR5_2 than canonical PDR5_1 with K_D values of 186 nM and 371 nM, respectively. Variant PDR5_4 has reduced binding with a K_D value of 883 nM. Overall R_1-152 and R_1-168 share a similar binding trend with the tightest affinity for PDR5_3 and weakest for PDR5_4 with K_D values of 113 nM and 938 nM, respectively. Again, variant PDR5_2 has a higher affinity than canonical PDR5_1 with K_D values of 308 nM and 534 nM, respectively. The longer Pdr1 construct, R_1-168, has slightly weaker binding affinities for all PDREs in comparison to R_1-152. In addition to the PDRE consensus motif, the 5bp flanking regions of the PDRE binding site determine DNA recognition of Pdr1 DBD.

6.1.4. Discussion

These results are significant for the understanding of how PDR transcriptional activators interact with multiple binding sites for the overall regulation of a target gene. Pdr1 DBD binding affinity ranks from tightest to weakest, PDR5_3 > PDR5_2 > PDR5_1 > PDR5_4. Surprisingly, a variant PDRE, PDR5_2 has higher affinity than a canonical PDRE, PDR5_1, indicating DNA recognition is not solely dependent on the consensus PDRE sequence. Sequential deletion studies of the *pdr5* promoter show that the first three PDRE sites are needed for basal expression of Pdr5, PDR5_4 can be eliminated without affecting basal levels (291). Pdr1 DBD binding affinity of correlates to the regulation of *pdr5* expression. Further studies to examine how the flanking regions enhanced or depressed binding affinity of Pdr1 DBD for canonical and variant PDREs
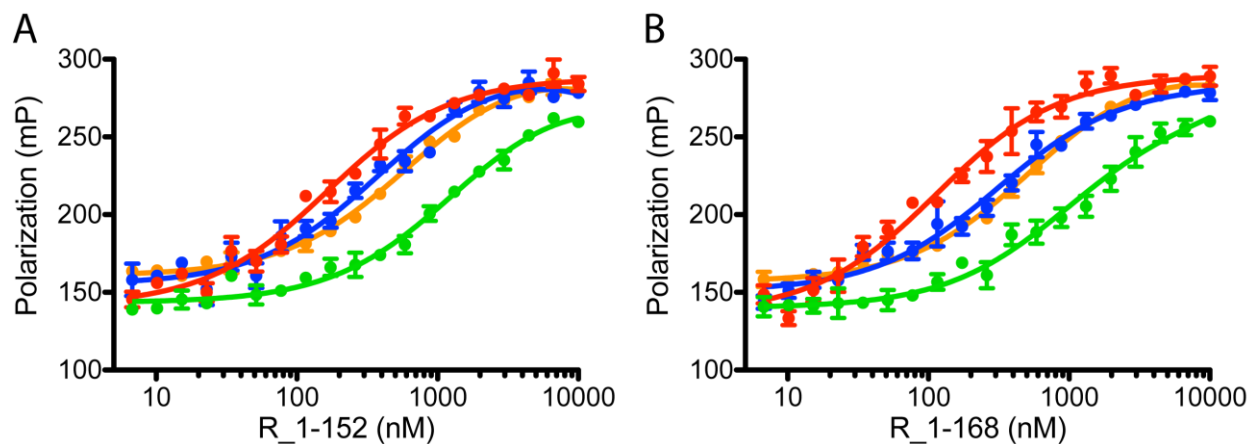
Figure 6.6. Flanking regions of PDREs influences Pdr1 DBD recognition. Fluorescence polarization of Pdr1 DBDs (A) R_1-152 and (B) R_1-168 binding the four PDREs from the promoter region of *pdr5*. Canonical PDREs PDR5_1 and PDR5_3 are represented by orange and red circles, respectively, and variant PDREs PDR5_2 and PDR5_4 are depicted by blue and green circles, respectively. Error bars represent data collected in triplicate, and a one-site binding model was used to fit the data shown with lines colored to match the corresponding PDRE.

Table 6.4. Pdr1 DBD equilibrium binding constants.

	R_1-152			R_1-168		
	K_D		σ	K_D		σ
PDR5_1	371	±	54	534	±	47
PDR5_2	186	±	31	308	±	51
PDR5_3	71	±	9	113	±	17
PDR5_4	883	±	223	938	±	247

* Standard deviation of triplicates

are needed. Mutating *pdr5* PDREs to the opposite canonical or variant site would provide a direct comparison for the influence of the flanking regions and consensus PDRE sequences on binding affinity of Pdr1 DBD.

The fluorescence polarization experiment developed in this study could be used to measure the DNA binding affinity of Pdr3 DBD. Optimization of Pdr3 DBD construct design is needed to improve protein expression and prevent protein degradation to produce a homogenous sample with high purity. Unfortunately, the temperature-sensitive nature of the DBD constructs have made other binding affinity experiments, such as SPR, difficult. One limitation of this study is that the Pdr1 DBD constructs are shorter than the predicted DBD (residues 1-207) needed for full transcriptional activity. The Pdr1 DBD constructs used are sufficient for DNA recognition but might be missing important regions needed for dimerization.

In a xenobiotic-dependent manner, Pdr1 and Pdr3 differentially regulate PDR genes despite the similarities in PDRE sequences. Expanding this study to determine how xenobiotics interact with Pdr1 and Pdr3 to influence the DNA recognition of DBD is an important next step. A detailed understanding of DBD DNA binding affinity and ligand-binding of the XBD will shed light on the mechanism of Pdr1 and Pdr3 xenobiotic-activated regulation of drug ABC transporters. More broadly, this research could be used to understand how pathogens acquire drug resistance, target drug design for increased therapeutic efficacy and find inhibitors to prevent drug resistance of pathogens.

REFERENCES

1. Chaturvedi, K. S., and Henderson, J. P. (2014) Pathogenic adaptations to host-derived antibacterial copper. *Front Cell Infect Microbiol* **4**, doi: 10.3389/fcimb.2014.00003

2. Higgins, C. F. (1992) ABC transporters: from microorganisms to man. *Annu Rev Cell Biol* **8**, 67-113

3. Berntsson, R. P., Smits, S. H., Schmitt, L., Slotboom, D. J., and Poolman, B. (2010) A structural classification of substrate-binding proteins. *FEBS Lett* **584**, 2606-2617

4. Higgins, C. F., and Linton, K. J. (2004) The ATP switch model for ABC transporters. *Nat Struct Mol Biol* **11**, 918-926

5. Rice, A. J., Park, A., and Pinkett, H. W. (2014) Diversity in ABC transporters: type I, II and III importers. *Crit Rev Biochem Mol Biol* **49**, 426-437

6. van der Heide, T., and Poolman, B. (2002) ABC transporters: one, two or four extracytoplasmic substrate-binding sites? *EMBO Rep* **3**, 938-943

7. Scheepers, G. H., Lycklama a Nijeholt, J. A., and Poolman, B. (2016) An updated structural classification of substrate-binding proteins. *FEBS Lett* **590**, 4393-4401

8. Biemans-Oldehinkel, E., Doeven, M. K., and Poolman, B. (2006) ABC transporter architecture and regulatory roles of accessory domains. *FEBS Lett* **580**, 1023-1035

9. ter Beek, J., Duurkens, R. H., Erkens, G. B., and Slotboom, D. J. (2011) Quaternary Structure and Functional Unit of Energy Coupling Factor (ECF)-type Transporters. *J Biol Chem* **286**, 5471-5475

10. Slotboom, D. J. (2014) Structural and mechanistic insights into prokaryotic energy-coupling factor transporters. *Nat Rev Microbiol* **12**, 79-87

11. Beis, K. (2015) Structural basis for the mechanism of ABC transporters. *Biochem Soc Trans* **43**, 889-893

12.   Locher, K. P. (2016) Mechanistic diversity in ATP-binding cassette (ABC) transporters. *Nat Struct Mol Biol* **23**, 487-493

13.   Rees, D. C., Johnson, E., and Lewinson, O. (2009) ABC transporters: the power to change. *Nat Rev Mol Cell Bio* **10**, 218-227

14.   Xu, K., Zhang, M. H., Zhao, Q., Yu, F., Guo, H., Wang, C. Y., He, F. Y., Ding, J. P., and Zhang, P. (2013) Crystal structure of a folate energy-coupling factor transporter from *Lactobacillus brevis*. *Nature* **497**, 268-271

15.   Eitinger, T., Rodionov, D. A., Grote, M., and Schneider, E. (2011) Canonical and ECF-type ATP-binding cassette importers in prokaryotes: diversity in modular organization and cellular functions. *FEMS Microbiol Rev* **35**, 3-67

16.   Vitreschak, A. G., Rodionov, D. A., Mironov, A. A., and Gelfand, M. S. (2002) Regulation of riboflavin biosynthesis and transport genes in bacteria by transcriptional and translational attenuation. *Nucleic Acids Res* **30**, 3141-3151

17.   Gutierrez-Preciado, A., Torres, A. G., Merino, E., Bonomi, H. R., Goldbaum, F. A., and Garcia-Angulo, V. A. (2015) Extensive Identification of Bacterial Riboflavin Transporters and Their Distribution across Bacterial Species. *PLoS One* **10**, doi: 10.1371/journal.pone.0126124

18.   Messenger, A. J. M., and Barclay, R. (1983) Bacteria, iron and pathogenicity. *Biochem Educ* **11**, 54-64

19.   Hood, M. I., and Skaar, E. P. (2012) Nutritional immunity: transition metals at the pathogen-host interface. *Nat Rev Microbiol* **10**, 525-537

20.   Weinberg, E. D. (1975) Nutritional immunity. Host's attempt to withold iron from microbial invaders. *JAMA* **231**, 39-41

21. Payne, S. M., Mey, A. R., and Wyckoff, E. E. (2016) Vibrio Iron Transport: Evolutionary Adaptation to Life in Multiple Environments. *Microbiol Mol Biol Rev* **80**, 69-90

22. Sheldon, J. R., and Heinrichs, D. E. (2015) Recent developments in understanding the iron acquisition strategies of gram positive pathogens. *FEMS Microbiol Rev* **39**, 592-630

23. Skaar, E. P. (2010) The Battle for Iron between Bacterial Pathogens and Their Vertebrate Hosts. *PLoS Path* **6**, doi: 10.1371/journal.ppat.1000949

24. Porcheron, G., Garenaux, A., Proulx, J., Sabri, M., and Dozois, C. M. (2013) Iron, copper, zinc, and manganese transport and regulation in pathogenic Enterobacteria: correlations between strains, site of infection and the relative importance of the different metal transport systems for virulence. *Front Cell Infect Microbiol* **3**, doi: 10.3389/fcimb.2013.00090

25. Palmer, L. D., and Skaar, E. P. (2016) Transition Metals and Virulence in Bacteria. *Annu Rev Genet* **50**, 67-91

26. Yang, X. H., Becker, T., Walters, N., and Pascual, D. W. (2006) Deletion of *znuA* virulence factor attenuates *Brucella abortus* and confers protection against wild-type challenge. *Infect Immun* **74**, 3874-3879

27. Ammendola, S., Pasquali, P., Pistoia, C., Petrucci, P., Petrarca, P., Rotilio, G., and Battistoni, A. (2007) High-affinity Zn^{2+} Uptake System ZnuABC is Required for Bacterial Zinc Homeostasis in Intracellular Environments and Contributes to the Virulence of *Salmonella enterica*. *Infect Immun* **75**, 5867-5876

28. Campoy, S., Jara, M., Busquets, N., de Rozas, A. M. P., Badiola, I., and Barbe, J. (2002) Role of the high-affinity zinc uptake znuABC system in *Salmonella enterica* serovar Typhimurium virulence. *Infect Immun* **70**, 4721-4725

29. Davis, L. M., Kakuda, T., and DiRita, V. J. (2009) A *Campylobacter jejuni znuA* orthologue is essential for growth in low-zinc environments and chick colonization. *J Bacteriol* **191**, 1631-1640

30. Murphy, T. F., Brauer, A. L., Kirkham, C., Johnson, A., Koszelak-Rosenblum, M., and Malkowski, M. G. (2013) Role of the zinc uptake ABC transporter of *Moraxella catarrhalis* in persistence in the respiratory tract. *Infect Immun* **81**, 3406-3413

31. Sabri, M., Houle, S., and Dozois, C. M. (2009) Roles of the extraintestinal pathogenic *Escherichia coli* ZnuACB and ZupT Zinc transporters during urinary tract infection. *Infect Immun* **77**, 1155-1164

32. Bobrov, A. G., Kirillina, O., Fetherston, J. D., Miller, M. C., Burlison, J. A., and Perry, R. D. (2014) The *Yersinia pestis* siderophore, yersiniabactin, and the ZnuABC system both contribute to zinc acquisition and the development of lethal septicaemic plague in mice. *Mol Microbiol* **93**, 759-775

33. Perry, R. D., Bobrov, A. G., and Fetherston, J. D. (2015) The role of transition metal transporters for iron, zinc, manganese, and copper in the pathogenesis of *Yersinia pestis*. *Metallomics* **7**, 965-978

34. Desrosiers, D. C., Bearden, S. W., Mier, I., Jr., Abney, J., Paulley, J. T., Fetherston, J. D., Salazar, J. C., Radolf, J. D., and Perry, R. D. (2010) Znu is the predominant zinc importer in *Yersinia pestis* during in vitro growth but is not essential for virulence. *Infect Immun* **78**, 5163-5177

35. Hood, M. I., Mortensen, B. L., Moore, J. L., Zhang, Y. F., Kehl-Fie, T. E., Sugitani, N., Chazin, W. J., Caprioli, R. M., and Skaar, E. P. (2012) Identification of an *Acinetobacter baumannii* zinc acquisition system that facilitates resistance to calprotectin-mediated zinc

sequestration. *PLoS Path* **8**, doi: 10.1371/journal.ppat.1003068

36.   Nielubowicz, G. R., Smith, S. N., and Mobley, H. L. (2010) Zinc uptake contributes to motility and provides a competitive advantage to *Proteus mirabilis* during experimental urinary tract infection. *Infect Immun* **78**, 2823-2833

37.   Kehres, D. G., Janakiraman, A., Slauch, J. M., and Maguire, M. E. (2002) SitABCD is the alkaline Mn(2+) transporter of *Salmonella enterica* serovar Typhimurium. *J Bacteriol* **184**, 3159-3166

38.   Kelliher, J. L., and Kehl-Fie, T. E. (2016) Competition for manganese at the host-pathogen interface. *Prog Mol Biol Transl* **142**, 1-25

39.   Boyer, E., Bergevin, I., Malo, D., Gros, P., and Cellier, M. F. (2002) Acquisition of Mn(II) in addition to Fe(II) is required for full virulence of *Salmonella enterica* serovar Typhimurium. *Infect Immun* **70**, 6032-6042

40.   Lim, K. H. L., Jones, C. E., vanden Hoven, R. N., Edwards, J. L., Falsetta, M. L., Apicella, M. A., Jennings, M. P., and McEwan, A. G. (2008) Metal binding specificity of the MntABC permease of *Neisseria gonorrhoeae* and its influence on bacterial growth and interaction with cervical epithelial cells. *Infect Immun* **76**, 3569-3576

41.   Liu, M., Bouhsira, E., Boulouis, H. J., and Biville, F. (2013) The *Bartonella henselae* SitABCD transporter is required for confronting oxidative stress during cell and flea invasion. *Res Microbiol* **164**, 827-837

42.   Litwin, C. M., and Calderwood, S. B. (1993) Role of Iron in Regulation of Virulence Genes. *Clin Microbiol Rev* **6**, 137-149

43.   Sabri, M., Caza, M., Proulx, J., Lymberopoulos, M. H., Bree, A., Moulin-Schouleur, M., Curtiss, R., 3rd, and Dozois, C. M. (2008) Contribution of the SitABCD, MntH, and

FeoB metal transporters to the virulence of avian pathogenic *Escherichia coli* O78 strain chi7122. *Infect Immun* **76**, 601-611

44. Zaharik, M. L., Cullen, V. L., Fung, A. M., Libby, S. J., Kujat Choy, S. L., Coburn, B., Kehres, D. G., Maguire, M. E., Fang, F. C., and Finlay, B. B. (2004) The *Salmonella enterica* serovar typhimurium divalent cation transport systems MntH and SitABCD are essential for virulence in an *Nramp1*^{G169} murine typhoid model. *Infect Immun* **72**, 5522-5525

45. Fetherston, J. D., Mier, I., Jr., Truszczynska, H., and Perry, R. D. (2012) The Yfe and Feo transporters are involved in microaerobic growth and virulence of *Yersinia pestis* in bubonic plague. *Infect Immun* **80**, 3880-3891

46. Festa, R. A., and Thiele, D. J. (2012) Copper at the front line of the host-pathogen battle. *PLoS Path* **8**, doi: 10.1371/journal.ppat.1002887

47. Warnes, S. L., Caves, V., and Keevil, C. W. (2012) Mechanism of copper surface toxicity in *Escherichia coli* O157:H7 and *Salmonella* involves immediate membrane depolarization followed by slower rate of DNA destruction which differs from that observed for Gram-positive bacteria. *Environ Microbiol* **14**, 1730-1743

48. Argüello, J. M., Gonzalez-Guerrero, M., and Raimunda, D. (2011) Bacterial Transition Metal P$_{1B}$-ATPases: Transport Mechanism and Roles in Virulence. *Biochemistry* **50**, 9940-9949

49. Argüello, J. M., Raimunda, D., and Padilla-Benavides, T. (2013) Mechanisms of copper homeostasis in bacteria. *Front Cell Infect Microbiol* **3**, doi: 10.3389/fcimb.2013.00073

50. Konieczna, I., Zarnowiec, P., Kwinkowski, M., Kolesinska, B., Fraczyk, J., Kaminski, Z., and Kaca, W. (2012) Bacterial urease and its role in long-lasting human diseases. *Curr*

Protein Pept Sc **13**, 789-806

51. Benoit, S. L., Miller, E. F., and Maier, R. J. (2013) *Helicobacter pylori* Stores Nickel To Aid Its Host Colonization. *Infect Immun* **81**, 580-584

52. Fischer, F., Robbe-Saule, M., Turlin, E., Mancuso, F., Michel, V., Richaud, P., Veyrier, F. J., De Reuse, H., and Vinella, D. (2016) Characterization in *Helicobacter pylori* of a Nickel Transporter Essential for Colonization That Was Acquired during Evolution by Gastric *Helicobacter* Species. *PLoS Path* **12**, doi: 10.1371/journal.ppat.1006018

53. Remy, L., Carriere, M., Derre-Bobillot, A., Martini, C., Sanguinetti, M., and Borezee-Durant, E. (2013) The *Staphylococcus aureus* Opp1 ABC transporter imports nickel and cobalt in zinc-depleted conditions and contributes to virulence. *Mol Microbiol* **87**, 730-743

54. Coulter, S. N., Schwan, W. R., Ng, E. Y. W., Langhorne, M. H., Ritchie, H. D., Westbrock-Wadman, S., Hufnagle, W. O., Folger, K. R., Bayer, A. S., and Stover, C. K. (1998) *Staphylococcus aureus* genetic loci impacting growth and survival in multiple infection environments. *Mol Microbiol* **30**, 393-404

55. Steeb, B., Claudi, B., Burton, N. A., Tienz, P., Schmidt, A., Farhan, H., Mazé, A., and Bumann, D. (2013) Parallel exploitation of diverse host nutrients enhances *Salmonella* virulence. *PLoS Path* **9**, doi: 10.1371/journal.ppat.1003301

56. Olive, A. J., and Sassetti, C. M. (2016) Metabolic crosstalk between host and pathogen: sensing, adapting and competing. *Nat Rev Microbiol* **14**, 221-234

57. Abu-Lubad, M., Meyer, T. F., and Al-Zeer, M. A. (2014) *Chlamydia trachomatis* inhibits inducible NO synthase in human mesenchymal stem cells by stimulating polyamine synthesis. *J Immunol* **193**, 2941-2951

58.   Wall, D. H., Nielsen, U. N., and Six, J. (2015) Soil biodiversity and human health. *Nature* **528**, 69-76

59.   Tullius, M. V., Harth, G., and Horwitz, M. A. (2003) Glutamine synthetase GlnA1 is essential for growth of *Mycobacterium tuberculosis* in human THP-1 macrophages and guinea pigs. *Infect Immun* **71**, 3927-3936

60.   de Oliveira, D. C., da Silva Lima, F., Sartori, T., Antunes Santos, A. C., Rogero, M. M., and Fock, R. A. (2016) Glutamine metabolism and its effects on immune response: molecular mechanism and gene expression. *Nutrire* **41**, doi: 10.1186/s41110-41016-40016-41118

61.   van Heeswijk, W. C., Westerhoff, H. V., and Boogerd, F. C. (2013) Nitrogen assimilation in *Escherichia coli*: putting molecular data into a systems perspective. *Microbiol Mol Biol Rev* **77**, 628-695

62.   Amon, J., Titgemeyer, F., and Burkovski, A. (2010) Common patterns - unique features: nitrogen metabolism and regulation in Gram-positive bacteria. *FEMS Microbiol Rev* **34**, 588-605

63.   Catlin, B. W. (1973) Nutritional profiles of *Neisseria gonorrhoeae*, *Neisseria meningitidis*, and *Neisseria lactamica* in chemically defined media and the use of growth requirements for Gonococcal typing. *J Infect Dis* **128**, 178-194

64.   Malinverni, J. C., and Silhavy, T. J. (2009) An ABC transport system that maintains lipid asymmetry in the Gram-negative outer membrane. *Proc Natl Acad Sci USA* **106**, 8009-8014

65.   Monaco, C., Talà, A., Spinosa, M. R., Progida, C., De Nitto, E., Gaballo, A., Bruni, C. B., Bucci, C., and Alifano, P. (2006) Identification of a meningococcal L-glutamate ABC

transporter operon essential for growth in low-sodium environments. *Infect Immun* **74**, 1725-1740

66. Colicchio, R., Ricci, S., Lamberti, F., Pagliarulo, C., Pagliuca, C., Braione, V., Braccini, T., Talà, A., Montanaro, D., Tripodi, S., Cintorino, M., Troncone, G., Bucci, C., Pozzi, G., Bruni, C. B., Alifano, P., and Salvatore, P. (2009) The meningococcal ABC-Type L-glutamate transporter GltT is necessary for the development of experimental meningitis in mice. *Infect Immun* **77**, 3578-3587

67. Talà, A., Monaco, C., Nagorska, K., Exley, R. M., Corbett, A., Zychlinsky, A., Alifano, P., and Tang, C. M. (2011) Glutamate utilization promotes meningococcal survival in vivo through avoidance of the neutrophil oxidative burst. *Mol Microbiol* **81**, 1330-1342

68. Takahashi, H., Kim, K. S., and Watanabe, H. (2011) Meningococcal internalization into human endothelial and epithelial cells is triggered by the influx of extracellular L-glutamate via GltT L-glutamate ABC transporter in *Neisseria meningitidis*. *Infect Immun* **79**, 380-392

69. Takahashi, H., Yanagisawa, T., Kim, K. S., Yokoyama, S., and Ohnishi, M. (2015) Multiple functions of glutamate uptake via Meningococcal GltT-GltM L-Glutamate ABC transporter in *Neisseria meningitidis* internalization into human brain microvascular endothelial cells. *Infect Immun* **83**, 3555-3567

70. Reitzer, L. (2003) Nitrogen assimilation and global regulation in *Escherichia coli*. *Annu Rev Microbiol* **57**, 155-176

71. Weiner, J. H., and Heppel, L. A. (1971) A binding protein for glutamine and its relation to active transport in *Escherichia coli*. *J Biol Chem* **246**, 6933-6941.

72. Klose, K. E., and Mekalanos, J. J. (1997) Simultaneous prevention of glutamine synthesis

and high-affinity transport attenuates *Salmonella* typhimurium virulence. *Infect Immun* **65**, 587-596

73. Hendriksen, W. T., Kloosterman, T. G., Bootsma, H. J., Estevão, S., De Groot, R., Kuipers, O. P., and Hermans, P. W. M. (2008) Site-specific contributions of glutamine-dependent regulator GlnR and GlnR-regulated genes to virulence of *Streptococcus pneumoniae*. *Infect Immun* **76**, 1230-1238

74. Hartel, T., Klein, M., Koedel, U., Rohde, M., Petruschka, L., and Hammerschmidt, S. (2011) Impact of glutamine transporters on pneumococcal fitness under infection-related conditions. *Infect Immun* **79**, 44-58

75. Tamura, G. S. (2002) A glutamine transport gene, *glnQ*, is required for fibronectin adherence and virulence of Group B Streptococci. *Infect Immun* **70**, 2877-2885

76. Haber, A., Friedman, S., Lobel, L., Burg-Golani, T., Sigal, N., Rose, J., Livnat-Levanon, N., Lewinson, O., and Herskovits, A. (2017) L-glutamine Induces Expression of *Listeria monocytogenes* Virulence Genes. *PLoS Path* **13**, doi: 10.1371/journal.ppat.1006161

77. Trakhanov, S., Vyas, N. K., Luecke, H., Kristensen, D. M., Ma, J., and Quiocho, F. A. (2005) Ligand-free and -bound structures of the binding protein (LivJ) of the *Escherichia coli* ABC leucine/isoleucine/valine transport system: Trajectory and dynamics of the interdomain rotation and ligand specificity. *Biochemistry* **44**, 6597-6608

78. Adams, M. D., Maguire, D. J., and Oxender, D. L. (1991) Altering the binding activity specificity of the leucine binding proteins of *Escherichia coli*. *J Biol Chem* **266**, 6209-6214

79. Rahmanian, M., Claus, D. R., and Oxender, D. L. (1973) Multiplicity of Leucine Transport Systems in *Escherichia coli* K-12. *J Bacteriol* **116**, 1258-1266

80. Koyanagi, T., Katayama, T., Suzuki, H., and Kumagai, H. (2004) Identification of the LIV-I/LS System as the Third Phenylalanine Transporter in *Escherichia coli* K-12. *J Bacteriol* **186**, 343-350

81. Luck, L. A., and Johnson, C. (2000) Fluorescence and ^{19}F NMR evidence that phenylalanine, 3-L-fluorophenylalanine and 4-L-fluorophenylalanine bind to the L-leucine specific receptor of *Escherichia coli*. *Protein Sci* **9**, 2573-2576

82. Magnusson, U., Salopek-Sondi, B., Luck, L. A., and Mowbray, S. L. (2004) X-ray structures of the leucine-binding protein illustrate conformational changes and the basis of ligand specificity. *J Biol Chem* **279**, 8747-8752

83. Basavanna, S., Khandavilli, S., Yuste, J., Cohen, J. M., Hosie, A. H. F., Webb, A. J., Thomas, G. H., and Brown, J. S. (2009) Screening of *Streptococcus pneumoniae* ABC Transporter Mutants Demonstrates that LivJHMGF, a Branched-Chain Amino Acid ABC Transporter, Is Necessary for Disease Pathogenesis. *Infect Immun* **77**, 3412-3423

84. Murphy, T. F., Brauer, A. L., Johnson, A., and Kirkham, C. (2016) ATP-binding cassette (ABC) transporters of the human respiratory tract pathogen, *Moraxella catarrhalis*: Role in virulence. *PLoS One* **11**, doi: 10.1371/journal.pone.0158689

85. Xayarath, B., Marquis, H., Port, G. C., and Freitag, N. E. (2009) *Listeria monocytogenes* CtaP is a multifunctional cysteine transport-associated protein required for bacterial pathogenesis. *Mol Microbiol* **74**, 956-973

86. Tuinema, B. R., Reid-Yu, S. A., and Coombes, B. K. (2014) *Salmonella* evades D-amino acid oxidase to promote infection in neutrophils. *MBio* **5**, doi: 10.1128/mBio.01886-01814

87. Osborne, S. E., Tuinema, B. R., Mok, M. C., Lau, P. S., Bui, N. K., Tomljenovic-Berube,

A. M., Vollmer, W., Zhang, K., Junop, M., and Coombes, B. K. (2012) Characterization of DalS, an ATP-binding cassette transporter for D-alanine, and its role in pathogenesis in *Salmonella enterica*. *J Biol Chem* **287**, 15242-15250

88.   Kohler, S., Voß, F., Gomez Mejia, A., Brown, J., and Hammerschmidt, S. (2016) Pneumococcal lipoproteins involved in bacterial fitness, virulence, and immune evasion. *FEBS Lett* **590**, 3820-3839

89.   Basavanna, S., Chimalapati, S., Maqbool, A., Rubbo, B., Yuste, J., Wilson, R., Hosie, A., Ogunniyi, A., Paton, J., Thomas, G., and Brown, J. (2013) The Effects of Methionine Acquisition and Synthesis on *Streptococcus pneumoniae* Growth and Virulence. *PLoS One* **8**, doi: 10.1371/journal.pone.0049638

90.   Saleh, M., Abdullah, M. R., Schulz, C., Kohler, T., Pribyl, T., Jensch, I., and Hammerschmidt, S. (2014) Following in real time the impact of Pneumococcal virulence factors in an acute mouse pneumonia model using bioluminescent bacteria. *J Vis Exp* **84**, doi: 10.3791/51174

91.   Lebrette, H., Brochier-Armanet, C., Zambelli, B., de Reuse, H., Borezee-Durant, E., Ciurli, S., and Cavazza, C. (2014) Promiscuous Nickel Import in Human Pathogens: Structure, Thermodynamics, and Evolution of Extracytoplasmic Nickel-Binding Proteins. *Structure* **22**, 1421-1432

92.   Terwilliger, A., Swick, M. C., Pflughoeft, K. J., Pomerantsev, A., Lyons, C. R., Koehler, T. M., and Maresso, A. (2015) *Bacillus anthracis* overcomes an amino acid auxotrophy by cleaving host serum proteins. *J Bacteriol* **197**, 2400-2411

93.   Al-quadan, T., Price, C. T., and Kwaik, Y. A. (2012) Exploitation of evolutionarily conserved amoeba and mammalian processes by *Legionella*. *Trends Microbiol* **20**, 299-

306

94.   Abouhamad, W. N., Manson, M., Gibson, M. M., and Higgins, C. F. (1991) Peptide transport and chemotaxis in *Escherichia coli* and *Salmonella Typhimurium*: characterization of the dipeptide permease (Dpp) and the dipeptide-binding protein. *Mol Microbiol* **5**, 1035-1047

95.   Alloing, G. v., Martin, B., Granadel, C., and Claverys, J. P. (1998) Development of competence in *Streptococcus pneumoniae*: Pheromone autoinduction and control of quorum sensing by the oligopeptide permease. *Mol Microbiol* **29**, 75-83

96.   Perego, M., Higgins, C. F., Pearce, S. R., Gallagher, M. P., and Hoch, J. A. (1991) The oligopeptide transport system of *Bacillus subtilis* plays a role in the initiation of sporulation. *Mol Microbiol* **5**, 173-185

97.   Jones, A. L., Knoll, K. M., and Rubens, C. E. (2000) Identification of *Streptococcus agalactiae* virulence genes in the neonatal rat sepsis model using signature-tagged mutagenesis. *Mol Microbiol* **37**, 1444-1455

98.   Pettersen, V. K., Mosevoll, K. A., Lindemann, P. C., and Wiker, H. G. (2016) Coordination of metabolism and virulence factors expression of extraintestinal pathogenic *Escherichia coli* purified from blood cultures of patients with sepsis. *Mol Cell Proteomics* **15**, 2890-2907

99.   Mason, K. M., Munson, R. S., Lauren, O., and Bakaletz, L. O. (2003) Nontypeable *Haemophilus influenzae* Gene Expression Induced In Vivo in a Chinchilla Model of Otitis Media *Infect Immun* **71**, 3553-3462

100.   Eriksson, S., Lucchini, S., Thompson, A., Rhen, M., and Hinton, J. C. D. (2003) Unravelling the biology of macrophage infection by gene expression profiling of

intracellular *Salmonella enterica*. *Mol Microbiol* **47**, 103-118

101. Hancock, R. E. W., and Chapple, D. S. (1999) Peptide antibiotics. *Antimicrob Agents Chemother* **43**, 1317-1323

102. Detmers, F. J. M., Lanfermeijer, F. C., Abele, R., Jack, R. W., Tampe, R., Konings, W. N., and Poolman, B. (2000) Combinatorial peptide libraries reveal the ligand-binding mechanism of the oligopeptide receptor OppA of *Lactococcus lactis*. *Proc Natl Acad Sci USA* **97**, 12487-12492

103. Berntsson, R. P., Doeven, M. K., Fusetti, F., Duurkens, R. H., Sengupta, D., Marrink, S. J., Thunnissen, A. M., Poolman, B., and Slotboom, D. J. (2009) The structural basis for peptide selection by the transport receptor OppA. *EMBO J* **28**, 1332-1340

104. Jones, M. M., Johnson, A., Koszelak-Rosenblum, M., Kirkham, C., Brauer, A. L., Malkowski, M. G., and Murphy, T. F. (2014) Role of the oligopeptide permease ABC transporter of *Moraxella catarrhalis* in nutrient acquisition and persistence in the respiratory tract. *Infect Immun* **82**, 4758-4766

105. Gominet, M., Slamti, L., Gilois, N., Rose, M., and Lereclus, D. (2001) Oligopeptide permease is required for expression of the *Bacillus thuringiensis* plcR regulon and for virulence. *Mol Microbiol* **40**, 963-975

106. Wang, C. H., Lin, C. Y., Luo, Y. H., Tsai, P. J., Lin, Y. S., Lin, M. T., Chuang, W. J., Liu, C. C., and Wu, J. J. (2005) Effects of oligopeptide permease in Group A Streptococcal infection. *Infect Immun* **73**, 2881-2890

107. Groisman, E. A., Parra-Lopez, C., Salcedo, M., Lipps, C. J., and Heffron, F. (1992) Resistance to host antimicrobial peptides is necessary for *Salmonella* virulence. *Proc Natl Acad Sci USA* **89**, 11939-11943

108. López-Solanilla, E., García-Olmedo, F., and Rodríguez-Palenzuela, P. (1998) Inactivation of the *sapA* to *sapF* locus of *Erwinia chrysanthemi* reveals common features in plant and animal bacterial pathogenesis. *Plant Cell* **10**, 917-924

109. Mason, K. M., Munson, R. S., and Bakaletz, L. O. (2005) A mutation in the *sap* operon attenuates survival of nontypeable *Haemophilus influenzae* in a chinchilla model of otitis media. *Infect Immun* **73**, 599-608

110. Mason, K. M., Raffel, F. K., Ray, W. C., and Bakaletz, L. O. (2011) Heme utilization by nontypeable *Haemophilus influenzae* is essential and dependent on sap transporter function. *J Bacteriol* **193**, 2527-2535

111. Raffel, F. K., Szelestey, B. R., Beatty, W. L., and Mason, K. M. (2013) The *Haemophilus influenzae* Sap transporter mediates bacterium-epithelial cell homeostasis. *Infect Immun* **81**, 43-54

112. Mount, K. L. B., Townsend, C. A., Rinker, S. D., Gu, X., Fortney, K. R., Zwickl, B. W., Janowicz, D. M., Spinola, S. M., Katz, B. P., and Bauer, M. E. (2010) *Haemophilus ducreyi* SapA contributes to cathelicidin resistance and virulence in humans. *Infect Immun* **78**, 1176-1184

113. Shelton, C. L., Raffel, F. K., Beatty, W. L., Johnson, S. M., and Mason, K. M. (2011) Sap transporter mediated import and subsequent degradation of antimicrobial peptides in *Haemophilus*. *PLoS Path* **7**, doi: 10.1371/journal.ppat.1002360

114. Rinker, S. D., Gu, X., Fortney, K. R., Zwickl, B. W., Katz, B. P., Janowicz, D. M., Spinola, S. M., and Bauer, M. E. (2012) Permeases of the *sap* transporter are required for cathelicidin resistance and virulence of *Haemophilus ducreyi* in humans. *J Infect Dis* **206**, 1407-1414

115.   Mason, K. M., Bruggeman, M. E., Munson, R. S., and Bakaletz, L. O. (2006) The non-typeable *Haemophilus influenzae* Sap transporter provides a mechanism of antimicrobial peptide resistance and SapD-dependent potassium acquisition. *Mol Microbiol* **62**, 1357-1372

116.   Eswarappa, S. M., Panguluri, K. K., Hensel, M., and Chakravortty, D. (2008) The *yejABEF* operon of *Salmonella* confers resistance to antimicrobial peptides and contributes to its virulence. *Microbiology* **154**, 666-678

117.   Wang, Z., Bie, P., Cheng, J., Lu, L., Cui, B., and Wu, Q. (2016) The ABC transporter YejABEF is required for resistance to antimicrobial peptides and the virulence of *Brucella melitensis*. *Sci Rep* **6**, doi: 10.1038/srep31876

118.   Rebuffat, S. (2012) Microcins in action : amazing defence strategies of Enterobacteria. *Biochem Soc Trans* **40**, 1456-1462

119.   Mistry, A., Warren, M. S., Cusick, J. K., Karkhoff-Schweizer, R. R., Lomovskaya, O., and Schweizer, H. P. (2013) High-level pacidamycin resistance in *Pseudomonas aeruginosa* is mediated by an *opp* oligopeptide permease encoded by the *opp-fabI* operon. *Antimicrob Agents Chemother* **57**, 5565-5571

120.   Pletzer, D., Braun, Y., Dubiley, S., Lafon, C., Köhler, T., Page, M. G. P., Mourez, M., and Severinov, K. (2015) The *Pseudomonas aeruginosa* PA14 ABC transporter NppA1A2BCD is required for uptake of peptidyl nucleoside antibiotics. *J Bacteriol* **197**, 2217-2228

121.   Novikova, M., Metlitskaya, A., Datsenko, K., Kazakov, T., Kazakov, A., Wanner, B., and Severinov, K. (2007) The *Escherichia coli* Yej transporter is required for the uptake of translation inhibitor Microcin C. *J Bacteriol* **189**, 8361-8365

122. Clarke, T. E., Braun, V., Tari, L. W., and Vogel, H. J. (2002) X-ray crystallographic structures of the *Escherichia coli* periplasmic protein FhuD bound to hydroxamate-type siderophores and the antibiotic albomycin. *J Biol Chem* **277**, 13966-13972

123. Pletzer, D., Lafon, C., Braun, Y., Köhler, T., Page, M. G. P., Mourez, M., and Weingart, H. (2014) High-throughput screening of dipeptide utilization mediated by the ABC transporter DppBCDF and its substrate-binding proteins DppA1-A5 in *Pseudomonas aeruginosa*. *PLoS One* **9**, doi: 10.1371/journal.pone.0111311

124. Shiver, A. L., Osadnik, H., Kritikos, G., Li, B., Krogan, N., Typas, A., and Gross, C. A. (2016) A chemical-genomic screen of neglected antibiotics reveals illicit transport of kasugamycin and blasticidin S. *PLoS Genet* **12**, doi: 10.1371/journal.pgen.1006124

125. Ilari, A., Pescatori, L., Di Santo, R., Battistoni, A., Ammendola, S., Falconi, M., Berlutti, F., Valenti, P., and Chiancone, E. (2016) *Salmonella enterica* serovar Typhimurium growth is inhibited by the concomitant binding of Zn(II) and a pyrrolyl-hydroxamate to ZnuA, the soluble component of the ZnuABC transporter. *Biochim Biophys Acta* **1860**, 534-541

126. Tanabe, M., Atkins, H. S., Harland, D. N., Elvin, S. J., Stagg, A. J., Mirza, O., Titball, R. W., Byrne, B., and Brown, K. A. (2006) The ABC Transporter Protein OppA Provides Protection against Experimental *Yersinia pestis* Infection. *Infect Immun* **74**, 3687-3691

127. Yang, M., Johnson, A., and Murphy, T. F. (2011) Characterization and evaluation of the *Moraxella catarrhalis* oligopeptide permease A as a mucosal vaccine antigen. *Infect Immun* **79**, 846-857

128. Brown, J. S., Ogunniyi, A. D., Woodrow, M. C., Holden, D. W., and Paton, J. C. (2001) Immunization with components of two iron uptake ABC transporters protects mice

against systemic *Streptococcus pneumoniae* infection. *Infect Immun* **69**, 6702-6706

129. Jomaa, M., Terry, S., Hale, C., Jones, C., Dougan, G., and Brown, J. (2006) Immunization with the iron uptake ABC transporter proteins PiaA and PiuA prevents respiratory infection with *Streptococcus pneumoniae*. *Vaccine* **24**, 5133-5139

130. Yang, H. J., Zhang, J. Y., Wei, C., Yang, L. Y., Zuo, Q. F., Zhuang, Y., Feng, Y. J., Srinivas, S., Zeng, H., and Zou, Q. M. (2016) Immunisation with Iimmunodominant linear B cell epitopes vaccine of manganese transport protein C confers protection against *Staphylococcus aureus* infection. *PLoS One* **11**, doi: 10.1371/journal.pone.0149638

131. Gribenko, A. V., Parris, K., Mosyak, L., Li, S., Handke, L., Hawkins, J. C., Severina, E., Matsuka, Y. V., and Anderson, A. S. (2016) High Resolution Mapping of Bactericidal Monoclonal Antibody Binding Epitopes on *Staphylococcus aureus* Antigen MntC. *PLoS Path* **12**, doi: 10.1371/journal.ppat.1005908

132. Begier, E., Seiden, D. J., Patton, M., Zito, E., Severs, J., Cooper, D., Eiden, J., Gruber, W. C., Jansen, K. U., Anderson, A. S., and Gurtman, A. (2017) SA4Ag, a 4-antigen *Staphylococcus aureus* vaccine, rapidly induces high levels of bacteria-killing antibodies. *Vaccine* **35**, 1132-1139

133. Murphy, T. F., Bakaletz, L. O., and Smeesters, P. R. (2009) Microbial Interactions in the Respiratory Tract. *Pediatr Infect Dis J* **28**, 121-126

134. Turk, D. C. (1984) The pathogenicity of *Haemophilus influenzae*. *J Med Microbiol* **18**, 1-16

135. Monsó, E., Ruiz, J., Rosell, A., Manterola, J., Fiz, J., Morera, J., and Ausina, V. (1995) Bacterial infection in chronic obstructive pulmonary disease. A study of stable and exacerbated outpatients using the protected specimen brush. *Am J Respir Crit Care Med*

152, 1316-1320

136. Rajan, S., and Saiman, L. (2002) Pulmonary infections in patients with cystic fibrosis. *Semin Respir Infect* **17**, 47-56

137. Murphy, T. F. (2003) Respiratory infections caused by non-typeable *Haemophilus influenzae*. *Curr Opin Infect Dis* **16**, 129-134

138. Venekamp, R. P., Burton, M. J., Dongen, T. M. v., Heijden, G. J. v. d., Zon, A. v., and Schilder, A. G. (2016) Antibiotics for otitis media with effusion in children. *Cochrane Database Syst Rev*, doi: 10.1002/14651858.CD14009163.pub14651853

139. Singh, K., Nordström, T., Mörgelin, M., Brant, M., Cardell, L. O., and Riesbeck, K. (2014) *Haemophilus influenzae* Resides in Tonsils and Uses Immunoglobulin D Binding as an Evasion Strategy. *J Infect Dis* **209**, 1418-1428

140. Harrison, A., Bakaletz, L. O., and Munson, R. S. (2012) *Haemophilus influenzae* and oxidative stress. *Front Cell Infect Microbiol* **2**, doi:10.3389/fcimb.2012.00040

141. Cundell, D. R., Taylor, G. W., Kanthakumar, K., Wilks, M., Tabaqchali, S., Dorey, E., Devalia, J. L., Roberts, D. E., Davies, R. J., Wilson, R., and Cole, P. J. (1993) Inhibition of Human Neutrophil Migration In Vitro by Low-Molecular-Mass Products of Nontypeable *Haemophilus influenzae*. *Infect Immun* **61**, 2419-2424

142. Stull, T. L. (1987) Protein sources of heme for *Haemophilus influenzae*. *Infect Immun* **55**, 148-153

143. Granick, S., and Gilder, H. (1946) The Porphyrin Requirements of *Haemophilus Influenzae* and Some Functions of the Vinyl and Propionic Acid Side Chains of Heme. *J Gen Physiol* **30**, 1-13

144. Morton, D. J., Smith, A., Ren, Z., Madore, L. L., VanWagoner, T. M., Seale, T. W.,

Whitby, P. W., and Stull, T. L. (2004) Identification of a haem-utilization protein (Hup) in *Haemophilus influenzae*. *Microbiology* **150**, 3923-3933

145. Jin, H., Ren, Z., Whitby, P. W., Morton, D. J., and Stull, T. L. (1999) Characterization of *hgpA*, a gene encoding a haemoglobin/haemoglobin-haptoglobin-binding protein of *Haemophilus influenzae*. *Microbiology* **145**, 905-914

146. Ren, Z., Jin, H., Morton, D. J., and Stull, T. L. (1998) *hgpB*, a Gene Encoding a Second *Haemophilus influenzae* Hemoglobin-and Hemoglobin-Haptoglobin-Binding Protein. *Infect Immun* **66**, 4733-4741

147. Morton, D. J., Whitby, P. W., Jin, H., Ren, Z., and Stull, T. L. (1999) Effect of Multiple Mutations in the Hemoglobin- and Hemoglobin-Haptoglobin-Binding Proteins, HgpA, HgpB, and HgpC, of *Haemophilus influenzae* Type b. *Infect Immun* **67**, 2729-2739

148. Cope, L. D., Yogev, R., Muller-Eberhard, U., and Hansen, E. J. (1995) A Gene Cluster Involved in the Utilization of Both Free Heme and Heme:Hemopexin by H*aemophilus influenzae* Type b. *J Bacteriol* **177**, 2644-2653

149. Cope, L. D., Thomas, S. E., Hrkal, Z., and Hansen, E. J. (1998) Binding of Heme-Hemopexin Complexes by Soluble HxuA Protein Allows Utilization of This Complexed Heme by *Haemophilus influenzae*. *Infect Immun* **66**, 4511-4516

150. Faraldo-Gómez, J. D., and Sansom, M. S. P. (2003) Acquisition of siderophores in Gram-negative bacteria. *Nat Rev Mol Cell Bio* **4**, 105-116

151. Saier, M. H. (2000) A Functional-Phylogenetic Classification System for Transmembrane Solute Transporters. *Microbiol Mol Biol Rev* **64**, 354-411

152. Morton, D. J., Seale, T. W., Vanwagoner, T. M., Whitby, P. W., and Stull, T. L. (2009) The dppBCDF gene cluster of *Haemophilus influenzae*: Role in heme utilization. *BMC*

Res Notes **2**, doi: 10.1186/1756-0500-1182-1166

153. Vogel, A. R., Szelestey, B. R., Raffel, F. K., Sharpe, S. W., Gearinger, R. L., Justice, S. S., and Mason, K. M. (2012) SapF-mediated heme-iron utilization enhances persistence and coordinates biofilm architecture of *Haemophilus*. *Front Cell Infect Microbiol* **2**, doi: 10.3389/fcimb.2012.00042

154. Vergauwen, B., Elegheert, J., Dansercoer, A., Devreese, B., and Savvides, S. N. (2010) Glutathione import in *Haemophilus influenzae* Rd is primed by the periplasmic heme-binding protein HbpA. *Proc Natl Acad Sci USA* **107**, 13270-13275

155. Carlsen, C. U., Møller, J. K. S., and Skibsted, L. H. (2005) Heme-iron in lipid oxidation. *Coord Chem Rev* **249**, 485-498

156. Tenhunen, R., Marver, H. S., and Schmidt, R. (1969) Microsomal Heme Oxygenase. Characterization of the enzyme. *J Biol Chem* **244**, 6388-6393

157. Guo, Y., Guo, G., Mao, X., Zhang, W., Xiao, J., Tong, W., Liu, T., Xiao, B., Liu, X., Feng, Y., and Zou, Q. (2008) Functional identification of HugZ, a heme oxygenase from *Helicobacter pylori*. *BMC Microbiol* **8**, 10.1186/1471-2180-1188-1226

158. Hanson, M. S., and Hansen, E. J. (1991) Molecular cloning, partial purification, and characterization of a haemin-binding lipoprotein from *Haemophilus influenzae* type-b. *Mol Microbiol* **5**, 267-278

159. Hiles, I. D., and Higgins, C. F. (1986) Peptide uptake by *Salmonella* typhimuium. *Eur J Biochem* **158**, 561-567

160. Parra-Lopez, C., Baer, M. T., and Groisman, E. A. (1993) Molecular genetic analysis of a locus required for resistance to antimicrobial peptides in *Salmonella* typhimurium. *EMBO J* **12**, 4053-4062

161. Morton, D. J., Madore, L. L., Smith, A., VanWagoner, T. M., Seale, T. W., Whitby, P. W., and Stull, T. L. (2005) The heme-binding lipoprotein (HbpA) of *Haemophilus influenzae*: Role in heme utilization. *FEMS Microbiol Lett* **253**, 193-199

162. Shepherd, M., Heath, M. D., and Poole, R. K. (2007) NikA Binds Heme: A New Role for an *Escherichia coli* Periplasmic Nickel-Binding Protein. *Biochemistry* **46**, 5030-5037

163. Park, J. T., Raychaudhuri, D., Li, H., Mengin-lecreulx, D., and Normark, S. (1998) MppA, a Periplasmic Binding Protein Essential for Import of the Bacterial Cell Wall Peptide L-Alanyl-γ-D-Glutamyl-*meso*-Diaminopimelate. *J Bacteriol* **180**, 1215-1223

164. Létoffé, S., Delepelaire, P., and Wandersman, C. (2006) The housekeeping dipeptide permease is the *Escherichia coli* heme transporter and functions with two optional peptide binding proteins. *Proc Natl Acad Sci USA* **103**, 12891-12896

165. Barr, I., and Guo, F. (2015) Pyridine Hemochromagen Assay for Determinig the Concentration of Heme Purified Protein Solutions. *Bio Protoc* **5**, doi: 10.21769/BioProtoc.21594

166. Waterhouse, A. M., Procter, J. B., Martin, D. M. A., Clamp, M., and Barton, G. J. (2009) Jalview Version 2-a multiple sequence alignment editor and analysis workbench. *Bioinformatics* **25**, 1189-1191

167. Fukami-Kobayashi, K., Tateno, Y., and Nishikawa, K. (1999) Domain Dislocation: a Change of Core Structure in Periplasmic Binding Proteins in their Evolutionary History. *J Mol Biol* **286**, 279-290

168. Hellman, L. M., and Fried, M. G. (2007) Electrophoretic mobility shift assay (EMSA) for detecting protein-nucleic acid interactions. *Nat Protoc* **2**, 1849-1861

169. Wu, L. F., and Mandrand-Berthelot, M. A. (1995) A family of homologous substrate-

binding proteins with a broad range of substrate specificity and dissimilar biological functions. *Biochimie* **77**, 744-750

170. Thompson, J. M., Jones, H. A., and Perry, R. D. (1999) Molecular Characterization of the Hemin Uptake Locus (*hmu*) from *Yersinia pestis* and Analysis of *hmu* Mutants for Hemin and Hemoprotein Utilization. *Infect Immun* **67**, 3879-3892

171. O'Neill, M. J., Bhakta, M. N., Fleming, K. G., and Wilks, A. (2012) Induced fit on heme binding to the *Pseudomonas aeruginosa* cytoplasmic protein (PhuS) drives interaction with heme oxygenase (HemO). *Proc Natl Acad Sci USA* **109**, 5639-5644

172. Lee, E. M., Ahn, S. H., Park, J. H., Lee, J. H., Ahn, S. C., and Kong, I. S. (2004) Identification of oligopeptide permease (*opp*) gene cluster in *Vibrio fluvialis* and characterization of biofilm production by *oppA* knockout mutation. *FEMS Microbiol Lett* **240**, 21-30

173. Flores-Valdez, M. A., Morris, R. P., Laval, F., Daffé, M., and Schoolnik, G. K. (2009) *Mycobacterium tuberculosis* modulates its cell surface via an oligopeptide permease (Opp) transport system. *FASEB J* **23**, 4091-4104

174. Guyer, C. A., Morgan, D. G., and Staros, J. V. (1986) Binding specificity of the periplasmic oligopeptide-binding protein from *Escherichia coli*. *J Bacteriol* **168**, 775-779

175. Tame, J. R. H., Murshudov, G. N., Dodson, E. J., Neil, T. K., Dodson, G. G., Higgins, C. F., Wilkinson, A. J., Neil, T. K., Dodson, G. G., Higgins, C. F., and Wilkinson, A. J. (1994) The Structural Basis of Sequence-Independent Peptide Binding by OppA Protein. *Science* **264**, 1578-1581

176. Tanabe, M., Mirza, O., Bertrand, T., Atkins, H. S., Titball, R. W., Iwata, S., Brown, K. A., and Byrne, B. (2007) Structures of OppA and PstS from *Yersinia pestis* indicate

variability of interactions with transmembrane domains. *Acta Crystallogr Sect D Biol Cryst* **63**, 1185-1193

177. Klepsch, M. M., Kovermann, M., Löw, C., Balbach, J., Permentier, H. P., Fusetti, F., De Gier, J. W., Slotboom, D. J., and Berntsson, R. P. A. (2011) *Escherichia coli* peptide binding protein OppA has a preference for positively charged peptides. *J Mol Biol* **414**, 75-85

178. Lassaux, P., Peri, C., Ferrer-Navarro, M., Gourlay, L. J., Gori, A., Conchillo-Solé, O., Rinchai, D., Lertmemongkolchai, G., Longhi, R., Daura, X., Colombo, G., and Bolognesi, M. (2013) A Structure-Based Strategy for Epitope Discovery in *Burkholderia pseudomallei* OppA Antigen. *Structure* **21**, 167-175

179. Levdikov, V. M., Blagova, E. V., Brannigan, J. A., Wright, L., Vagin, A. A., and Wilkinson, A. J. (2005) The Structure of the Oligopeptide-binding Protein, AppA, from *Bacillus subtilis* in Complex with a Nonapeptide. *J Biol Chem* **345**, 879-892

180. Berntsson, R. P. A., Schuurman-Wolters, G. K., Dunny, G., Slotboom, D. J., and Poolman, B. (2012) Structure and Mode of Peptide Binding of Pheromone Receptor PrgZ*. *J Biol Chem* **287**, 37165-37170

181. Kabsch, W. (2010) *XDS. Acta Crystallogr Sect D Biol Cryst* **66**, 125-132

182. Winn, M. D., Ballard, C. C., Cowtan, K. D., Dodson, E. J., Emsley, P., Evans, P. R., Keegan, R. M., Krissinel, E. B., Leslie, A. G. W., McCoy, A., McNicholas, S. J., Murshudov, G. N., Pannu, N. S., Potterton, E. A., Powell, H. R., Read, R. J., Vagin, A., and Wilson, K. S. (2011) Overview of the *CCP4* suite and current developments. *Acta Crystallogr Sect D Biol Cryst* **67**, 235-242

183. Long, F., Vagin, A. A., Young, P., and Murshudov, G. N. (2007) *BALBES*: A molecular-

replacement pipeline. *Acta Crystallogr Sect D Biol Cryst* **64**, 125-132

184. Langer, G., Cohen, S. X., Lamzin, V. S., and Perrakis, A. (2008) Automated macromolecular model building for X-ray crystallography using ARP/wARP version 7. *Nat Protoc* **3**, 1171-1179

185. Emsley, P., and Cowtan, K. (2004) *Coot*: Model-building tools for molecular graphics. *Acta Crystallogr Sect D Biol Cryst* **60**, 2126-2132

186. Murshudov, G. N., Vagin, A. A., and Dodson, E. J. (1997) Refinement of macromolecular structures by the maximum-likelihood method. *Acta Crystallogr Sect D Biol Cryst* **53**, 240-255

187. Chen, V. B., Arendall, W. B., Headd, J. J., Keedy, D. A., Immormino, R. M., Kapral, G. J., Murray, L. W., Richardson, J. S., and Richardson, D. C. (2010) *MolProbity*: All-atom structure validation for macromolecular crystallography. *Acta Crystallogr Sect D Biol Cryst* **66**, 12-21

188. Laskowski, R. A., and Swindells, M. B. (2011) LigPlot+: Multiple Ligand-Protein Interaction Diagrams for Drug Discovery. *J Chem Inf Model* **51**, 2778-2786

189. Niesen, F. H., Berglund, H., and Vedadi, M. (2007) The use of differential scanning fluorimetry to detect ligand interactions that promote protein stability. *Nat Protoc* **2**, 2212-2221

190. Lyskov, S., Chou, F. C., Conchúir, S. Ó., Der, B. S., Drew, K., Kuroda, D., Xu, J., Weitzner, B. D., Renfrew, P. D., Sripakdeevong, P., Borgo, B., Havranek, J. J., Kuhlman, B., Kortemme, T., Bonneau, R., Gray, J. J., and Das, R. (2013) Serverification of Molecular Modeling Applications: The Rosetta Online Server That Includes Everyone (ROSIE). *PLoS One* **8**, doi: 10.1371/journal.pone.0063906

191. Silhavy, T. J., Szmelcman, S., Boos, W., and Schwartz, M. (1975) On the significance of the retention of ligand by protein. *Proc Natl Acad Sci USA* **72**, 2120-2124

192. Lanfermeijer, F. C., Picon, A., Konings, W. N., and Poolman, B. (1999) Kinetics and Consequences of Binding of Nona- and Dodecapeptides to the Oligopeptide Binding Protein (OppA) of *Lactococcus lactis*. *Biochemistry* **38**, 14440-14450

193. Goodell, E. W., and Higgins, C. F. (1987) Uptake of Cell Wall Peptides by *Salmonella* typhimurium and *Escherichia coli*. *J Bacteriol* **169**, 3861-3865

194. Tame, J. R., Dodson, E. J., Murshudov, G., Higgins, C. F., and Wilkinson, A. J. (1995) The crystal structures of the oligopeptide-binding protein OppA complexed with tripeptide and tetrapeptide ligands. *Structure* **3**, 1395-1406

195. Richarme, G., and Caldas, T. D. (1997) Chaperone Properties of the Bacterial Periplasmic Substrate-binding Proteins. *J Biol Chem* **272**, 15607-15612

196. Lennon, C. W., Thamsen, M., Friman, E. T., Cacciaglia, A., Sachsenhauser, V., Sorgenfrei, F. A., Wasik, M. A., and Bardwell, J. C. A. (2015) Folding Optimization *In Vivo* Uncovers New Chaperones. *J Mol Biol* **427**, 2983-2994

197. Klotman, M. E., and Chang, T. L. (2006) Defensins in innate antiviral immunity. *Nat Rev Immunol* **6**, 447-456

198. Silva, P. M., Gonçalves, S., and Santos, N. C. (2014) Defensins: Antifungal lessons from eukaryotes. *Front Microbiol* **5**, doi: 10.3389/fphar.2014.00275

199. Vale, N., Aguiar, L., and Gomes, P. (2014) Antimicrobial peptides: A new class of antimalarial drugs? *Front Pharma* **5**, doi: 10.3389/fphar.2014.00275

200. Lee, T. H., Hall, K. N., and Aguilar, M. I. (2016) Antimicrobial Peptide Structure and Mechanism of Action: A Focus on the Role of Membrane Structure. *Curr Top Med Chem*

16, 25-39

201. Sørensen, O., Arnljots, K., Cowland, J. B., Bainton, D. F., and Borregaard, N. (1997) The Human Antibacterial Cathelicidin, hCAP-18, Is Synthesized in Myelocytes and Metamyelocytes and Localized to Specific Granules in Neutrophils. *Blood* **90**, 2796-2803

202. Alalwani, S. M., Sierigk, J., Herr, C., Pinkenburg, O., Gallo, R., Vogelmeier, C., and Bals, R. (2010) The antimicrobial peptide LL-37 modulates the inflammatory and host defense response of human neutrophils. *Eur J Immunol* **40**, 1118-1126

203. Scott, M. G., Davidson, D. J., Gold, M. R., Bowdish, D., and Hancock, R. E. W. (2002) The Human Antimicrobial Peptide LL-37 Is a Multifunctional Modulator of Innate Immune Responses. *J Immunol* **169**, 3883-3891

204. Selsted, M. E., Harwig, S. S., Ganz, T., Schilling, J. W., and Lehrer, R. I. (1985) Primary structures of three human neutrophil defensins. *J Clin Invest* **76**, 1436-1439

205. Singh, P. K., Jia, H. P., Wiles, K., Hesselberth, J., Liu, L., Conway, B. A. D., Greenberg, E. P., Valore, E. V., Welsh, M. J., Ganz, T., Tack, B. F., and McCray, P. B. J. (1998) Production of β-defensins by human airway epithelia. *Proc Natl Acad Sci USA* **95**, 14961-14966

206. Yount, N. Y., and Yeaman, M. R. (2004) Multidimensional signatures in antimicrobial peptides. *Proc Natl Acad Sci USA* **101**, 7363-7368

207. Territo, M. C., Ganz, T., Selsted, M. E., and Lehrer, R. (1989) Monocyte-Chemotactic Activity of Defensins from Human Neutrophils. *J Clin Invest* **84**, 2017-2020

208. Michiel, D. F., Chertov, O., Michiel, D. F., Xu, L., Wang, J. M., Tani, K., Murphy, W. J., Longo, D. L., Taub, D. D., and Oppenheim, J. J. (1996) Identification of Defensin-1, Defensin-2, and CAP37/Azurocidin as T-cell Chemoattractant Proteins Released from

Interleukin-8-stimulated Neutrophils. *J Biol Chem* **271**, 2935-2940

209.   Yang, D., Chertov, O., Bykovskaia, S. N., Chen, Q., Buffo, M. J., Shogan, J., Anderson, M., Schröder, J. M., Wang, J. M., Howard, O. M. Z., and Oppenheim, J. J. (1999) β-Defensins: Linking Innate and Adaptive Immunity Through Dendritic and T Cell CCR6. *Science* **286**, 525-529

210.   Imasato, A., Desbois-Mouthon, C., Han, J., Kai, H., Cato, A. C. B., Akira, S., and Li, J. D. (2002) Inhibition of p38 MAPK by Glucocorticoids via Induction of MAPK Phosphatase-1 Enhances Nontypeable Haemophilus influenzae-induced Expression of Toll-like Receptor 2. *J Biol Chem* **277**, 47444-47450

211.   Lee, H. Y., Andalibi, A., Webster, P., Moon, S. K., Teufert, K., Kang, S. H., Li, J. D., Nagura, M., Ganz, T., and Lim, D. J. (2004) Antimicrobial activity of innate immune molecules against *Streptococcus pneumoniae*, *Moraxella catarrhalis* and nontypeable *Haemophilus influenzae*. *BMC Infect Dis* **4**, doi: 10.1186/1471-2334-1184-1112

212.   Bishop-Hurley, S. L., Schmidt, F. J., Erwin, A. L., and Smith, A. L. (2005) Peptides Selected for Binding to a Virulent Strain of *Haemophilus influenzae* by Phage Display Are Bactericidal. *Antimicrob Agents Chemother* **49**, 2972-2978

213.   Underwood, M., and Bakaletz, L. (2011) Innate Immunity and the Role of Defensins in Otitis Media. *Curr Allergy Asthma Rep* **11**, 499-507

214.   McGillivary, G., Mason, K. M., Jurcisek, J. A., Peeples, M. E., and Bakaletz, L. O. (2009) Respiratory syncytial virus-induced dysregulation of expression of a mucosal beta-defensin augments colonization of the upper airway by non-typeable *Haemophilus influenzae*. *Cell Microbiol* **11**, 1399-1408

215.   McGillivary, G., Ray, W. C., Bevins, C. L., Munson, R. S. J., and Bakaletz, L. O. (2007)

A member of the cathelicidin family of antimicrobial peptides is produced in the upper airway of the chinchilla and its mRNA expression is altered by common viral and bacterial co-pathogens of otitis media. *Mol Immunol* **44**, 2446-2458

216. Murphy, T. F., and Kirkham, C. (2002) Biofilm formation by nontypeable *Haemophilus influenzae*: strain variability, outer membrane antigen expression and role of pili. *BMC Microbiol* **2**, doi: 10.1186/1471-2180-1182-1187

217. Mandrell, R. E., McLaughlin, R., Kwaik, Y. A., Lesse, A., Yamasaki, R., Gibson, B., Spinola, S. M., and Apicella, M. A. (1992) Lipooligosaccharides (LOS) of Some *Haemophilus* Species Mimic Human Glycosphingolipids, and Some LOS Are Sialylated. *Infect Immun* **60**, 1322-1328

218. Clementi, C. F., and Murphy, T. F. (2011) Non-typeable *Haemophilus influenzae* invasion and persistence in the human respiratory tract. *Front Cell Infect Microbiol* **1**, doi: 10.3389/fcimb.2011.00001

219. Juneau, R. A., Pang, B., Weimer, K. W. D., Armbruster, C. E., and Swords, W. E. (2011) Nontypeable *Haemophilus influenzae* Initiates Formation of Neutrophil Extracellular Traps. *Infect Immun* **79**, 431-438

220. Harms, C., Domoto, Y., Celik, C., Rahe, E., Stumpe, S., Schmid, R., Nakamura, T., and Bakker, E. P. (2001) Identification of the ABC protein SapD as the subunit that confers ATP dependence to the K+-uptake systems TrkH and TrKG from *Escherichia coli* K-12. *Microbiology* **147**, 2991-3003

221. Holm, L., and Sander, C. (1995) Dali: a network tool for protein structure comparison. *Trends Biochem Sci* **20**, 478-480

222. Melo, M., Ferre, R., and Castanho, M. (2009) Antimicrobial peptides: linking partition,

activity and high membrane-bound concentrations. *Nat Rev Microbiol* **7**, 245-250

223. Gonçalves, S., Abade, J., Teixeira, A., and Santos, N. C. (2012) Lipid composition is a Determinant for Human Defensin HNP1 Selectivity. *Biopolymers* **98**, 313-321

224. Gonçalves, S., Teixeira, A., Abade, J., De Medeiros, L. N., Kurtenbach, E., and Santos, N. C. (2012) Evaluation of the membrane lipid selectivity of the pea defensin Psd1. *Biochim Biophys Acta* **1818**, 1420-1426

225. Bonucci, A., Balducci, E., Pistolesi, S., and Pogni, R. (2013) The defensin-lipid interaction: Insights on the binding states of the human antimicrobial peptide HNP-1 to model bacterial membranes. *Biochim Biophys Acta* **1828**, 758-764

226. Mathew, B., and Nagaraj, R. (2017) Variations in the interaction of human defensins with *Escherichia coli*: Possible implications in bacterial killing. *PLoS One* **12**, doi: 10.1371/journal.pone.0175858

227. Leeuw, E. d., Li, C., Zeng, P., Li, C., Buin, M. D. d., Lu, W. Y., Breukink, E., and Lu, W. (2010) Functional interaction of human neutrophil peptide-1 with the cell wall precursor lipid II. *FEBS Lett* **584**, 1543-1548

228. Sass, V., Schneider, T., Wilmes, M., Körner, C., Tossi, A., Novikova, N., Shamova, O., and Sahl, H. G. (2010) Human β-defensin 3 inhibits cell wall biosynthesis in staphylococci. *Infect Immun* **78**, 2793-2800

229. Wu, Z., Hoover, D. M., Yang, D., Boulègue, C., Santamaria, F., Oppenheim, J. J., Lubkowski, J., and Lu, W. (2003) Engineering disulfide bridges to dissect antimicrobial and chemotactic activities of human beta-defensin 3. *Proc Natl Acad Sci USA* **100**, 8880-8885

230. Varkey, J., and Nagaraj, R. (2005) Antibacterial Activity of Human Neutrophil Defensin

HNP-1 analogs without Cysteines. *Antimicrob Agents Chemother* **49**, 4561-4566

231. Mandal, M., and Nagaraj, R. (2002) Antibacterial activities and conformations of synthetic α-defensin HNP-1 and analogs with one, two and three disulfide bridges. *J Pept Res* **59**, 95-104

232. Krishnakumari, V., and Nagaraj, R. (2012) Binding of peptides corresponding to the carboxy-terminal region of human-β-defensins-1-3 with model membranes investigated by isothermal titration calorimetry. *Biochim Biophys Acta* **1818**, 1386-1394

233. Hoover, D. M., Wu, Z., Tucker, K., Lu, W., and Lubkowski, J. (2003) Antimicrobial Characterization of Human β-Defensin 3 Derivatives. *Antimicrob Agents Chemother* **47**, 2804-2809

234. Nigro, E., Colavita, I., Sarnataro, D., Scudiero, O., Zambrano, G., Granata, V., Daniele, A., Carotenuto, A., Galdiero, S., Folliero, V., Galdiero, M., Urbanowicz, R. A., Ball, J. K., Salvatore, F., and Pessi, A. (2015) An ancestral host defence peptide within human β-defensin 3 recapitulates the antibacterial and antiviral activity of the full-length molecule. *Sci Rep* **5**, doi: 10.1038/srep18450

235. Zhang, Y., Lu, W., and Hong, M. (2010) The Membrane-Bound Structure and Topology of a Human α-Defensin Indicate a Dimer Pore Mechanism for Membrane Disruption. *Biochemistry* **49**, 9770-9782

236. Faya, M., Kalhapure, R. S., Kumalo, H. M., Waddad, A. Y., Omolo, C., and Govender, T. (2018) Conjugates and nano-delivery of antimicrobial peptides for enhancing therapeutic activity. *J Drug Deliv Sci Technol* **44**, 153-171

237. Boto, A., De La Lastra, J. M. P., and González, C. C. (2018) The road from host-defense peptides to a new generation of antimicrobial drugs. *Molecules* **23**, doi:

10.3390/molecules23020311

238. Handali, M., Roychowdhury, H., Neupane, D. P., and Yukl, E. T. (2015) AztD, a Periplasmic Zinc Metallochaperone to an ATP-Binding Cassette (ABC) Transporter System in *Paracoccus denitrificans*. *J Biol Chem* **290**, 29984-29992

239. Ilari, A., Alaleona, F., Tria, G., Petrarca, P., Battistoni, A., Zamparelli, C., Verzili, D., Falconi, M., and Chiancone, E. (2014) The *Salmonella enterica* ZinT structure, zinc affinity and interaction with the high-affinity uptake protein ZnuA provide insight into the management of periplasmic zinc. *Biochim Biophys Acta* **1840**, 535-544

240. Carter, D. M., Miousse, I. R., Gagnon, J. N., Martinez, â., Clements, A., Lee, J., Hancock, M. A., Gagnon, H., Pawelek, P. D., and Coulton, J. W. (2006) Interactions between TonB from *Escherichia coli* and the Periplasmic Protein FhuD. *J Biol Chem* **281**, 35413-35424

241. James, K. J., Hancock, M. A., Gagnon, J. N., and Coulton, J. W. (2009) TonB Interacts with BtuF, the *Escherichia coli* Periplasmic Binding Protein for Cyanocobalamin. *Biochemistry* **48**, 9212-9220

242. Tanaka, K. J., Song, S., Mason, K., and Pinkett, H. W. (2018) Selective substrate uptake: The role of ATP-binding cassette (ABC) importers in pathogenesis. *Biochim Biophys Acta* **1860**, 868-877

243. Garmory, H. S., and Titball, R. W. (2004) ATP-Binding Cassette Transporters Are Targets for the Development of Antibacterial Vaccines and Therapies. *Infect Immun* **72**, 6757-6763

244. Sjuts, H., Vargiu, A. V., Kwasny, S. M., Nguyen, S. T., Kim, H.-S., Ding, X., Ornik, A. R., Ruggerone, P., Bowlin, T. L., Nikaido, H., Pos, K. M., and Opperman, T. J. (2016)

Molecular basis for inhibition of AcrB multidrug efflux pump by novel and powerful pyranopyridine derivatives. *Proc Natl Acad Sci USA* **113**, 3509-3514

245. Oldham, M. L., Hite, R. K., Steffen, A. M., Damko, E., Li, Z., Walz, T., and Chen, J. (2016) A mechanism of viral immune evasion revealed by cryo-EM analysis of the TAP transporter. *Nature* **529**, 537-540

246. Stojiljkovic, I., Kumar, V., and Srinivasan, N. (1999) Non-iron metalloporphyrins : potent antibacterial compounds that exploit haem/Hb uptake systems of pathogenic bacteria. *Mol Microbiol* **31**, 429-442

247. Arivett, B. A., Fiester, S. E., Ohneck, E. J., Penwell, W. F., Kaufman, C. M., Relich, R. F., and Actis, L. A. (2015) Antimicrobial Activity of Gallium Protoporphyrin IX against *Acinetobacter baumannii* Strains Displaying Different Antibiotic Resistance Phenotypes. *Antimicrob Agents Chemother* **59**, 7657-7665

248. Richter, K., Thomas, N., Zhang, G., Prestidge, C. A., Coenye, T., Wormald, P.-J., and Vreugde, S. (2017) Deferiprone and Gallium-Protoporphyrin Have the Capacity to Potentiate the Activity of Antibiotics in *Staphylococcus aureus* Small Colony Variants. *Front Cell Infect Microbiol* **7**, doi: 10.3389/fcimb.2017.00280

249. Sierra, J. M., Fusté, E., Rabanal, F., Vinuesa, T., and Viñas, M. (2017) An overview of antimicrobial peptides and the latest advances in their development. *Expert Opin Biol Ther* **17**, 663-676

250. Rajchakit, U., and Sarojini, V. (2017) Recent Developments in Antimicrobial-Peptide-Conjugated Gold Nanoparticles. *Bioconj Chem* **28**, 2673-2686

251. Mensa, B., Howell, G. L., Scott, R., and DeGrado, W. F. (2014) Comparative mechanistic studies of brilacidin, daptomycin, and the antimicrobial peptide LL16.

Antimicrob Agents Chemother **58**, 5136-5145

252. Rank, G. H., Gerlach, J. H., and Robertson, A. J. (1976) Some physiological alterations associated with pleiotropic cross resistance and collateral sensitivity in *Saccharomyces cerevisiae*. *Mol Gen Genet* **144**, 281-288

253. Sanglard, D., Ischer, F., and Calabrese, D. (1999) The ATP Binding Cassette Transporter Gene CgCDR1 from *Candida glabrata* Is Involved in the Resistance of Clinical Isolates to Azole Antifungal Agents. *Antimicrob Agents Chemother* **43**, 2753-2765

254. Slaven, J. W., Anderson, M. J., and Sanglard, D. (2002) Increased expression of a novel *Aspergillus fumigatus* ABC transporter gene, *atrF*, in the presence of itraconazole in an itraconazole resistant clinical isolate. *Fungal Genet Biol* **36**, 199-206

255. Fling, M., Kopf, J., Tamarkin, A., Gorman, J. A., Smith, H. A., and Koltin, Y. (1991) Analysis of a *Candida albicans* gene that encodes a novel mechanism for resistance to benomyl and methotrexate. *Mol Gen Genet* **227**, 318-329

256. Goffeau, A. (2008) Drug resistance: the fight against fungi. *Nature* **452**, 541-542

257. Sá-Correia, I., and Tenreiro, S. (2002) The multidrug resistance transporters of the major facilitator superfamily, 6 years after disclosure of *Saccharomyces cerevisiae* genome sequence. *J Biotechnol* **98**, 215-226

258. Shahi, P., and Moye-Rowley, W. S. (2009) Coordinate control of lipid composition and drug transport activities is required for normal multidrug resistance in fungi. *Biochim Biophys Acta* **1794**, 852-859

259. Gulshan, K., and Moye-Rowley, W. S. (2007) Multidrug resistance in fungi. *Eukaryot Cell* **6**, 1933-1942

260. Balzi, E., Chen, W., Ulaszewski, S., Capieaux, E., and Goffeau, A. (1987) The multidrug

resistance gene PDR1 from *Saccharomyces cerevisiae*. *J Biol Chem* **262**, 16871-16879

261. Subik, J., Ulaszewski, S., and Goffeau, A. (1986) Genetic mapping of nuclear mucidin resistance mutations in *Saccharomyces cerevisiae*. A new pdr locus on chromosome II. *Curr Genet* **10**, 665-670

262. Kolaczkowska, A., and Goffeau, A. (1999) Regulation of pleiotropic drug resistance in yeast. *Drug Resist Updat* **2**, 403-414

263. DeRisi, J., van den Hazel, B., Marc, P., Balzi, E., Brown, P., Jacq, C., and Goffeau, A. (2000) Genome microarray analysis of transcriptional activation in multidrug resistance yeast mutants. *FEBS Lett* **470**, 156-160

264. Delahodde, A., Delaveau, T., and Jacq, C. (1995) Positive autoregulation of the yeast transcription factor Pdr3p, which is involved in control of drug resistance. *Mol Cell Biol* **15**, 4043-4051

265. Balzi, E., Wang, M., Leterme, S., Van Dyck, L., and Goffeau, A. (1994) PDR5, a novel yeast multidrug resistance conferring transporter controlled by the transcription regulator PDR1. *J Biol Chem* **269**, 2206-2214

266. Decottignies, A., Lambert, L., Catty, P., Degand, H., Epping, E. A., Moye-Rowley, W. S., Balzi, E., and Goffeau, A. (1995) Identification and characterization of SNQ2, a new multidrug ATP binding cassette transporter of the yeast plasma membrane. *J Biol Chem* **270**, 18150-18157

267. Katzmann, D. J., Hallstrom, T. C., Voet, M., Wysock, W., Golin, J., Volckaert, G., and Moye-Rowley, W. S. (1995) Expression of an ATP-binding cassette transporter-encoding gene (YOR1) is required for oligomycin resistance in *Saccharomyces cerevisiae*. *Mol Cell Biol* **15**, 6875-6883

268. Cui, Z., Shiraki, T., Hirata, D., and Miyakawa, T. (1998) Yeast gene YRR1, which is required for resistance to 4-nitroquinoline N-oxide, mediates transcriptional activation of the multidrug resistance transporter gene SNQ2. *Mol Microbiol* **29**, 1307-1315

269. Akache, B., and Turcotte, B. (2002) New regulators of drug sensitivity in the family of yeast zinc cluster proteins. *J Biol Chem* **277**, 21254-21260

270. Carvajal, E., van den Hazel, H. B., Cybularz-Kolaczkowska, A., Balzi, E., and Goffeau, A. (1997) Molecular and phenotypic characterization of yeast PDR1 mutants that show hyperactive transcription of various ABC multidrug transporter genes. *Mol Gen Genet* **256**, 406-415

271. Nourani, A., Papajova, D., Delahodde, A., Jacq, C., and Subik, J. (1997) Clustered amino acid substitutions in the yeast transcription regulator Pdr3p increase pleiotropic drug resistance and identify a new central regulatory domain. *Mol Gen Genet* **256**, 397-405

272. Kolaczkowski, M., Kolaczowska, A., Luczynski, J., Witek, S., and Goffeau, A. (1998) *In Vivo* Characterization of the Drug Resistance Profile of the Major ABC Transporters and Other Components of the Yeast Pleiotropic Drug Resistance Network. *Microb Drug Resist* **4**, 143-158

273. Meyers, S., Schauer, W., Balzi, E., Wagner, M., Goffeau, A., and Golin, J. (1992) Interaction of the yeast pleiotropic drug resistance genes *PDR1* and *PDR5*. *Curr Genet* **21**, 431-436

274. Fardeau, V., Lelandais, G., Oldfield, A., Salin, H., Lemoine, S., Garcia, M., Tanty, V., Le Crom, S., Jacq, C., and Devaux, F. (2007) The Central Role of PDR1 in the Foundation of Yeast Drug Resistance. *J Biol Chem* **282**, 5063-5074

275. Sidorova, M., Drobna, E., Dzugasova, V., Hikkel, I., and Subik, J. (2007) Loss-of-

function *pdr3* mutations convert the Pdr3p transcription activator to a protein suppressing multidrug resistance in *Saccharomyces cerevisiae*. *FEMS Yeast Res* **7**, 254-264

276. Wendler, F., Bergler, H., Prutej, K., Jungwirth, H., Zisser, G., Kuchler, K., and Högenauer, G. (1997) Diazaborine Resistance in the Yeast *Saccharomyces cerevisiae* Reveals a Link between *YAP1* and the Pleiotropic Drug Resistance Genes *PDR1* and *PDR3*. *J Biol Chem* **272**, 27091-27098

277. Hellauer, K., Rochon, M. H., and Turcotte, B. (1996) A novel DNA binding motif for yeast zinc cluster proteins: the Leu3p and Pdr3p transcriptional activators recognize everted repeats. *Mol Cell Biol* **16**, 6096-6102

278. Bauer, B. E., Wolfger, H., and Kuchler, K. (1999) Inventory and function of yeast ABC proteins: about sex, stress, pleiotropic drug and heavy metal resistance. *Biochim Biophys Acta* **1461**, 217-236

279. Devaux, F., Marc, P., Bouchoux, C., Delaveau, T., Hikkel, I., Potier, M. C., and Jacq, C. (2001) An artificial transcription activator mimics the genome-wide properties of the yeast Pdr1 transcription factor. *EMBO Rep* **2**, 493-498

280. Kolaczkowska, A., Kolaczkowski, M., Delahodde, A., and Goffeau, A. (2002) Functional dissection of Pdr1p, a regulator of multidrug resistance in *Saccharomyces cerevisiae*. *Mol Genet Genomics* **267**, 96-106

281. Simonics, T., Kozovska, Z., Michalkova-Papajova, D., Delahodde, A., Jacq, C., and Subik, J. (2000) Isolation and molecular characterization of the carboxy-terminal pdr3 mutants in *Saccharomyces cerevisiae*. *Curr Genet* **38**, 248-255

282. Thakur, J. K., Arthanari, H., Yang, F., Pan, S.-J., Fan, X., Breger, J., Frueh, D. P., Gulshan, K., Li, D. K., Mylonakis, E., Struhl, K., Moye-Rowley, W. S., Cormack, B. P.,

Wagner, G., and Näär, A. M. (2008) A nuclear receptor-like pathway regulating multidrug resistance in fungi. *Nature* **452**, 604-609

283. Kolaczkowska, A., Kolaczkowski, M., Goffeau, A., and Moye-Rowley, W. S. (2008) Compensatory activation of the multidrug transporters Pdr5p, Snq2p, and Yor1p by Pdr1p in *Saccharomyces cerevisiae*. *FEBS Lett* **582**, 977-983

284. Wolfger, H., Mahé, Y., Parle-McDermott, A., Delahodde, A., and Kuchler, K. (1997) The yeast ATP binding cassette (ABC) protein genes PDR10 and PDR15 are novel targets for the Pdr1 and Pdr3 transcriptional regulators. *FEBS Lett* **418**, 269-274

285. Dzugasova, V., Borecka, S., Batova, M., Pilisiova, R., Hervayova, N., and Subik, J. (2010) Site-directed mutagenesis of Asp853 in Pdr3p transcriptional activator from *Saccharomyces cerevisiae*. *Yeast* **27**, 277-284

286. MacPherson, S., Larochelle, M., and Turcotte, B. (2006) A Fungal Family of Transcriptional Regulators: the Zinc Cluster Proteins. *Microbiol Mol Biol Rev* **70**, 583-604

287. Schjerling, P., and Holmberg, S. (1996) Comparative amino acid sequence analysis of the C6 zinc cluster family of transcriptional regulators *Nucleic Acids Res* **24**, 4599-4607

288. Mamane, Y., Hellauer, K., Rochon, M. H., and Turcotte, B. (1998) A linker region of the yeast zinc cluster protein leu3p specifies binding to everted repeat DNA. *J Biol Chem* **273**, 18556-18561

289. Mamnun, Y. M., Pandjaitan, R., Mahé, Y., Delahodde, A., and Kuchler, K. (2002) The yeast zinc finger regulators Pdr1p and Pdr3p control pleiotropic drug resistance (PDR) as homo- and heterodimers in vivo. *Mol Microbiol* **46**, 1429-1440

290. Katzmann, D. J., Burnett, P. E., Golin, J., Mahé, Y., and Moye-Rowley, W. S. (1994)

Transcriptional control of the yeast PDR5 gene by the PDR3 gene product. *Mol Cell Biol* **14**, 4653-4661

291. Katzmann, D. J., Hallstrom, T. C., Mahé, Y., and Moye-Rowley, W. S. (1996) Multiple Pdr1p/Pdr3p Binding Sites are Essential for Normal Expression of the ATP Binding Cassette Transporter Protein-encoding Gene *PDR5*. *J Biol Chem* **271**, 23049-23054

VITA

AWARDS

National Science Foundation Graduate Research Fellowship Program – Honorable Mention 2012

NIH Molecular Biophysics Training Grant – granted 2011, renewed 2012

PUBLICATIONS AND PRESENTATIONS

Publications:

Tanaka, K. J. and Pinkett, H. W. Multifunctional substrate binding of nontypeable *Haemophilus influenzae* oligopeptide-binding protein (OppA). (2019) *Journal of Biological Chemistry* doi: 10.1074/jbc.RA118.004479

Tanaka, K. J., Song, S., Mason, K., and Pinkett, H. W. Selective substrate uptake: The role of ATP-binding cassette (ABC) importers in pathogenesis. (2018) *Biochimica et Biophysica Acta – Biomembranes* **1860,** 868-877

Penn, R. L., Tanaka, K. and Erbs, J. Size dependent kinetics of oriented aggregation. (2007) *Journal of Crystal Growth* **309**, 97-102

Podium Presentations:

Multifunctional Substrate Binding of Oligopeptide-Binding Protein (OppA). 9th Annual Biophysics Symposium. June 20th, 2018; Northwestern University, IL.

Multifunctional Sap Transporter: Role in Nutrient Uptake and Antimicrobial Resistance. 7th Annual Biophysics Symposium. June 15th, 2016; Northwestern University, IL.

Nutrient Uptake and Antimicrobial Resistance of Bacteria. IBiS (Interdisciplinary Biological Sciences) Retreat. September 4th, 2015; Northwestern University, IL.

Poster Presentations:

Heimlich, D.R., Tanaka, K.J., Pinkett, H.W., and Mason, K.M. Persistence of Nontypeable *Haemophilus influenzae* is Dependent upon Selective Import of Nutrients and Host Antimicrobial Peptides. 18th International Symposium on Recent Advances in Otitis Media. June 7-11, 2015; National Harbor, MD.

Heimlich, D.R., Tanaka, K.J., Pinkett, H.W., and Mason, K.M. Transporter remodeling for selectivity of substrate transport is critical for *Haemophilus* persistence. 21st Annual Midwest Microbial Pathogenesis Conference. September 12-14, 2014; Chicago, IL.

Tanaka, K.J. and Pinkett, H.W. The Role of Zinc Custer Proteins in Antifungal Resistance. Biophysical Society 57th Annual Meeting, Protein/Nucleic Acids Interactions. February 2-6, 2013; Philadelphia, PA.

Tanaka, K.J. and Pinkett, H.W. Controlling Drug Resistance in Fungal Systems. 26th Annual Symposium of The Protein Society, Proteins and Disease. August 5-8, 2012; San Diego, CA.

TEACHING EXPERIENCE

Teaching Assistant - *Biochemistry*

    Spring 2013, Northwestern University

Laboratory Instructor **-** *Genetics and Molecular Biology*

    Fall 2011, Northwestern University

Laboratory Assistant **-** *Organic Chemistry*

    Fall 2007, Macalester College